

Physicochemical controls on the compositions of the Earth and planets

Paolo A. Sossi^{*,1}, Remco C. Hin², Thorsten Kleine³, Alessandro Morbidelli^{4,5}, and Francis Nimmo⁶

¹Institute of Geochemistry and Petrology, ETH Zürich, Clausiusstrasse 25, CH-8092, Zürich, Switzerland

²Institute of Environmental Geology and Geoengineering, Consiglio Nazionale delle Ricerche (CNR), Via Sandro Botticelli 23, 20133, Milan, Italy

³Max Planck Institute for Solar System Research, Justus-von-Liebig-Weg 3, 37077, Göttingen, Germany

⁴Laboratoire Lagrange, Université Côte d'Azur, Observatoire de la Côte d'Azur, CNRS, CS 34229, F-06304, Nice, France

⁵Collège de France, CNRS, PSL Université, Sorbonne Université, F-75014, Paris, France

⁶Department of Earth & Planetary Sciences, University of California Santa Cruz, CA 95064, Santa Cruz, USA

*corresponding author. email: paolo.sossi@eps.ethz.ch

December 2, 2025

Abstract

Despite the fact that the terrestrial planets all formed from the protoplanetary disk, their bulk compositions show marked departures from that of material condensing from a canonical H_2 -rich solar nebula. Metallic cores fix the oxygen fugacities ($f\text{O}_2$ s) of the planets to between ~ 5 (Mercury) and ~ 1 log units below the iron-wüstite buffer, orders of magnitude higher than that of the nebular gas. Their oxidised character is coupled with a lack of volatile elements with respect to the solar nebula. Here we show that condensates from a canonical solar gas at different temperatures (T_0) produce bulk compositions with Fe/O (by mass) ranging from ~ 0.93 ($T_0 = 1250$ K) to ~ 0.81 ($T_0 = 400$ K), far lower than that of Earth at 1.06. Because the reaction $\text{Fe(s)} + \text{H}_2\text{O(g)} = \text{FeO(s)} + \text{H}_2\text{(g)}$ proceeds only below ~ 600 K, temperatures at which most moderately volatile elements (MVEs) have already condensed, oxidised planets are expected to be rich in volatiles, and vice-versa. That this is not observed suggests that planets *i*) did not accrete from equilibrium nebular condensates and/or *ii*) underwent additional volatile depletion/ $f\text{O}_2$ changes at conditions distinct from those of the solar nebula. Indeed, MVEs in small telluric bodies (Moon, Vesta) are consistent with evaporation/condensation at $\Delta\text{IW}-1$ and ~ 1400 - 1800 K, while the extent of mass-dependent isotopic fractionation observed implies this occurred near- or at equilibrium. On the other hand, the volatile-depleted elemental- yet near-chondritic isotopic compositions of larger telluric bodies (Earth, Mars) reflect mixing of bodies that had themselves experienced different extents of volatile depletion, overprinted by accretion of volatile-undepleted material. On the basis of isotopic anomalies in Cr- and Ti in the BSE, such undepleted matter has been proposed to be CI chondrites, which would comprise 40 % by mass if the proto-Earth were ureilite-like. However, this would result in an overabundance of volatile elements in the BSE, requiring significant loss thereafter, which has yet to be demonstrated. On the other hand, 6 % CI material added late to an enstatite chondrite-like proto-Earth would broadly match the BSE composition. However, because the Earth is an end-member in isotopic anomalies of heavier elements, no combination of existing meteorites alone can account for its chemical- and isotopic composition. Instead, the Earth is most likely made partially or essentially entirely from an NC-like missing component. If so, the oxidised-, yet volatile-poor nature of differentiated bodies in the inner solar system, including Earth and Mars, is a property intrinsic to the NC reservoir.

1 Introduction

The present-day locations and properties of the terrestrial planets, Mercury, Venus, Earth and Mars (section 2), are the culmination of chemical- and physical processes occurring through space and time that followed the collapse of the molecular cloud. Observations of young stars show that these systems are governed by the interaction of an H_2 -rich gas with the central star (section 3). Temporal evolution from a ‘protostellar’ or Class 0 stage in which molecular cloud material infalls to the central star occurs within $\sim 10^4$ to 10^5 yr (Class I) and forms envelopes extending from $\sim 10^3$ to 10^4 au. Over timescales of 10^6 to 10^7 yr, these envelopes develop into the more common T-Tauri stars, which are invariably surrounded by a circumstellar disk of 1 – 10 Jupiter masses [Montmerle *et al.*, 2006]. The lifetimes of such disks range from ~ 1 – 10 Myr [Hartmann *et al.*, 1998; Hillenbrand, 2008], with that of our Sun having been inferred to have dissipated by 3.8 Myr after the condensation of the first solids by measurements of magnetic fields preserved in angrite meteorites [Wang *et al.*, 2017].

The theory for the evolution of disks was initially developed assuming that turbulence is the main source of viscosity in disks, so that viscosity is proportional to the product of the square of scale height (the size of the largest turbulent eddies) and of the orbital frequency [Lynden-Bell and Pringle, 1974]. However, it now appears that turbulent viscosity can be high only in the initial phase of the disk, due to ionising temperatures [Balbus and Hawley, 1998], Reynolds stresses due to gas infalling onto the disk [Kuznetsova *et al.*, 2022] and/or gravitational instabilities [Rafikov, 2016]. Once this initial phase is over, turbulence becomes too weak in most parts of the disk to account for the observed gas accretion rates [e.g., Cassen, 2006, see section 3]. This mismatch implies an alternative driver of accretion in protoplanetary disks. The strong X-ray emission of T-Tauri stars is testament to the magnetisation of both the star and disk [Feigelson and Montmerle, 1999]. It is now understood that the magnetic effects not only govern the collapse of gas from the initial cloud onto the protostar and its disk [Matsumoto and Tomisaka, 2004; Joos *et al.*, 2012; Krumholz and Federrath, 2019], but also the transport of gas through the disk thanks to the removal of angular momentum in disk winds [Suzuki and Inutsuka, 2009; Bai and Stone, 2013; Gressel *et al.*, 2015]. Disk evolution under disk winds [Tabone *et al.*, 2022] leads, on a typical timescale of ~ 5 Myr, to accretion rates that are sufficiently low so as to result in the removal of the remaining gas by photoevaporation [Alexander *et al.*, 2006].

Chemically, these protoplanetary disks are composed predominantly of H_2 (~ 91 mol. %) and He (~ 8 mol %), with diminishing quantities of other major components, namely, in order of decreasing abundance O, C, Ne, N, Mg, Si and Fe [Lodders, 2010]. Relative to the protoplanetary disk (and hence the Sun), the terrestrial planets are impoverished in H, C, N, He and other rare gases [Aston, 1924] that attests to their accretion from predominantly condensed matter rather than from capture of large quantities of nebular gas. The composition of this material has typically been reconciled in the framework of equilibrium condensation [Larimer, 1967; Grossman and Larimer, 1974; Lodders, 2003, see section 4]. Chemical equilibrium, though not mandated, is invoked for these calculations throughout the entire temperature range over which condensation occurs at an assumed, and constant, pressure of 10^{-4} bar, taken to be representative of the midplane for a Sun-like star.

The first solids predicted to have condensed in these calculations are analogous to calcium-aluminium-rich inclusions (CAIs) preserved in some meteorites [MacPherson, 2006]. They are also the oldest materials to have originated within the Solar System [establishing the t_0 age in relative chronology, Amelin *et al.*, 2002; Connelly *et al.*, 2012], lending credence to the concept of equilibrium condensation. The ‘matrix’ component of chondrites may also result from near-complete condensation of the nebular gas (save for the ice-forming elements; H, C, N, O and the noble gases) [Grossman and Larimer, 1974]. The third component, chondrules, may have originally condensed from the solar nebula, but subsequently experienced partial melting [e.g., Hewins *et al.*, 2005; Ebel *et al.*, 2018; Hellmann *et al.*, 2020]. Mixtures between these components likely gave rise to the chemical variability observed in chondrites [Humayun

and Cassen, 2000; Braukmüller et al., 2018; Alexander, 2019], yet the nature of the processes producing such mixtures, and whether they reflect nebular-wide gradients, remains unclear [Li et al., 2021; Boyce et al., 2024].

The importance of the chondrites lies in their adoption, to first order, as the building blocks of the planets [Ringwood, 1966; Safronov, 1969]. While the constancy of the ratios of refractory lithophile elements (RLEs) to within $\sim 10\%$ among chondrites substantiates this approximation, the abundances of the major planet-forming elements (Fe, Mg, Si, O) vary markedly [up to a factor ~ 2 , Yoshizaki and McDonough, 2020]. In detail, the core/mantle ratios of rocky bodies, which range from ~ 0.65 for Mercury to 0.01 for the Moon by mass [section 2, Ringwood, 1966; Richter et al., 2006], contrasts with the range expected from chondrites, at roughly $0.2 - 0.3$ [e.g., Bercovici et al., 2022]. Indeed, no set of mixtures of chondrites is readily able to reproduce the chemical compositions of the planets [Drake and Richter, 2002; Campbell and O'Neill, 2012], which may instead reflect chemical transformations unique to growing planets (section 5).

One such macroscopic difference is the differentiation of planetary bodies into a core and mantle, implying they experienced melting. Moreover, the terrestrial planets, as well as small telluric bodies (such as Vesta or the Moon), are depleted in volatile elements in a manner unlike that observed in chondritic meteorites [Witt-Eickchen et al., 2009; Mezger et al., 2021]. Sossi et al. [2022] noted that the depletion of elements as a function of their volatilities approximates a cumulative normal distribution, suggesting that rocky bodies accreted by the stochastic combination of many smaller bodies that each experienced volatile depletion at different temperatures. Whether a heliocentric gradient in the temperatures, and hence compositions of bodies is required is unclear [see also Palme, 2000]. This observation only supports the notion that mixing of material with disparate thermal histories led to the formation of the planets, but does not speak to the locus or conditions at which volatile depletion occurred.

An enduring but as yet inconclusive thesis states that the volatile depletion that affected small telluric bodies occurred under different physicochemical conditions to those prevailing during the formation of chondrites [Kreutzberger et al., 1986; Wulf et al., 1995; O'Neill and Palme, 2008; Visscher and Fegley, 2013; Norris and Wood, 2017; Sossi et al., 2019, section 6]. The observation that at least the Earth, with a single-stage Hf-W age of 34 ± 3 Myr [Kleine and Walker, 2017] experienced protracted growth permits the possibility that melting and evaporation took place *after* dispersal of the nebular gas and hence under more oxidised (i.e., higher fO_2) conditions. Evidence for such 'post-nebular' evaporation may be found in the Mn/Na ratio, which is elevated in all small telluric bodies with respect to chondrites, while the bulk silicate Earth falls within the chondritic range [O'Neill and Palme, 2008; Siebert et al., 2018].

The mass-dependent variations in the stable isotopic compositions of these elements provide another means with which to interrogate the origin of volatile depletion among planetary materials (section 6). The coupled isotopic variations in Fe, Si and potentially Mg to superchondritic (i.e., heavy) values suggest that volatile depletion processes, rather than core formation, were most likely responsible for the range of isotopic compositions of planetary materials [Poitrasson et al., 2004; Pringle et al., 2014; Dauphas et al., 2015; Sossi et al., 2016; Hin et al., 2017; Bourdon et al., 2018; Sossi and Shahar, 2021]. On the other hand, the mass-dependent isotopic ratios of moderately volatile elements, such as K and Zn, are near-chondritic in the Earth and Mars [Wang et al., 2016; Sossi et al., 2018b; Paquet et al., 2023], whereas small telluric bodies, such as Vesta, are isotopically heavy [or extremely light in the case of the angrite parent body, Hu et al., 2022]. These observations support the inference of Sossi et al. [2022], in which volatile element depletion affecting small telluric bodies generates isotopic fractionation, which is then progressively overprinted by mixing as the body accretes isotopically unfractionated, volatile-undepleted material.

Such undepleted material is often equated with CI chondrites, an hypothesis reinforced by the discovery, in 2011 [Warren, 2011], of two discrete clusters of meteorites in their isotopic compositions of Cr and Ti [Trinquier et al., 2007, 2009], when normalised to mass-dependent variations. These observations prompted the proposal that two reservoirs

existed in the early Solar System; the NC and CC groups (section 7). That this dichotomy is likely spatial rather than temporal in nature comes from the overlap in accretion ages of both NC- and CC bodies [Kruijer *et al.*, 2017; Bollard *et al.*, 2017], with the former presumed to represent the inner- and the latter the outer solar system. Furthermore, within these groups, isotopically distinct reservoirs exist, implying that mixing, should it have taken place during the accretion of planetary bodies, was likely local in nature. Whether this decreases the likelihood of dynamical scenarios in which the bodies of the early solar system were agitated and resulted in eccentric, crossing orbits, such as in the Grand Tack [Mah and Brasser, 2021; Mah *et al.*, 2022; Woo *et al.*, 2022], remains to be seen.

Earth and Mars fall close to- or within the NC group for these two elements [e.g., Warren, 2011; Dauphas, 2017]. Some small, telluric bodies also occupy the NC group space, and, for Cr, Ti and other iron-peak elements, together define an ‘NC trend’ that passes linearly through or near to the composition of CI chondrites [Trinquier *et al.*, 2009; Williams *et al.*, 2020; Palme and Mezger, 2024]. On this basis, some models argue that the Earth is made predominantly (~ 95 %) of EH-like material [Kleine *et al.*, 2023; Dauphas *et al.*, 2024], whereas others suggest a ureilite-like NC end-member and require up to ~ 40 % CC material [Schiller *et al.*, 2018]. However, the perceived necessity for the addition of carbonaceous chondrites may be circumstantial, since CCs lie on fractionation lines distinct from terrestrial in triple O isotope space [Clayton and Mayeda, 1999], implying that they, in combination with ureilites or EH-like material, are unlikely to represent a significant portion of the Earth on a mass basis. Moreover, for the isotopes of the heavy elements, notably Mo and Zr, there is no suitable member of the extant CC group that would produce the composition of the Earth from an existing NC member. Possible solutions state that the Earth accreted some ‘missing’ material not represented in the meteorite collection for an EH-like proto-Earth [Burkhardt *et al.*, 2021] or preferentially lost *s*-process-depleted material via envelope processing for a ureilite-like end-member [Onyett *et al.*, 2023].

Here, we synthesise the major physical properties of the terrestrial planets and other differentiated telluric bodies and compare them with chondrites on an empirical basis (section 2). Section 3 describes the thermophysical states of protoplanetary disks and their evolution in time so as to identify possible loci and times of planet formation. In section 4, we characterise the chemistry of solids that condense from the solar nebula under the assumption of equilibrium, before exploring the effects of non-equilibrium condensation on the stability and compositions of condensates. Whether mixtures of such condensates are consistent with the bulk compositions of telluric bodies are evaluated in section 5, and the influence of chemical equilibrium between core- and mantle at a range of pressure-temperature conditions on the gross structure of differentiated bodies is examined. The effect of planetary mass on the chemical and isotopic effects of volatile depletion processes are characterised in section 6. Finally, a critical assessment of the distribution of nucleosynthetic anomalies, both across planetary materials and among different elements in the Earth and Mars is undertaken in section 7, with a view to developing a coherent astrophysical model for planetary formation.

2 Physical- and chemical nature of terrestrial planets

2.1 Physical structure and distribution

The distribution of the mass of rocky material in the inner Solar System is concentrated in the terrestrial planets, with two, Earth and Venus, together comprising 91.8 % (see Table 1). The integrated mean of the mass therefore is nearly symmetrically centred about 0.897 AU, an observation that is used to inform models of the initial mass distribution of the protoplanetary disk [Weidenschilling, 1977]. Despite the symmetry in mass distribution, the constitution of the planets is not uniform. The internal structures of the terrestrial planets are *differentiated* and can be approximated by silicate mantles and iron-rich cores, but the core/mantle ratio of the terrestrial planets

broadly decreases with increasing semi-major axis [e.g., *Ringwood*, 1966], ranging from 0.67 ± 0.06 in Mercury [*Hauck et al.*, 2013] to 0.204 ± 0.015 in Mars [*Khan et al.*, 2023] and $0.008\text{--}0.015$ in the Moon [*Sossi et al.*, 2025]. In detail, however, Venus has a slightly lower uncompressed density (by 2 %) than does the Earth, but its moment of inertia [0.337 ± 0.024 , *Margot et al.*, 2021] overlaps with that of the Earth [0.3307 , *Williams*, 1994], meaning its core/mantle ratio is indistinguishable, within error, from that of the Earth (0.325).

Table 1: Selected physical and chemical properties of planetary bodies.

	Semi-major axis (AU)	ξ	log(mass, kg)	ξ	CMF	ξ	FeO (wt. %)	ξ	Mg#	ξ	ΣFe	ξ	ΔIW	ξ
Mercury	0.387	-	23.519	-	0.67	0.06	0.21	0.10	0.98	0.02	0.604	0.054	-5.40	0.40
Venus	0.723	-	24.687	-	0.27	0.05	9.0	3.0	0.88	0.04	0.294	0.056	-2.11	0.35
Earth	1.000	-	24.776	-	0.325	-	8.1	0.2	0.890	0.005	0.335	-	-2.20	0.02
Moon	1.000	-	22.866	-	0.012	0.003	11	3	0.84	0.04	0.095	0.025	-1.58	0.26
Mars	1.524	-	23.807	-	0.204	0.015	13.8	1.0	0.81	0.02	0.298	0.029	-1.74	0.07
Vesta	2.36	-	20.413	-	0.15	0.07	24.4	3.0	0.68	0.03	0.296	0.068	-1.24	0.12
UPB	2.7*	0.5	21*	1	0.20	0.09	22.5	7.0	0.70	0.07	0.31	0.10	-1.36	0.25
APB	2.7*	0.5	21*	1	0.17	0.04	22	4	0.71	0.04	0.295	0.048	-1.33	0.11

CMF = core mass fraction. ΣFe = fraction of planetary mass comprised by total Fe (FeO+Fe). ΔIW = Oxygen fugacity with respect to the iron-wüstite buffer, $\Delta\text{IW} = \log f\text{O}_2 - \log f\text{O}_2(\text{IW})$. References: Mercury - [*Hauck et al.*, 2013; *Namur et al.*, 2016], Venus [*BVSP*, 1981; *Helbert et al.*, 2021; *Shah et al.*, 2022; *Rodríguez-Mozos and Moya*, 2022], Earth [*Frost and McCammon*, 2008; *Palme and O'Neill*, 2014], Moon [*Sossi et al.*, 2025], Mars [*Khan et al.*, 2022, 2023], Vesta - [*Zuber et al.*, 2011; *Toplis et al.*, 2013], Ureilite Parent Body (UPB) - [*Goodrich et al.*, 2007], Angrite Parent Body (APB) - [*Longhi*, 1999; *McKibbin and O'Neill*, 2018; *Tissot et al.*, 2022]. The semi-major axes and masses of the UPB and APB are unknown. They are thought to reside (or have resided) in the asteroid belt, and to have (or have had) masses similar to that of Vesta.

Nominal ranges of 2.7 ± 0.5 AU and $10^{21 \pm 1}$ kg for semi-major axis and mass, respectively, are given here.

2.2 Chemical composition

2.2.1 Major rock-forming elements

The core/mantle ratio, is, to first order, an indicator of the relative proportions of Fe/O accreted by the planetary body [as seen for chondritic meteorites; *Urey and Craig*, 1953]. There is no requirement for planets to adhere to the chondritic range, not only due to potential chemical gradients in the solar nebula [e.g., *Larimer and Bartholomay*, 1979; *Palme*, 2000] but also owing to giant impacts [e.g., *Fegley and Cameron*, 1987; *O'Neill and Palme*, 2008]. Irrespective of the pathway via which differentiated bodies accreted, at equilibrium, the amount of oxygen that is available to oxidise metallic iron is described by;

$$\text{Fe}(\text{core}) + \frac{1}{2}\text{O}_2 = \text{FeO}(\text{mantle}), \quad (1)$$

in which FeO is dissolved in a multicomponent silicate (e.g., liquid phase), and metallic iron forms a discrete phase (including minor Ni, Co and light elements), that then constitutes the core of the body. Equation 1 represents the iron-wüstite (IW) buffer, and can be used to constrain the oxygen fugacity, $f\text{O}_2$, relative to IW, which is given by;

$$\Delta\text{IW} = \log_{10} f\text{O}_2(\text{body}) - \log_{10} f\text{O}_2(\text{IW}) = 2\log_{10} \left(\frac{a\text{FeO}}{a\text{Fe} \cdot K_{(1)}} \right) - 2\log_{10} \left(\frac{1}{K_{(1)}} \right) = 2\log_{10} \left(\frac{a\text{FeO}}{a\text{Fe}} \right), \quad (2)$$

where a refers to the activity and $K_{(1)}$ the equilibrium constant of eq. 1 [see, for example, *O'Neill and Pownceby*, 1993]. If the mantle FeO content of a given planetary body (see Table 1) is assumed to be well-mixed and to represent a quantity determined by equilibrium with the core, there is a general tendency for the $f\text{O}_2$ to increase as a function of heliocentric distance (Fig. 1a), but also with decreasing mass (Fig. 1b). The small telluric bodies in the asteroid belt define values near ΔIW -1.3, Mars has an intermediate value of ΔIW -1.7, and the Earth the most reduced, ΔIW -2.2 [see also *Wadhwa*, 2008; *Frost and McCammon*, 2008]. The Moon is displaced to higher values with respect to the

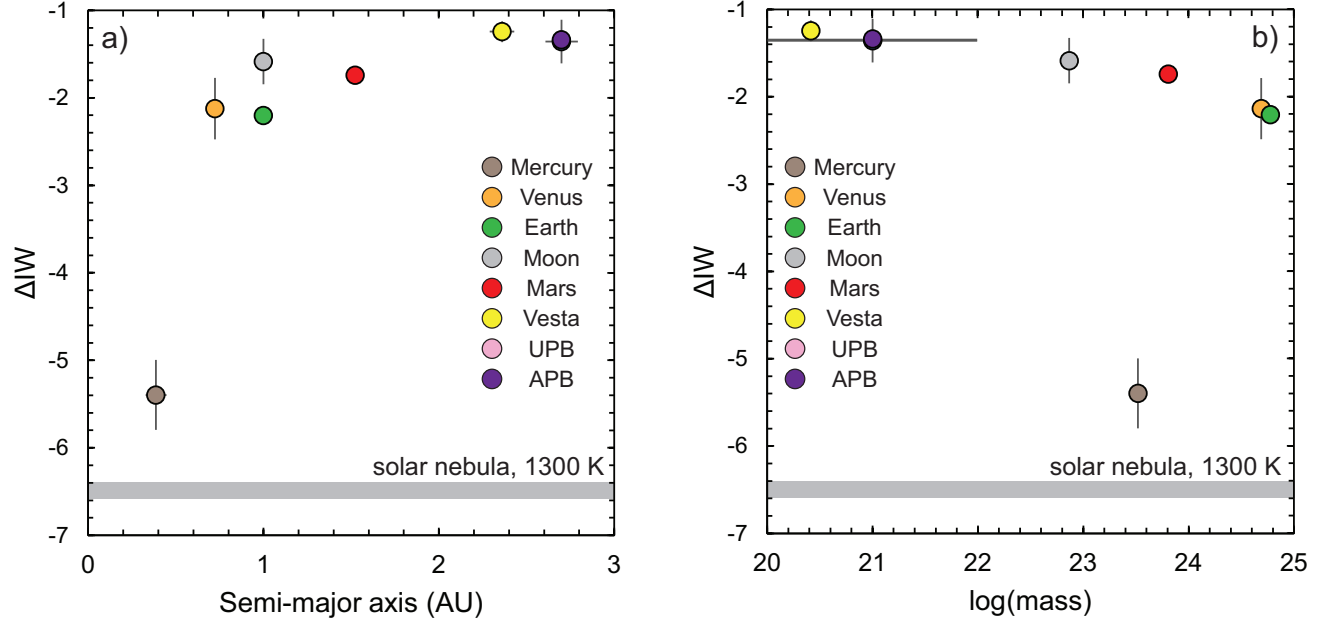


Figure 1: Oxygen fugacities, with respect to the iron-wüstite (IW) buffer [O'Neill and Pownceby, 1993] of the planets as a function of a) heliocentric distance (in AU) and b) the \log_{10} of their masses. Also shown is the fO_2 defined by a solar gas at 1300 K and 10^{-4} bar [Grossman et al., 2008]. Source data is shown in Table 1.

Earth [see O'Neill, 1991; Sossi et al., 2025], whereas Mercury has a conspicuously lower fO_2 [Namur et al., 2016]. Even so, the fO_2 inferred for core formation on Mercury is similar to that for a gas of solar composition at 1300 K, which has an H_2/H_2O ratio of 5×10^{-4} , corresponding to $\Delta IW = -6.5$ [e.g., Grossman et al., 2008]. Thus, the fO_2 s recorded by all differentiated planetary bodies, with the possible exception of Mercury, are more oxidised than that expected for equilibrium with the solar nebula.

Most bodies are consistent with an amount of total iron ($\sum Fe \sim 28 - 33$ wt. %, Table 1) that overlaps with those found in chondrites [18 - 30 wt. %, Wasson and Kallemeyn, 1988], though it should be noted that estimates for core mass fractions for the small telluric bodies are made on the assumption of a chondritic bulk composition [e.g., Toplis et al., 2013]. This notwithstanding, Mercury and the Moon are again exceptions and require roughly 60 wt. % and 10 wt. % total Fe, respectively (Table 1; Fig. 2). Comparisons of the oxygen fugacities of differentiated bodies with those of chondritic meteorites are hampered because the most primitive examples (i.e., type 3 chondrites) are a collection of unequilibrated grains and therefore the fO_2 is undefined. A relative scale of oxidation may be instead provided by the Mg# of silicates contained therein (calculated on a molar basis);

$$Mg\# = \frac{Mg}{[Mg + Fe^{2+}]} \quad (3)$$

Because Mg is lithophile and Ni is siderophile, plots of the Fe/Mg and Ni/Mg ratios of groups of bulk chondrites can be used in conjunction with eq. 1 to infer the oxygen fugacity at which their silicates formed [Larimer and Anders,

1970]. As Ni is almost entirely hosted in metal grains, the Fe/Mg ratio of the silicate fraction of a given chondrite group is recovered at Fe/Ni = 0. Carbonaceous chondrites yield higher intercepts $(\text{Fe/Mg})_0 = 0.35 \pm 0.16$ than do the ordinary chondrites $(\text{Fe/Mg})_0 = 0.16 \pm 0.03$, while that for enstatite chondrites cannot be reliably assessed from only two groups, but their constituent silicates have Fe/Mg very near 0 [see also *O'Neill and Palme, 1998*] and here we adopt 0.01 ± 0.01 . These are compared to the range of Mg#s observed among planetary mantles, as a proxy for $f\text{O}_2$, in Fig. 2.

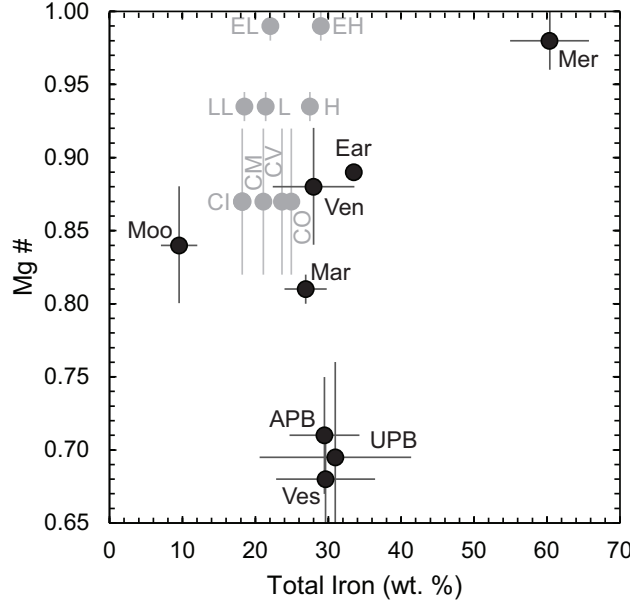


Figure 2: The Mg # of differentiated (black) and undifferentiated (grey) bodies as a function of their total iron contents. Source data is from *Wasson and Kallemeyn [1988]* for chondritic meteorites.

Chondritic meteorites occupy but a limited parameter space, down to Mg#s ~ 0.82 , within uncertainty. Strikingly, all small telluric bodies (STBs) and Mars have mantle Mg#s far below even silicate phases in carbonaceous chondrites (CI, CM, CV, CO in Fig. 2). It should be noted that chemical equilibration in the presence of S could result in $f\text{O}_2$ s higher than the IW buffer [*Bercovici et al., 2022*]. Hence, the STBs must have experienced additional oxidation relative to that observed in at least the ordinary and enstatite meteorites, and potentially also the carbonaceous chondrites, considering some cores of STBs are thought to be S-poor [*Steenstra et al., 2020*], though others are inferred to contain up to 19 wt.% S [*Hirschmann et al., 2021*]. To first order, the vertical trend in Fig. 2 implies differences in Fe/O ratios at constant total iron contents. This could not have been produced through physical, binary mixtures of metal and silicate, which would instead give rise to coupled changes in Fe/O and ΣFe , as vaguely defined by the trend passing through the Moon, Venus, Earth and Mercury. Therefore, and unlike refractory elements, there is no *a priori* reason to expect chondritic ratios (which differ even between themselves) among the major rock-forming elements (Fe, Mg, Si, O) in the terrestrial planets [see also *Yoshizaki and McDonough, 2020*].

2.2.2 Volatile elements

Unlike the major, rock-forming elements, abundances of the volatile elements vary by orders of magnitude among planetary materials. In order to derive their abundances in planetary mantles, they are typically referenced to a refractory element of similar geochemical character during partial melting of the mantle, such as La or U for the moderately volatile K, or Sr for Rb [e.g., *Halliday and Porcelli, 2001*]. Furthermore, both K and U are natural gamma-ray emitters and their abundances can thus be inferred via remote sensing [e.g., *Prettyman et al., 2006; Peplowski et al., 2012*]. Ratios of these elements for the mantles of bodies in which they are well constrained, are plotted as a function of the escape velocity of the body, $v_e = \sqrt{\frac{2GM}{r}}$, in Fig. 3.

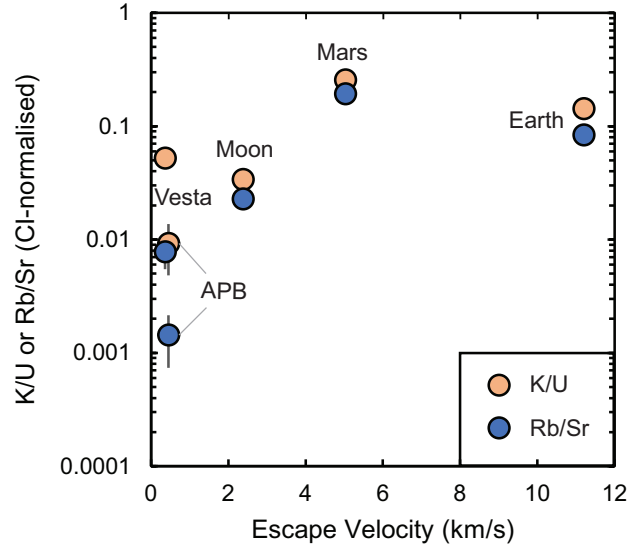


Figure 3: The K/U and Rb/Sr ratios, normalised to those in CI chondrites, of differentiated planetary bodies. References: Angrite parent body - [*Dauphas et al., 2022*], Vesta - [*Sossi et al., 2022*], Moon - [*Sossi et al., 2025*], Mars and Earth - [*Dauphas et al., 2022*].

In broad terms, the planets, Mars and Earth, are more volatile-rich, as attested to by their markedly higher K/U and Rb/Sr ratios, than are the small telluric bodies, the Moon, Vesta and the APB [see also *McCubbin and Barnes, 2019*]. In detail, however, Mars appears to have higher quantities of volatile elements than does the Earth [*Yoshizaki and McDonough, 2020; Khan et al., 2022; Dauphas et al., 2022*], a conclusion reinforced from higher S content of the Martian core [~ 10 wt. % *Khan et al., 2023*] relative to that of Earth [~ 2 wt. % S, *Dreibus and Palme, 1996; Suer et al., 2017*]. Moreover, despite the greater mass of the Moon relative to Vesta, both exhibit similar degrees of volatile depletion (Fig. 3). The exception is Mn, which is essentially undepleted with respect to Mg and CI chondrites in Vesta, but is lower, by nearly a factor of 4, in the Moon [*Sossi et al., 2025*]. This observation was used as evidence to suggest that the Moon was derived from the Earth’s mantle after core formation [*Ringwood and Kesson, 1977; Sossi et al., 2025*]. The APB remains the most highly volatile-depleted body known in the solar system, and thus defines a hierarchy from (most volatile-rich) Mars > Earth > Moon \sim Vesta > APB (least volatile-rich). Therefore, differences in the present-day escape velocities of planetary bodies (proportional to mass for constant density) may only partially

account for the observed range in their volatile element contents. Available observations do not support any trend in K/U with heliocentric distance [McCubbin and Barnes, 2019], either, though volatile abundances in Mercury and Venus remain essentially unconstrained at the resolution required to draw such conclusions. The surface of Mercury, as revealed by MESSENGER, compared to the Earth and even Mars, is rich in C [1.4 ± 0.9 wt. %, Peplowski *et al.*, 2016; Nittler *et al.*, 2018] and S [~ 2.5 wt. %, Nittler *et al.*, 2011; Weider *et al.*, 2016], which, in the canonical nebular condensation sequence, are regarded as ice-forming and moderately volatile elements, respectively. This leaves at least three possibilities; i) the Hermean surface is richer in these elements than is its interior, ii) the region of the inner disk from which Mercury formed did not experience extensive volatile depletion and/or iii) C and S did not behave in a volatile manner as expected for a typical solar nebular composition.

3 Thermal states of accreting disks

The first steps of planet formation – condensation of the first solids, aggregation of dust into planetesimals, formation of protoplanets – occur in a protoplanetary disk. The temperature of the protoplanetary disk dictates which chemical species are in the solid or gaseous forms, and therefore influences the volatile element content (both moderately and highly) of the bodies depending on where and when they form. At a given time and location, gas in the disk can be moving either outwards or inwards. The following discussion details physics applicable to typical solar-mass (G-type) stars.

3.1 Disks dominated by internal viscosity

When modelling viscous disks, following Shakura and Sunyaev [1973, 1976], it is customary to assume that the viscosity is

$$\nu = \alpha H^2 \Omega = \alpha c_s H, \quad (4)$$

where Ω is the orbital frequency at distance r from the central star, c_s is the sound speed and

$$H = \frac{c_s}{\Omega} = \sqrt{\frac{\gamma_{ad} R T r^3}{\mu G M_*}} \quad (5)$$

is the pressure scale height of the disk assumed to be vertically isothermal and in hydrostatic equilibrium, T is the temperature and γ_{ad} , R , μ are the adiabatic index-, constant- and mean molecular weight of an ideal gas, with G gravitational constant, and M_* the mass of the star. The coefficient α is a proportionality parameter with values between 0 and 1. Its precise value is not well known as it depends on the physical conditions inside the disk (degree of ionisation, coupling with the magnetic field, as discussed below in section 3.3). A viscous disk spreads radially. Over most of the radial extension of the disk, the gas is transported towards the central star at a speed $v_r = -\frac{3}{2} \frac{\nu}{r}$, but near the disk’s outer edge, the gas radial velocity becomes positive. This allows the disk to grow in radial extent over time, while transporting gas inwards (hence the name “accretion disk”) and angular momentum outwards. The radius where the radial velocity of the gas changes sign increases over time [Lynden-Bell and Pringle, 1974] (see Fig. 6); as a consequence, a fixed point in the disk (relative to the star) will see outwards-then-inwards gas motion.

The accretion rate on the star is given by:

$$\dot{M} = 2\pi r v_r \Sigma \quad (6)$$

where Σ is the surface density of the disk at distance r . The friction among different “rings” of the disk in differential rotation generates heat on the disk’s midplane at a rate

$$Q_+^{visc} = \frac{9}{4}\nu\Sigma\Omega^2 = \frac{3}{4\pi}\dot{M}\Omega^2 \quad (7)$$

The irradiation from the central star deposits heat at the disk's effective surface H_s , where it is absorbed at a rate

$$Q_+^{irr} = \frac{\phi L_*}{2\pi r^2}, \quad (8)$$

where L_* is the stellar luminosity and ϕ is the incidence angle between the H_s surface and the stellar rays. Notice that viscous heating is proportional to the accretion rate \dot{M} , hence to the product $\nu\Sigma$ while irradiation heating is independent of both. The disk cools at the H_s surface by radiating in space as a black body, at the rate

$$Q_- = 2\sigma_{SB}T_{eff}^4, \quad (9)$$

where σ_{SB} is the Stefan-Boltzmann constant and T_{eff} is the temperature of the disk at the surface H_s . The energy balance equation

$$Q_- = Q_+^{visc} + Q_+^{irr} \quad (10)$$

sets T_{eff} assuming steady state has been reached. The temperature on the midplane T is then related to T_{eff} via the equation

$$T = \left[\frac{(Q_+^{irr} + \frac{3\tau}{4}Q_+^{visc})}{Q_-} \right]^{1/4} T_{eff} \quad (11)$$

where $\tau = \kappa\Sigma$ is the optical depth of the disk and κ its opacity (see *Dullemond* [2013] for more details). These simplified analytical calculations are useful to get a general view of the structure of the disk and its dependence on physical parameters. A more precise calculation can be obtained with hydrodynamical simulations, where Q_+^{visc} is imposed on each cell of the disk (substituting Σ with ρdz , where ρ is the local density and dz the vertical extent of the cell) and Q_+^{irr} and Q_- are computed for each cell accounting for the local gas optical depth (see for instance *Bitsch et al.* [2014, 2015]).

Fig. 4 shows the radial distribution of the midplane disk temperature as a function of the stellar accretion rate. The latter is constrained by observations *Hartmann et al.* [1998] to be dependent on the age of the star-disk system, as

$$\log \dot{M} = -8 \pm 0.1 - (1.4 \pm 0.3)\log t, \quad (12)$$

where \dot{M} is measured in M_\odot/y and t is the time in Myr. The transition from a viscous-dominated to an irradiation-dominated disk is in the 5–10 au region. The calculation presented in the figure is made for a specific value of $\alpha = 5.4 \times 10^{-3}$. In the region dominated by the viscous heating the midplane temperature is proportional to $(\dot{M}^2/\alpha)^{1/5}$ [*Batygin and Morbidelli*, 2022]. Also, notice that the temperature at 1 au barely exceeds 500 K, even in the highest accretion case of $\dot{M} = 10^{-7} M_\odot/\text{y}$. We return to this in section 3.4.

3.2 Dust dynamics and disk chemistry

By looking at Fig. 4 one could naively think that, as the disk cools over time (i.e. with decreasing \dot{M}) the gas condenses increasingly volatile species and that the chemical composition of the disk in its solid and gaseous parts simply depends on the local temperature. This is not true in general because (i) the radial motion of gas towards the central star is typically faster than the rate of radial displacement of a condensation line (i.e. the disk cooling rate) and (ii)

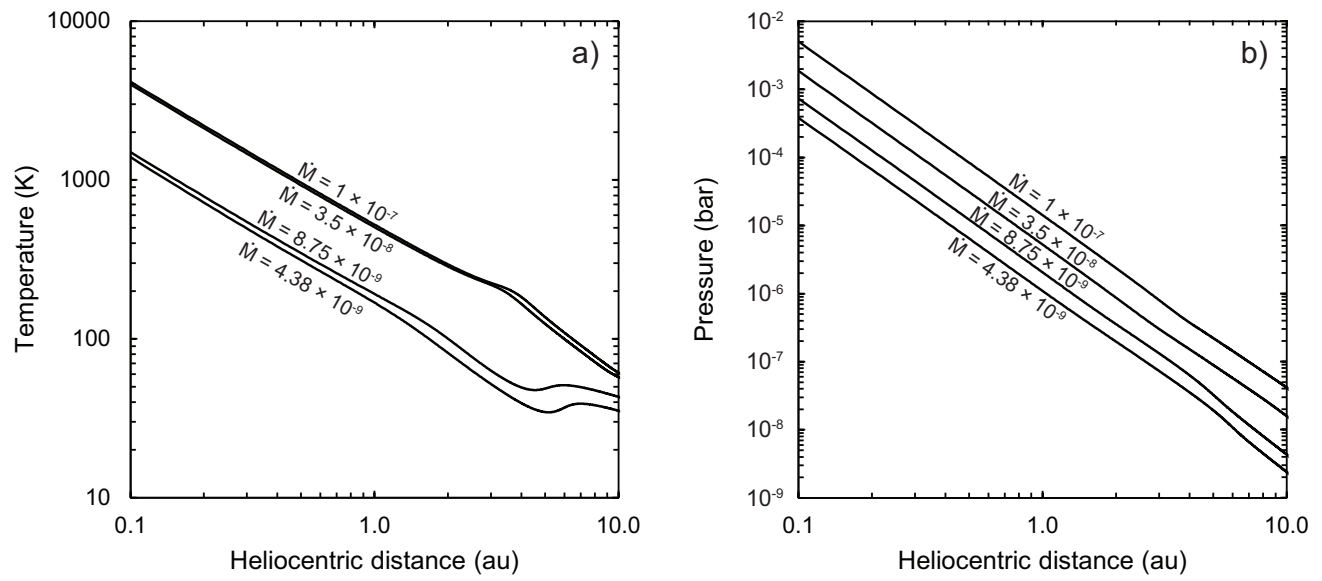


Figure 4: Radial distribution of **a)** temperature in Kelvin and **b)** pressure in bar in the midplane of the disk for different stellar mass accretion rates (\dot{M}) in solar masses/yr. Here $\alpha = 0.0054$. The temperature of the snowline (i.e., the temperature at which the reaction $\text{H}_2\text{O}(\text{g}) = \text{H}_2\text{O}(\text{s})$ proceeds to the right) is roughly between 220 – 150 K, depending on pressure. NB: Temperatures and pressures inward of 1 au are extrapolated. Constructed with data from *Bitsch et al.* [2015].

the solid material is carried by dust particles that rapidly grow to sizes at which grain dynamics partially decouples from gas dynamics [Cassen, 2001; Morbidelli *et al.*, 2015].

The consequence of (i) is that “all [gas] trajectories pass from the cool side of the [condensation] front to the hot side; no condensation occurs” [Cassen, 2001, their Fig. 13]; the only exception being in the region where the gas radial motion is outward or near the radius where the radial velocity of the gas changes sign and so is small, as illustrated schematically in Fig. 5. Condensation can occur only if there is a continuous presence of the concerned species in gaseous form just inward of the condensation front, sustained by inward radial drift of dust and sublimation.

The consequence of (ii) is that, because, typically the inward radial flow of dust is faster than the flow of gas, the evaporated species has, in general, a higher concentration, relative to hydrogen, at the locus of evaporation than in the initial stellar composition (i.e., the mean solar nebula). This is illustrated in the top panel of Fig. 5.

On the other hand, if the radial drift of the dust is blocked by a pressure maximum appearing in the disk (for instance due to the formation of a gap-opening planet, but also to the formation of rings due to magnetic effects Béthune *et al.* [2017]), there is no evaporation at the condensation front and therefore no possible recondensation during disk cooling (bottom panel, Fig. 5). Morbidelli *et al.* [2015] proposed that the blockage of the radial drift of icy grains, possibly due to the formation of Jupiter, prevented the inner disk from becoming enriched in ice relative to the solar value, even when the snowline was eventually able to pass inward of 1 au, as expected from the decay of \dot{M} over time and the related effect on the disk’s temperature (Fig. 4, eq. 12). This scenario can explain the deficit in water (and other volatile elements) in bodies formed in the inner solar system [McCubbin and Barnes, 2019, see also section 7].

One can imagine also more complicated scenarios. For instance, if the dust trap is located between the H₂O and CO condensation lines, CO(g) would be released but water vapour would not. As a result, the inner disk would have an enhanced C/O ratio relative to the original ratio in the disk and the star. Thus, depending on the location, number and efficacy of dust traps, various scenarios can arise that influence the chemistry of the disk inward of the trap(s). Predicting the actual evolution of the dust, which, in turn, depends on dust growth, radial extension of the disk, formation of pressure maxima, and so on, is currently an active field of research.

3.3 Disks dominated by magnetised winds

Up to this point, we have considered that the disk evolves and is heated under the effect of its own viscosity (cf. eq. 4). However, the origin of the disk’s viscosity is elusive. In the α -disk model expounded in section 3.1, the disk evolution timescale is given [Hartmann *et al.*, 1998; Cassen, 2006]:

$$t = \frac{r_d^2}{\nu} \quad (13)$$

where r_d is the characteristic length scale of the disk. For a typical disk extent of 100 AU at 1 Myr, as constrained by observations, ν is 10^{15} cm²/s. Molecular viscosity would be several orders of magnitude smaller, $\sim 10^6$ cm²/s [Cassen, 2006], than the viscosity considered in the simulations of Bitsch *et al.* [2015], as shown in Fig. 4. Thus, an additional source of viscosity is needed to reconcile the viscous disk model with observed disk properties. For a decade or so, it was generally believed that this additional viscosity contribution arises from turbulence within the disk, itself generated by the so-called magneto-rotational instability [Balbus and Hawley, 1998]. However, this instability occurs only if there is a strong coupling between the magnetic field and the gas, which requires a large amount of gas ionisation. Ionisation is expected to occur only at locations in the disk where it is very hot and the alkali elements have sublimed, i.e. above $\sim 1,000$ K or so [Umebayashi, 1983; Turner *et al.*, 2007; Flock *et al.*, 2017].

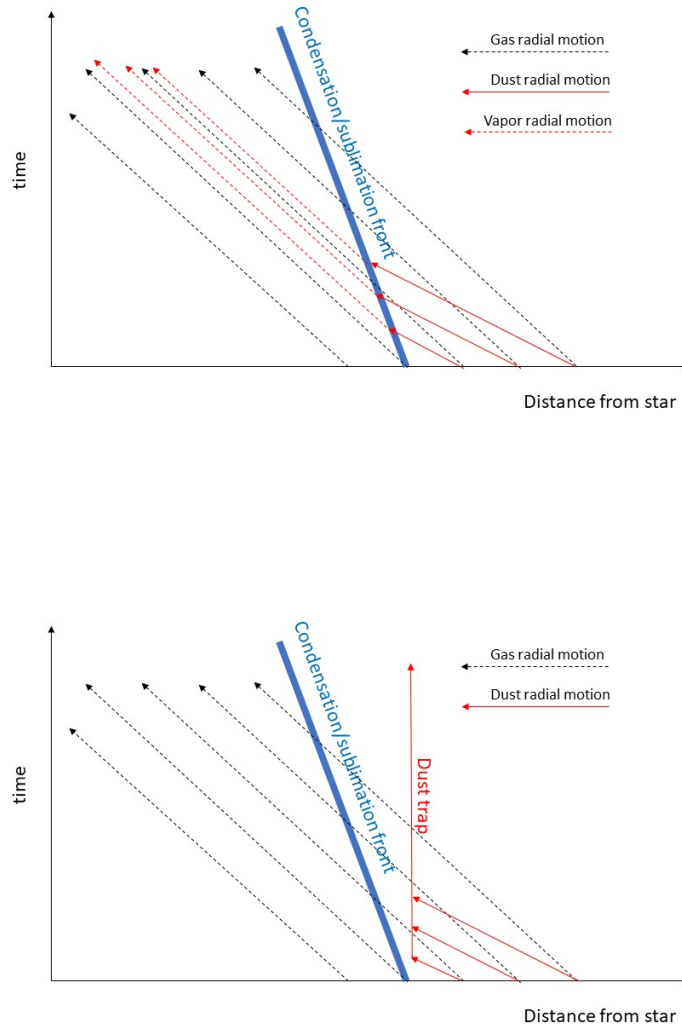


Figure 5: A schematic illustration of the radial motion of the evaporation/condensation front of gas and dust. The top panel shows the situation prevailing in a continuous disk. The radial motion of the gas (mostly hydrogen) towards the central star (dashed black arrows) is faster than the radial displacement of the evaporation/condensation front (thick blue line) that is due to disk cooling over time (cf. eq. 12). The dust moves towards the star (solid red arrows) even faster than does the gas. When crossing the evaporation front, the released vapour then moves inward (red dashed arrows) at the same speed as the gas. As a consequence, the vapour/hydrogen ratio is increased with respect to its initial ratio (i.e. the stellar abundance). Indeed, the red dashed arrows are denser in space than the black dashed lines, which indicates an enhanced density of the evaporated species. The bottom panel shows the case where the dust is trapped at some location beyond the evaporation front, due to the formation of a pressure maximum. In this case, the dust does not reach the evaporation front. Therefore, even if the disk cools, there is no further condensation possible.

A strong effective viscosity can also be generated if there are hydro-dynamical stresses in the disk. These may be the consequence of the formation of spiral waves in the disk, such as those generated when the disk is so dense so as to become nearly gravitationally unstable [Rafikov, 2016]. The accretion of gas from the molecular cloud onto the disk can also generate large effective viscosities [Kuznetsova *et al.*, 2022]. In the absence of these non-generic mechanisms, the viscosity in the disk is now expected to be small, with a value α of the order of 10^{-4} or smaller, set by weak disk instabilities such as the vertical shear instability [Stoll and Kley, 2014] or the convective overstability [Klahr and Hubbard, 2014].

If the transport of gas towards the central star were solely due to disk’s (i.e., molecular) viscosity, such low values of α would imply very massive disks (i.e. large Σ , large r_d , eq. 13) in order to account for the values of \dot{M} that are observed. But the observed disk masses do not seem as high as required [Manara *et al.*, 2016, 2018]. This suggests that another mechanism than internal viscosity is responsible for the mass transport towards the central star.

The emerging view is that, in weakly ionised disks (i.e., beyond ~ 1 au), the interaction with magnetic fields generates a magnetised wind, which ejects ions and extracts angular momentum from the disk, promoting the inward radial motion of the remaining gas [B  thune *et al.*, 2017; Lesur *et al.*, 2023]. These magnetic fields are thought to have been inherited from the molecular cloud collapse stage, and subsequently lace the protoplanetary disk [Stephens *et al.*, 2017; Fu *et al.*, 2021]. Though there is no consensus as to how such fields evolve [Lesur, 2021], stellar accretion due to magnetised winds breaks the relationship between \dot{M} , α and Σ that is typical of viscous disks (section 3.1). The main consequence, for what concerns this chapter, is that \dot{M} is no longer related to the disk’s temperature, unlike in the curves shown in Fig. 4. In absence of viscous heating, disks are solely heated by stellar irradiation and therefore are expected to be cold [Chiang and Youdin, 2010], with a snowline (~ 170 K) inwards of 1 au. Because such temperatures would have resulted in water-rich bodies in the inner solar system, which are not observed, disks clearly must have been much warmer than this, at least initially, owing to the high viscosity induced by one of the sources of stress in the disk (see above). An additional source of heating could come from the existence of a current sheet at about $3H$ [Latter *et al.*, 2010; Gressel *et al.*, 2015], but the effect is expected to be small [Mori *et al.*, 2019].

3.4 A view of disk evolution

In light of the foregoing discussion, we can envision a general view of disk evolution. Initially, when stellar collapse starts and the disk forms, the disk is small and dense. Its effective viscosity can be very high (even $\alpha = 0.01 - 0.1$) due to stresses exerted on it by the infalling gas and by the anisotropy in the gas distribution generated by conditions close to gravitational instability. The disk is therefore very hot (it is also strongly irradiated by the accretion shock at the stellar surface) and spreads very rapidly outwards [Hueso and Guillot, 2005; Pignatale *et al.*, 2017; Morbidelli *et al.*, 2022; Marschall and Morbidelli, 2023]; see Fig. 6. At this time, the disk is at its hottest; significantly higher than that of a standard accretion disk (compare Fig. 6 with Fig. 4), reaching $\sim 1,000$ K at 1 au. During the radial expansion stage, the gas flows from the hot side of the condensation fronts towards the cold side (inward to outward), whereas this is reversed in the later evolutionary stage. Thus, the outward expansion stage is likely to result in direct condensation of gas, such as that leading to the formation of primitive grains, namely calcium-aluminium-rich inclusions, CAIs and amoeboid-olivine-aggregates, AOAs [Pignatale *et al.*, 2017; Marschall and Morbidelli, 2023]. Notice that, from Fig. 6, the CAI condensation temperature is met at 0.3–0.6 au during the early stages of the disk, where these grains are thought to have formed [e.g., Gounelle *et al.*, 2001]. It should be noted that such refractory grains show evidence for having formed by very rapid cooling [within $\sim 10^{-1} - 10^{-2}$ yr, Marrocchi *et al.*, 2019], and it is therefore unlikely that the thermal regime under which they condensed is representative of gross disk structure.

When the rate of infall of new gas onto the protoplanetary disk wanes, typically after a few 10^5 yr according to observations, and once the disk has spread sufficiently in the radial direction to be far from gravitationally unstable

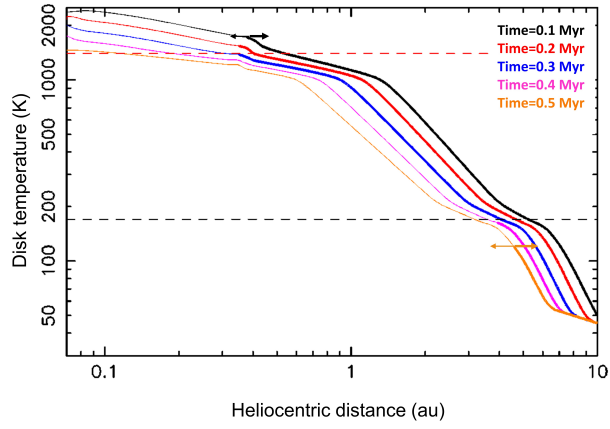


Figure 6: Temperature in the disk as a function of time during the epoch when the disk is accreting material from the envelope surrounding the forming star. The thick part of each curve shows the region where the radial velocity of the gas is positive (outward), whereas the thin part depicts the accretion part of the disk (negative radial velocity), as also indicated by the black and orange arrows. The horizontal dashed lines mark the condensation temperature of water ($T = 170$ K, black), and rocks ($T = 1400$ K, red). The intersection of these lines with the various coloured curves identify the location of the condensation/sublimation fronts of these elements as a function of time. From *Morbidelli et al.* [2022].

conditions, the viscosity rapidly drops to low values, corresponding to $\alpha < 10^{-4}$. Consequently, the temperature also drops very rapidly to approach that of a passively irradiated disk [Chiang and Youdin, 2010]. We remind readers that such a disk has a temperature of 120 K at 1 au and decaying as $1/r^{3/7}$. The transport of gas towards the central star is now dominated by the process of angular momentum removal in magnetised disk’s winds.

The relative timing of the radial spreading of the disk and subsequent accretion (inward transport) stages is unclear and the formation ages of planetary bodies are also used to inform models. For instance, Lichtenberg *et al.* [2021] assume an outflow phase that results in condensation from ~ 0.2 Myr and persists until 0.7 Myr over 1.5 – 7 au, in order to explain the inferred iron meteorite (and other achondrite parent body) formation times. The disk cools and contracts thereafter, resulting in the formation of a second generation of planetesimals from 3 – 15 au at 0.7 – 5 Myr after t_0 . By contrast, models which approximate alpha disks with a decreasing value of α lead to the contemporaneous generation of two [Morbideilli *et al.*, 2022] or three [Izidoro *et al.*, 2022] planetesimal populations from ~ 0.1 – 0.5 Myr at 1, 5 and, in Izidoro *et al.* [2022], 30 au for nominally ‘rock’, ‘ice’ and ‘soot’, respectively.

While the formation times and locations detailed above are based on the temperature in the disk (which evolves with time), they do not describe how these dust grains migrate in the disk thereafter. One should expect a generalised condensation of volatiles during the rapid cooling phase of the disk. However, if an obstacle to the radial drift of dust appears in the disk before the rapid cooling phase starts, as suggested by the preservation of the so-called isotopic dichotomy (see section 7) established during the disk’s radial expansion phase [Kruijer *et al.*, 2017; Nanne *et al.*, 2019; Brasser and Mojzsis, 2020; Morbidelli *et al.*, 2022], the inner disk may remain volatile depleted because volatile-rich dust cannot penetrate the inner disk to be accreted by the local planetesimals [Morbideilli *et al.*, 2015].

The efficiency with which particles are able to traverse any such barrier between the outer- and inner disks is inversely proportional to their size, owing to the better coupling of smaller particles to the surrounding gas [Kalyaan *et al.*, 2023; Stammer *et al.*, 2023]. Consequently, such barriers are expected to have been permeable to small grains. Empirical constraints on plausible threshold sizes were first provided by Haugbølle *et al.* [2019] on the basis of the size distribution of CAI grains in an ordinary chondrite, concluding that only grains smaller than 100 – 300 μm would be able to penetrate the barrier. This estimate was subsequently revised downward to $46 \pm 48 \mu\text{m}$ by Dunham *et al.* [2023] after having examined some 76 sections across a range of chondrites, both NC and CC. This figure overlaps with the 50 μm size distribution peak observed by Hezel *et al.* [2008] in CCs. Furthermore, the region occupied by CAIs, on average, in NC chondrites is 0.0097 ± 0.0002 %, compared to an average of 3-5 % for the most CAI-rich CCs [CK and CV, Hezel *et al.*, 2008; Ebel *et al.*, 2024]. Therefore, CAIs are up to $500\times$ less abundant in the NC-forming region than they were in the CC-forming region. Although these CAIs likely formed in close proximity to the Sun, their abundance in CCs implies they were rapidly transported to regions of the disk at which they formed, plausibly the outer solar system [Shu *et al.*, 1997; Desch *et al.*, 2010; Jacquet *et al.*, 2024]. If true and such CAIs resided in the outer solar system, then, at most, 1 % of these particles were able to (re-)enter the inner solar system. Interestingly, the NC chondritic planetesimals, which are thought to have formed in the inner solar system (parent bodies of ordinary and enstatite chondrites), are highly depleted in water [McCubbin and Barnes, 2019], but only mildly depleted in more moderately volatile elements such as Na, Zn, K [Wasson and Kallemeyn, 1988]. This may suggest that the drift of dust was blocked after that the temperature at 1-2 au had decreased below ~ 800 K, but before it decreased to 170 K.

4 Condensation of the solar nebula

4.1 Equilibrium condensation

The discussion in section 3 has highlighted the dynamic nature of the protoplanetary disk, both in time and in space. This contrasts with the ‘static’ picture afforded by the canonical cosmochemical understanding of disk evolution, which is frequently tied to nebular condensation temperatures of the elements, T_c , from a gas of fixed composition (the Sun) and pressure [10^{-4} bar; *Lodders, 2003; Wood et al., 2019*]. The utility of this volatility scale lies in its simplicity; it quantifies the temperature at which half of the mass of a given element exists in its condensed (liquid or solid) state [*Larimer, 1967*]. However, this simplicity comes at the expense of information as to the condensing mineral assemblage, and thus the temperature range over which condensation occurs. For oxides and metals, condensation stoichiometries take the general form:

$$M^{x+n}O_{\frac{x+n}{2}}(l, s) = M^xO_{\frac{x}{2}}(g) + \frac{n}{4}O_2(g) \quad (14)$$

where x is the oxidation state of the metal, M , in the gas phase and n the number of electrons exchanged. The condensation temperature of M in the above reaction can be described by [e.g., *Sossi et al., 2019; Ebel, 2023*]:

$$T = \frac{-\Delta H}{R \left(\frac{n}{4} \ln f_{O_2} + \ln P + \ln f_{vap}^{i,T} \right) - \Delta S} \quad (15)$$

where P is the total pressure, ΔH and ΔS are the enthalpy and entropy change of eq. 14, respectively, and $f_{vap}^{i,T}$ is the fraction of element i remaining in the vapour;

$$f_{vap}^{i,T} = N_{vap}^{i,T} / N_{vap}^{i,0} \quad (16)$$

where N is the number of moles of i in the gas phase at any given temperature, T , relative to the total abundance, 0. Values therefore range between $0 < f_{vap}^{i,T} < 1$. Condensation curves of the elements for any given reaction occur over a similar temperature interval, relating to the fact that gas-solid reactions have similar $\Delta G/RT$ among one another (cf. eq. 15), where ΔG is the change in Gibbs energy. Because ΔG is large relative to RT , the temperature intervals over which condensation occurs are small ($\sim 50 - 100$ K) [*Larimer, 1967*]. This is typically the case for the major elements (Mg, Fe, and Si), whose condensation reactions are *not* limited by the availability of other elements in the gas phase. However, the 50 % condensation temperature is not an intrinsic thermodynamic property of the element, but is related to the nature of the particular condensation reaction(s) for a given composition, pressure and temperature. When a single equilibrium predominates, a constant ΔH with respect to T is a good approximation, and the first derivative of eq. 15 with respect to $f_{vap}^{i,T}$ yields the condensation rate;

$$dT = \frac{\Delta H R}{f_{vap}^{i,T} \left(R \left(\frac{n}{4} \ln f_{O_2} + \ln P + \ln f_{vap}^{i,T} \right) - \Delta S \right)^2} df_{vap}^i \quad (17)$$

The functional form of eq. 17 indicates that the temperature interval is proportional to $1/[f_{vap} \ln f_{vap}^2]$, leading to decreasing condensation rates as temperature declines. These phenomena are best understood by examining the equilibrium condensation curves of the elements from a solar gas at 10^{-4} bar in Fig. 7.

It is evident that some elements condense largely into a single phase, such as Al into Al_2O_3 (corundum) or S into FeS (troilite). The behaviour of others, however, is dictated by several condensation reactions occurring at different temperatures, the most prominent example being Si, which condenses into olivine at ~ 1345 K via the reaction;

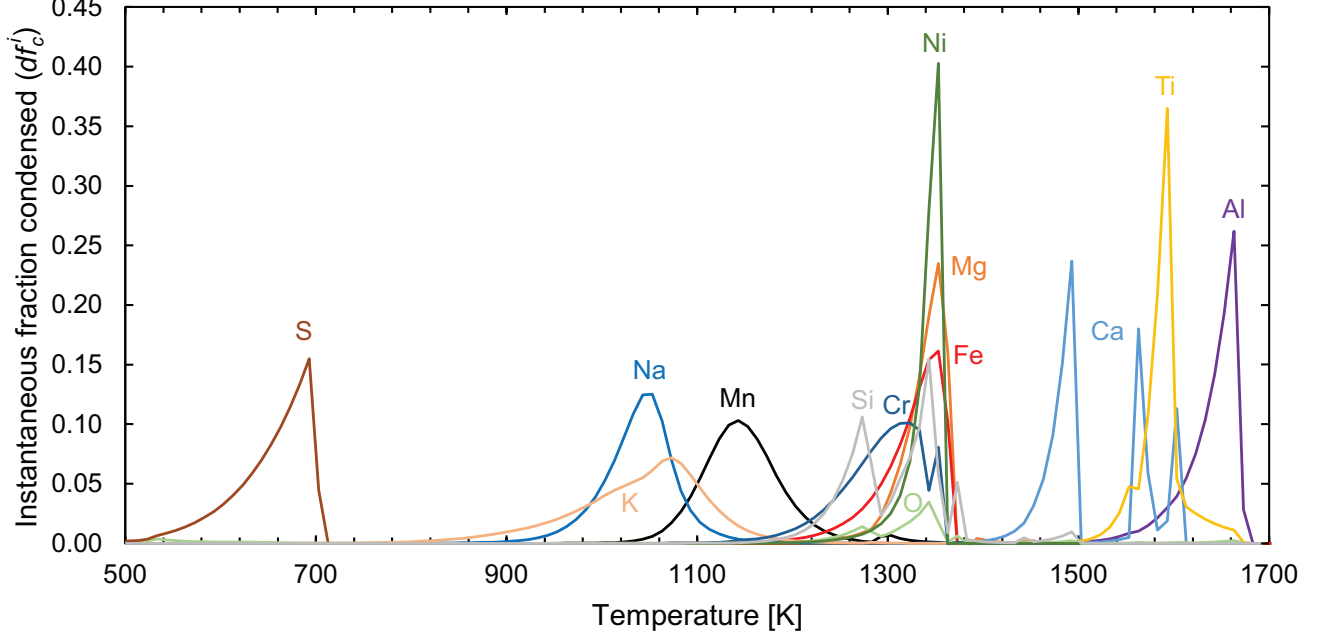
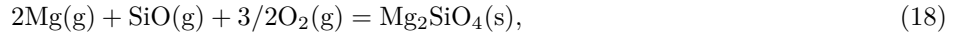


Figure 7: Condensation curves of the elements from a gas of solar composition [Lodders, 2010] at 10^{-4} bar total pressure as calculated with FactSage 8.2. It shows curves of the instantaneous fraction condensed (df_c^i) of a given element, i , as a function of temperature computed at 10 K intervals (dT). The quantity $df_c^i = f_c^{i,T_2} - f_c^{i,T_1}$, where $f_c^{i,T} = 1 - f_{vap}^{i,T}$. Elements with multiple peaks (notably Ca and Si) condense via a series of reactions. See text for details.



which then reacts with remaining SiO(g) to form orthopyroxene at ~ 1275 K, according to:



This gives rise to a T_c^{50} of roughly 1320 K, which, thermodynamically, does not correspond to any particular reaction, but rather the arithmetic average of the two major reactions. The root of the second derivative of the instantaneous fraction condensed with respect to temperature, d^2f/dT^2 gives the peak of the condensation curve, and each of the major reactions (contributing $>5\%$ to the total condensed fraction of an element, $f_c > 0.05$) are shown, together with f_c at that temperature, in Table 2.

Equation 18 proceeds through the consumption of O_2 gas. As a result, the f_{O_2} of the solar nebula decreases relative to those defined by solid-solid buffers as condensation of the major elements (notably Mg and Si) occur (Fig. 8). That of Fe (and Ni) is oxygen-neutral, as its reaction involves no electron exchange, yet would result in net increase in f_{O_2} of the gas phase by increasing its O/Fe ratio, given that f_{O_2} is proportional to $x_{\text{O}_2}P$, and the total pressure is held constant. This does not arise, however, because this effect is not sufficient to offset the decrease in f_{O_2} caused by reaction 18 occurring at the same temperature (Fig. 8). Little condensation occurs thereafter, and oxygen fugacity

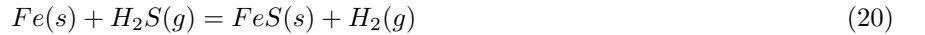
Table 2: Major condensation reactions in the solar nebula

Element	Major Gas(es)	Mineral	Mineral Name	T [K]	$f_c^{i,T}$
Al	Al > AlOH > Al ₂ O	Al ₂ O ₃	Corundum	1663	0.29
Ti	TiO >> Ti	CaTiO ₃	Perovskite	1593	0.54
Ca	Ca >> CaOH	CaAl ₁₂ O ₁₉	Hibonite	1603	0.11
Ca	Ca >> CaOH	CaAl ₄ O ₇	Grossite	1563	0.38
Ca	Ca >> CaOH	Ca ₂ Al ₂ SiO ₇	Melilite	1493	0.63
Ni	Ni >> NiH, NiS	Fe alloy	Fe alloy	1353	0.40
Mg	Mg	Mg ₂ SiO ₄	Olivine	1343	0.24
Fe	Fe	Fe alloy	Fe alloy	1340	0.35
Cr	Cr >> Cr(OH) ₂	Fe alloy	Fe alloy	1353	0.08
Cr	Cr >> Cr(OH) ₂	MgCr ₂ O ₄	Spinel	1318	0.37
Si	SiO > SiS	CaAl ₂ Si ₂ O ₈	Feldspar	1373	0.09
Si	SiO > SiS	Mg ₂ SiO ₄	Olivine	1343	0.31
Si	SiO > SiS	MgSiO ₃	Orthopyroxene	1273	0.76
O	CO ~ H ₂ O >> SiO	Mg ₂ SiO ₄	Olivine	1343	0.08
O	CO ~ H ₂ O >> SiO	MgSiO ₃	Orthopyroxene	1273	0.17
Mn	Mn	Mg ₂ SiO ₄	Olivine	1143	0.48
Na	Na > NaCl	CaAl ₂ Si ₂ O ₈	Feldspar	1048	0.49
K	K > KCl	CaAl ₂ Si ₂ O ₈	Feldspar	1083	0.40
S	H ₂ S	FeS	Troilite	693	0.20

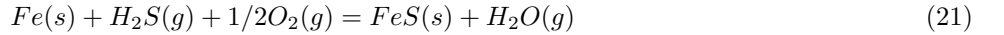
T refers to the root of the second derivative of $f_c^{i,T}$ (the fraction condensed) with respect to temperature (i.e., the peak temperature in Fig. 7).

then increases monotonically below 1250 K owing to internal gas phase reactions (chiefly $\text{H}_2\text{O} = 0.5\text{O}_2 + \text{H}_2$ and $\text{CO}_2 = 0.5\text{O}_2 + \text{CO}$) that favour the left-hand-side down-temperature. This increase in $f\text{O}_2$ relative to the iron-wüstite buffer is accelerated upon troilite precipitation (Fig. 8).

Mineralogically, oxidation is manifest in the redistribution of Fe from its host predominantly in Fe metal above ~ 700 K into increasingly fayalitic olivine and troilite (FeS) below this temperature threshold. The latter transformation is described by the well-known equilibrium [Lewis, 1972]:



which, owing to the equal number of molecules of gas in the reactants and products, is independent of total pressure. Although O is not shown in eq. 20, because the gas is in chemical equilibrium, it can equally be written;



explicitly highlighting the increasing $f\text{O}_2$ that attends FeS condensation. This reaction results in a reduction of the modal abundance of Fe metal by a factor 2, from ~ 27 % (by mass) to 13 % by 600 K, causing a concomitant increase in FeS to 15 %. The consumption of the remaining condensed Fe^0 proceeds due to increasing $f\text{O}_2$ ($f\text{H}_2\text{O}/f\text{H}_2$) below ~ 600 K [Lewis, 1972];



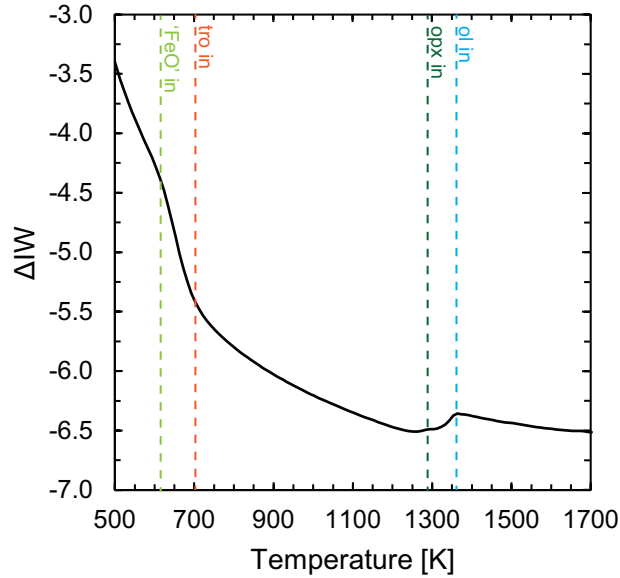
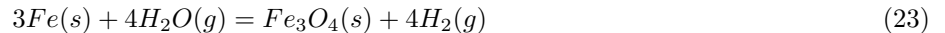


Figure 8: Evolution of oxygen fugacity (f_{O_2}) relative to the iron-wüstite buffer [O'Neill and Pownceby, 1993] during cooling and equilibrium condensation of the solar nebula gas at 10^{-4} bar. Dashed vertical lines show the onset of condensation of major phases; ol = olivine (blue), opx = orthopyroxene (dark green), tro = troilite (orange) and FeO as a component in olivine, 'FeO' (light green).

here, FeO is treated as a component in olivine, and reaction 22 tempers the f_{O_2} increase shown in Fig. 8. The Mg# (molar Mg/[Mg + Fe²⁺]) in olivine decreases from ~ 0.98 at 700 K to 0.71 by 520 K in our computation [see also Grossman, 1972], consuming almost the entirety of the remainder of the Fe⁰ by this temperature. Like eq. 20, eq. 22 is pressure-independent. Consequently, and because reactions 20 and 22 occur at similar temperatures, the abundance of S and the FeO/Fe ratio of condensed material are correlated. The small fractions of remaining metal are oxidised below ~ 380 K by:



though diffusion-controlled growth rates mean that reaction 23 is unlikely to proceed far [Hong and Fegley Jr, 1998]. At lower temperatures still (below ~ 350 K), olivine and orthopyroxene may be consumed by the condensation of H₂O to form serpentine, talc and brucite, however, the low temperatures mean that reaction kinetics are sluggish, and such minerals are unlikely to form by direct condensation [Fegley, 2000].

4.2 Non-equilibrium and fractional condensation

The idealised condensation sequence presented above is subject to the implicit assumption that all condensed material remains in contact with the same parcel of gas over its entire cooling history. This assumption characterises all such equilibrium models [e.g., Grossman, 1972; Wood and Hashimoto, 1993; Lodders, 2003; Wood et al., 2019]. For this condition to hold, it implies a static, slow-cooling solar nebula, in which the gas-solid equilibration timescale (t_{eq}) is

at least as rapid as the cooling timescale (t_{cool}). Observations of T-Tauri stars indicate mean nebular lifetimes of $\sim 1 - 10$ Myr [e.g., *Armitage et al.*, 2003]. Kinetic considerations show that $t_{eq} < t_{cool}$ is not met, even in a static disk, below ~ 400 K owing to the exponential dependence of diffusion coefficients with reciprocal temperature, putting a lower limit on the equilibrium assumption [*Fegley*, 2000].

Temperatures of 400 K represent a lower limit because the analysis in section 3 emphasises the dynamic nature of disks. Gas and dust not only move radially inward or outward depending on their location in the disk, but also vertically as condensed grains coagulate and settle to the midplane [*Cassen*, 2001]. The degree to which settling occurs depends on the relative timescales of coagulation (t_{coag}) to the dynamical evolution of the disk (t_{dyn}), with the former of the order of 10^4 yr [*Weidenschilling and Cuzzi*, 1993] and the latter $\sim 10^5$ yr (and increasing with time). Perfect equilibrium is therefore unlikely on dynamical grounds. Settling of coagulated dust to the midplane has several consequences; *i*) it reduces disk opacities, leading to enhanced cooling rates (see section 3), *ii*) it fractionates volatile from refractory elements and *iii*) it enhances the dust/gas ratio of the midplane.

The presence of CAIs in contact with chondrules and matrix is evidence of disequilibrium among chondritic meteorites; the condensation sequence illustrated in Fig. 7 predicts that refractory phases (corundum, perovskite, hibonite, melilite) are no longer present below ~ 1400 K, having been replaced by feldspar, pyroxenes and olivine [e.g., *Grossman and Larimer*, 1974]. Settling to the midplane and subsequent isolation from the evolving gas is one plausible mechanism for preserving CAIs. Alternatively, the cooling rate of the disk could have been so rapid (see section 3.2) so as to prevent equilibration of newly condensed phases down-temperature. This occurs when the reciprocal cooling rate dt^{-1} is of the order of the condensation rate, dN_i/dt , which is in turn approximated by the Hertz-Knudsen equation:

$$\frac{dN_i}{dt} = A \frac{\gamma_{cond}(p_{i,eq} - p_i)}{\sqrt{2\pi m_i k_B T}}, \quad (24)$$

where N is the number of gaseous particles of i , t is the time, A is the surface area, γ_{cond} the dimensionless condensation coefficient with value $0 < \gamma_{cond} < 1$, m is the mass of i and k_B the Boltzmann constant. This process would engender supersaturation (i.e., $p_i > p_{i,eq}$) of the remaining gas phase components that are unable to condense at their equilibrium $P - T$ conditions, thereby resulting in condensation of new solids at higher-than-equilibrium temperatures [see *Grossman et al.*, 2012]. More sluggish are reactions that involve the conversion of an already condensed phase plus a gas to a new condensed phase;

$$solid(1) + gas = solid(2). \quad (25)$$

Equation 19 is an example of one such reaction. Simple collision theory (SCT) has been developed to predict the rates of these reactions [*Fegley Jr*, 1988; *Fegley*, 2000], which scale the Hertz-Knudsen equation (eq. 24) by an additional activation energy, E_a ,

$$\frac{dN_i}{dt}_{rxn} = \frac{dN_i}{dt} e^{-\frac{E_a}{RT}}, \quad (26)$$

resulting in a linear scaling for evaporation/condensation kinetics with time. After some time, however, the growth rim of the new solid(2) becomes diffusion-limited, producing a parabolic growth curve where dN_i is proportional to \sqrt{dt} [*Fegley*, 2000]. A detailed investigation of how cooling rates affect the mineralogy of the resulting phases is underway [*Charnoz et al.*, 2025].

Chemical evidence for deviations from canonical solar nebula conditions and/or equilibrium comes from the low Mg# (0.86 ± 0.003) of olivine and pyroxene in chondrules [*Larimer and Anders*, 1970; *Huang et al.*, 1996; *O'Neill and*

Palme, 1998, Fig. 2]. For the canonical case of equilibrium condensation of a solar gas, these Mg#s would be achieved by ~ 575 K. At these temperatures, chondrules should have their full complement of S, Zn and other moderately volatile elements, which is not observed [Wasson and Kallemeyn, 1988]. Ebel and Grossman [2000] suggest high FeO contents could arise from CI-like dust enrichment in the disk (either at the midplane or globally), resulting in $f\text{O}_2$ of $\Delta\text{IW}-3.1$, $\Delta\text{IW}-1.7$, and $\Delta\text{IW}-1.2$ for dust enrichment factors of 100CE, 500CE and 1000CE, respectively. Resulting olivine Mg#s at 1200 K are 0.96, 0.8 and 0.65-0.60, respectively [Ebel and Grossman, 2000], suggesting $\sim 300 - 400\text{CE}$ dust enrichment is required. Using the FactSage model, Mokhtari and Bourdon [2025] find slightly lower Mg#, 0.90, at 1200 K and $100\times$ CI dust enrichment, implying roughly $150\times$ dust enrichment is required to achieve $\text{Mg\#} = 0.86$. Enrichment factors above ~ 100 at the midplane are difficult to obtain, however, in dynamical models of the solar nebula [Cassen, 2001]. Appealing to the accretion of ices to oxidise iron requires comparable degrees of enrichment ($\sim 250\times$) to achieve a similar $\text{H}_2\text{O}/\text{H}_2$ ratio [7.6×10^{-2} , Fegley Jr and Palme, 1985] which are, in turn, higher than thought plausible by transport of ice-rich planetesimals into the inner disk ($5-100\times$) in the α -disk-based model of Ciesla and Cuzzi [2006].

5 Mixing and differentiation during planet formation

5.1 Estimating bulk compositions

In predicting the bulk compositions of the planets, T_c is of limited use, as it is undefined for elements that do not condense to more than 50 % relative to their initial mass. This is particularly relevant in the case of O, whose abundance in the planets is much higher than its T_c (180 K) would suggest. Roughly 20 % of the total nebular O budget is condensed by 1200 K, owing to the formation of solids in which it is bound with metals, yet only a further ~ 3 % condenses by 500 K, associated with the oxidation of Fe to FeO (eq. 22). Hence, the remaining ~ 77 % condenses as $\text{H}_2\text{O}(s)$ at much lower temperatures [~ 180 K; Lodders, 2003].

Therefore, the use of nebular condensation temperatures alone is insufficient to define the bulk compositions of planetary bodies. To test the extent to which the composition of the Earth and planets can be reproduced through mixing of components formed by nebular condensation, a Gaussian distribution (eq. 27) is employed to sample the compositions of the equilibrium condensates over a range of temperatures. This model, shown to provide a sound match to the volatile element composition of the Earth [Sossi *et al.*, 2022], takes the form here:

$$N_{i,body} = \sum_T \left[\frac{N_{i,body}^T}{\sigma\sqrt{2\pi}} \exp\left(-\frac{1}{2} \left[\frac{T-T_0}{\sigma}\right]^2\right) \right] \quad (27)$$

where $N_{i,body}$ is the number of moles of element i in the mixture (planetary body), T_0 is the mean temperature of the Gaussian distribution and σ its standard deviation, and is therefore the sum across all temperatures (T) of the product of the number of moles in the body at each temperature step ($N_{i,body}^T$) and the Gaussian probability distribution calculated at T . The mole fraction is then given:

$$x_{i,body} = \frac{N_{i,body}}{\sum_i N_{i,body}} \quad (28)$$

The values of T_0 and σ are varied between ranges of 400 – 1250 K and 50 – 300 K, respectively and results shown in Fig. 9.

The Earth’s composition [BE, Fischer and McDonough, 2025] is not captured by such models; falling to higher Fe/O than any mixture of equilibrium nebular condensates. This results from both a high Fe abundance (nearly 32 %

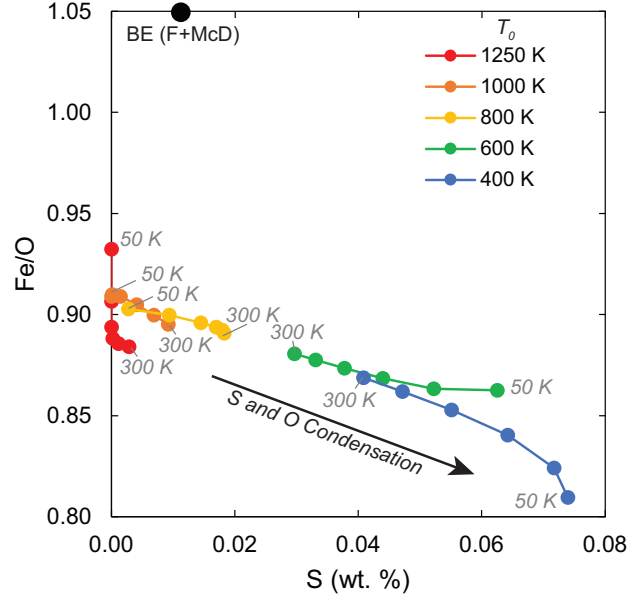


Figure 9: Modelled bulk planetary compositions emerging from mixing of equilibrium nebular condensates from a Gaussian distribution as a function of temperature at 10^{-4} bar. The coloured lines correspond to different values of T_0 (red = 1250 K, orange = 1000 K, yellow = 800 K, green = 600 K, blue = 400 K) and grey numbers denote the standard deviation of the Gaussian distribution, σ . The black point illustrates the composition of the Bulk Earth [BE, *Fischer and McDonough, 2025*].

by mass) and a low O abundance (~ 30 % by mass) in the BE compared to condensate mixtures; 27–29.5 % for Fe and 32–33 % for O. Such iron enrichment in the Earth has been cited as evidence of its ‘non-chondritic’ bulk composition [cf. *O’Neill and Palme, 2008*]. Mechanisms causing departures from chondritic compositions include, but are not limited to the physical ‘sorting’ of nebular condensates, such as the preferential incorporation of early-condensed forsterite into feedstocks for the Earth relative to later-condensing enstatite, as inferred on the basis of Si isotopes [*Dauphas et al., 2015*]. Erosion of mantle- relative to core material is another plausible process, mooted to have given rise to the Earth’s superchondritic Fe/Mg ratio [2.1 by mass, *O’Neill and Palme, 2008*]. Numerical simulations support the dynamical plausibility of collisional erosion in producing superchondritic Fe/Mg ratios [*Carter et al., 2015, 2018*]. The potential for evaporative loss at a post-nebular stage to fractionate Fe/Mg is explored in section 6.

Importantly, the Fe/O ratios and S contents of mixtures of nebular condensates are anticorrelated. This reflects the co-condensation of S, starting near 700 K at 10^{-4} bar, and additional O into the fayalite component of olivine near 550 K (eq. 22, Fig. 7). At $T_0 > 700$ K, increasing σ at constant T_0 leads to increasing S contents, whereas the opposite is true for $T_0 < 700$ K. Thus, the more volatile-rich the body, the more oxidised it is expected to be. Concretely, values of T_0 around 900 K would be required [at constant $\sigma = 225$ K, see *Sossi et al., 2022*] in order to condense quantities of S sufficient to match its estimated BE abundance [~ 1 wt. % *Fischer and McDonough, 2025*]. However, at this T_0 value, the Earth would be too enriched in moderately volatile elements (Na, K, Zn, among others)

relative to observations [which indicate T_0 for the Earth of ~ 1150 K, *Sossi et al.*, 2022]. This problem is exacerbated in the small telluric bodies; Vesta, APB and the Moon are more oxidised than the Earth (Fig. 1) yet more depleted in volatile elements (Fig. 3). Together, these considerations are grounds to reject the hypothesis that the composition of the Earth (and, by extension, those of the other terrestrial planets) reflect mixing of components produced by equilibrium condensation of a canonical solar nebula alone.

5.2 Internal differentiation

In order to translate planetary bulk compositions into those of their observable mantle and core, internal differentiation must be considered [e.g., *Ringwood*, 1966]. Core-mantle differentiation in growing planets is thought to have occurred during transient periods of (partial) melting at high pressures (several – to tens of GPa) and temperatures (>2000 K) informed by experiments and *ab-initio* simulations [e.g., *Ringwood et al.*, 1991; *Thibault and Walter*, 1995; *O'Neill et al.*, 1998; *Gessmann et al.*, 2001; *Rubie et al.*, 2004; *Wade and Wood*, 2005; *Ricolleau et al.*, 2011; *Fischer et al.*, 2015, 2020; *Suer et al.*, 2017; *Huang and Badro*, 2018; *Li et al.*, 2020; *Huang et al.*, 2021; *Blanchard et al.*, 2022].

To leverage these constraints, here we develop a model that takes as input parameters the pressure and temperature of core-mantle equilibrium, and the bulk composition of the material (section 5.1) in the system Si-Al-Ca-Mg-Fe-Ni-O, which, together, comprise ~ 98.5 wt. % of the Earth [*Palme and O'Neill*, 2014]. This approach was first formalised by *Rubie et al.* [2004] and expanded by *Frost et al.* [2008] and *Rubie et al.* [2011]. Our treatment is formally incomplete as it neglects other, minor core-forming elements, notably Co, S, C and H, which, together, likely comprise ~ 2.5 wt.% of the core [*Hirose et al.*, 2021]. The partitioning of the alloying elements - Ni, O and Si - are described according to eq. (29) and in Table 3 over a range from 1 bar to 100 GPa at a temperature corresponding to the peridotite liquidus of *Andrault et al.* [2011]. Three compositions are taken from mixtures of nebular condensates at different T_0 and σ values from section 5.1, and the fourth is the Bulk Earth composition (Table 4).

Table 3: Parameters for metal-silicate partitioning exchange reactions.

	$\log K$	$\ln \gamma$	n	Reference
Si	0.52-13000/ T	0.5-5500/ T	4	S13, F15
Fe	-	0	2	Ri11
O	0.7-5000/ T +(22 P)/ T	0	-	Ri11, S13, F15
Ni	1.06+1553/ T -(98 P)/ T	0	2	Ru11

Ri11 = *Ricolleau et al.* [2011], Ru11 = *Rubie et al.* [2011], S13 = *Siebert et al.* [2013], F15 = *Fischer et al.* [2015]

As iron is the dominant element in planetary cores, and is typically present at several weight percent in the coexisting mantles (cf. Table 1), element partitioning is described by an exchange coefficient with Fe [e.g., *Wade and Wood*, 2005],

$$\frac{n}{2}Fe + MO_{\frac{n}{2}} = \frac{n}{2}FeO + M \quad (29)$$

which circumvents the definition of fO_2 but requires that n , the number of electrons transferred in the reaction, be known. The abundances of Ni, O and Si in the mantle are allowed to vary in order to satisfy the equation;

$$x(M)_{core} = \frac{K_{(29)}(aFe)^{\frac{n}{2}}aMO_{\frac{n}{2}}}{\gamma M(aFeO)^{\frac{n}{2}}} = \frac{(xM)_T - (xM)_{mantle}(1 - CMF)}{CMF} \quad (30)$$

where the subscript T is the total mass and CMF the core mass fraction. The values of $(xM)_{mantle}$ and CMF are iterated until the left-hand side is equivalent to the right-hand side. The iteration is performed with the additional constraints that;

$$x(O)_{mantle} = 1.5[x(Al)_{mantle}] + x(Ca)_{mantle} + x(Mg)_{mantle} + 2[x(Si)_{mantle}] + x(Fe)_{mantle} + x(Ni)_{mantle} \quad (31)$$

and

$$\sum_M x(M)_{mantle} = 1 \quad (32)$$

The remaining elements, Al, Ca and Mg, are assumed to be perfectly lithophile, hence their mantle abundances are given analytically by $C_{mantle} = C_T/(1 - CMF)$. This leaves *four unknowns* - $x(Fe)_{mantle}$, $x(Ni)_{mantle}$, $x(Si)_{mantle}$ and CMF , which are soluble with four constraints (eq. 30 for $M = Ni, Si$ and O and eq. 32).

Table 4: Modelled bulk compositions using the parameters for eq. 27 as described in section 5.1. All elements in wt. fraction. Bulk Earth from *Fischer and McDonough* [2025].

	Fully reduced	Bulk Earth	Intermediate	Fully oxidised
Parameters				
T_0	1250	-	600	400
σ	50	-	50	50
Elements				
Al	0.0166	0.0159	0.0141	0.0138
Ca	0.0174	0.0167	0.0148	0.0145
Mg	0.1668	0.1578	0.1524	0.1491
Si	0.1636	0.1567	0.1721	0.1684
Fe	0.2971	0.3268	0.2913	0.2850
O	0.3187	0.3073	0.3377	0.3520
Ni	0.0198	0.0187	0.0176	0.0172
Fe/O	0.932	1.063	0.863	0.809

As first proposed by *Javoy* [1995], even for precursor materials that contain all Fe as Fe^0 (i.e., in reduced form), the process of core-mantle equilibration at increasing $P - T$ results in progressively higher FeO contents in the mantle (Fig. 10). This behaviour arises due to the competition between the incorporation of Si in the core via;

$$SiO_2(mantle) + 2Fe(core) = Si(core) + 2FeO(mantle) \quad (33)$$

and that of O by;

$$FeO(mantle) = Fe(core) + O(core) \quad (34)$$

Both reactions are self-limiting [cf. *O'Neill et al.*, 1998]: FeO contents tend to converge as $P - T$ increase along the peridotite liquidus, which reflects the tendency for both Si and O to partition into the core as $P - T$ increases (Fig. 10a). At a given $P - T$, whether Si or O predominantly enters the core depends on the Fe/O ratio. For initially high Fe/O, the low a_{FeO} promotes Si dissolution in the core, which, in turn, engenders an increase in a_{FeO} via eq. 33; a negative feedback that results in a keeling over of mantle FeO content (red and black curves, Fig. 10). Because mass is conserved, any change in mantle FeO content must be compensated for by a concomitant adjustment in the core mass fraction (Fig. 10b). At low Fe/O, the CMF increases because both Fe and O enter the core (eq. 34). Conversely, the CMF decreases when eq. 33 prevails over eq. 34, as the reduction of 1 mole of SiO_2 to Si in turn oxidises 2 moles of

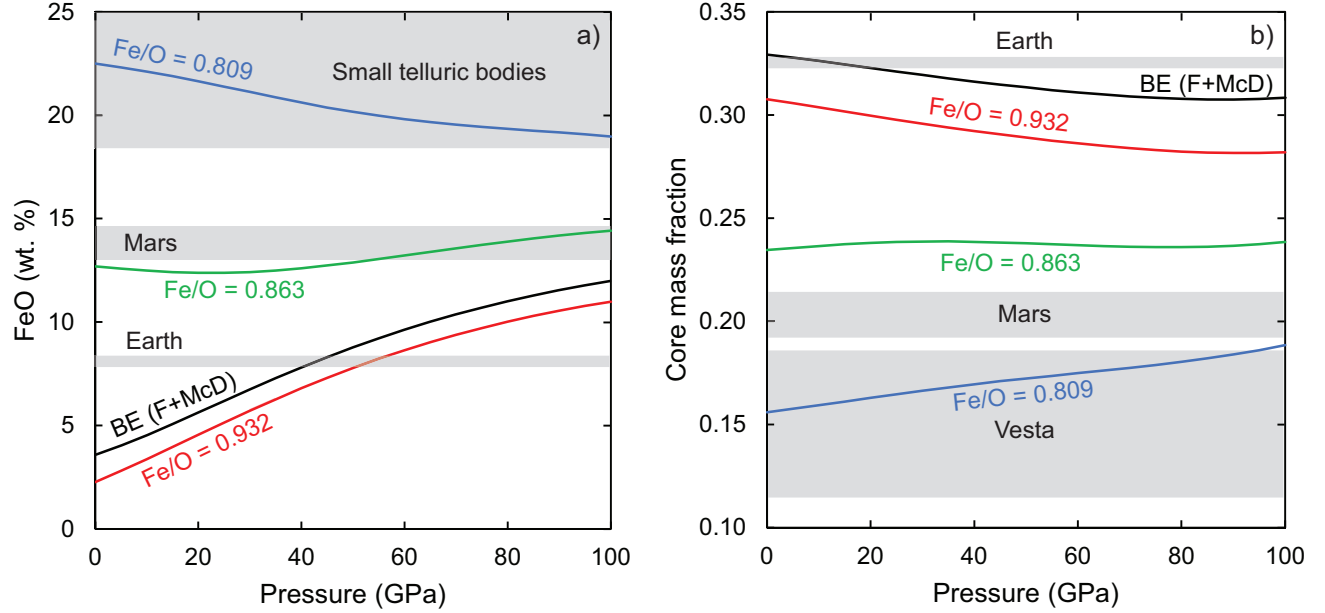


Figure 10: The equilibrium a) FeO content in the mantle and b) core mass fraction of synthetic rocky planets calculated along the peridotite liquidus of *Andraut et al.* [2011] plotted as a function of pressure for different bulk compositions with Fe/O (by weight) ratios ranging from fully reduced (all Fe as Fe^0), 0.932 (red), 0.863 (green) and 0.809 (blue, fully oxidised, all Fe as FeO). These bulk compositions are derived from the model presented in section 5.1 at different T_0 and σ values. The black curve has Fe/O = 1.063 and is the Bulk Earth composition of *Fischer and McDonough* [2025]. All compositions are shown in Table 4. Observed FeO contents and core mass fractions of selected telluric bodies are shown as grey horizontal bars (see Table 1 for data sources).

Fe to FeO. A corollary of the model is that the $f\text{O}_2$ of core formation changes as a function of P and T at *constant* bulk composition [see also *Rubie et al.*, 2011, their Fig. 2].

For single-stage core formation with the BE composition, we find FeO = 8.33 wt. % and Ni = 1881 ppm in the mantle with a CMF of 0.315 at $P = 40$ GPa and $T = 3150$ K. These values compare well with the 8.1 ± 0.2 wt. % FeO and 1860 ± 93 ppm Ni in the BSE [*Palme and O'Neill*, 2014] and a CMF of ~ 0.325 (Table 1). At these conditions, our model predicts Si = 3.6 wt. % and O = 1.2 wt. % in the core, consistent with other estimates [*O'Neill and Palme*, 1998; *Badro et al.*, 2014; *Dauphas et al.*, 2015; *Hirose et al.*, 2021]. That there is no single composition that fits the observed CMF and FeO at a given pressure should not be taken as evidence against single-stage core formation. At 40 GPa, this is likely remedied by the additional S (~ 2 wt. %), Co + P + Cr (~ 1.5 wt. %) in the core, which are not included in our model. Addition of these quantities to the CMF value of 0.315 at 40 GPa would result in the observed CMF of 0.325.

Such estimates also match the 30–50 GPa and 3000 K inferred from D_{Ni} and D_{Co} [*Thibault and Walter*, 1995; *Li and Agee*, 1996; *Bouhifd and Jephcoat*, 2003; *Wade and Wood*, 2005; *Kegler et al.*, 2008]. *Wade and Wood* [2005]

and *Rubie et al.* [2011, 2015] emphasised that, although homogeneous accretion models are readily able to satisfy the observed FeO, Ni and Co abundances in Earth’s mantle (as also shown here), they lead to elevated mantle Cr and V contents, which would instead require temperatures ~ 650 K higher. A notable caveat to their models lies in the implicit assumption that the extant families of chondrites *de facto* formed Earth. Should this assumption be relaxed, it remains to be seen whether heterogeneous accretion is required from a chemical standpoint. Moreover, *Siebert et al.* [2013] demonstrated V and Cr abundances could be fit, independent of whether accretion were homogeneous or heterogeneous with respect to composition, at (mean) pressures of equilibrium between 40 and 60 GPa, by virtue of the negative interaction parameters between Cr-O and V-O in iron-rich alloys. In either case, as is evident from Fig. 10 and highlighted by *Rubie et al.* [2015], the composition of Earth-forming material would need to have been initially somewhat reducing ($\text{Fe/O} > 0.9$) and high in total Fe (~ 32 wt. %; Table 4), as lower Fe/O ratios lead to mantle FeO contents that are too high relative to that observed (8.1 ± 0.02 wt. %; Table 1).

On the other hand, small telluric bodies have mantle FeO contents and core mass fractions (Table 1) that appear to require oxidised starting materials ($\text{Fe/O} < 0.86$; Fig. 10) because the low-pressure (< 5 GPa) core formation that must have occurred on these bodies would have led to temperatures insufficient [e.g., *Cartier et al.*, 2024], for self-oxidation to operate to the extent to reach the ~ 20 wt. % FeO observed *via* eq. 33 in their mantles. Mantle FeO contents inferred for the silicate mantles of iron meteorite parent bodies are almost invariably high, with all but the IIABs lying between 10–25 wt. % [*Grewal et al.*, 2024]. Rather, the volatile-poor nature of STBs, such as Vesta and the angrite parent body [e.g., *O’Neill and Palme*, 2008] together with the wide range of volatile contents in iron meteorites [*Scott and Wasson*, 1975; *Hirschmann et al.*, 2021] at near constant mantle FeO [*Grewal et al.*, 2024] indicates that the relationship between $f\text{O}_2$ and volatile element content expected for nebular condensation (Figs. 8, 9) decoupled during the formation of STBs. Finally, even at the lowest Fe/O ratios considered here, FeO contents relevant to Mercury’s mantle [0.2 ± 0.1 wt. % *Namur et al.*, 2016; *Nittler et al.*, 2018, Table 1] are not obtained, suggesting it accreted material more reduced and with higher metal/silicate ratios than that produced through equilibrium condensation and/or contains significant S or C that are not considered in this model.

6 Physicochemical conditions of volatile depletion

One possible explanation for the divergence in the compositions of the terrestrial planets and STBs relative to chondrites is that they (or their components) underwent chemical fractionation under conditions that differed from those set by the nebular gas [e.g., *O’Neill and Palme*, 2008].

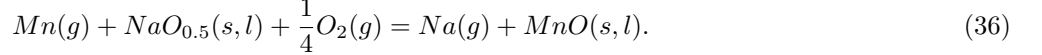
6.1 Chemical fractionation

Here we examine the *relative* fractionation between two volatile elements, $M1$ and $M2$, such that the physical mechanism by which the two elements were lost cancels from the operation and their relative fractionation is dependent on the thermodynamics of the presumed vaporisation reaction alone.

For most metals, vaporisation reactions are simple because one condensed component (e.g., MnO) and one gas species (e.g., Mn) predominate over a range of planetary- and nebular conditions [Table 2, *O’Neill*, 1991; *Sossi et al.*, 2019]. When comparing the fraction of an element vaporised ($fM1$) relative to that of a second comparator element ($fM2$), the total pressure of the system cancels, as does the total budget of the element in the system, to yield [*Sossi et al.*, 2025]:

$$\frac{f_{M1}^{vap}}{(1 - f_{M1}^{vap})} = \frac{f_{M2}^{vap}}{(1 - f_{M2}^{vap})} \left(\frac{\gamma_{M1}}{\gamma_{M2}} \right) (fO_2)^{\frac{\Delta n_{M2-M1}}{4}} \exp \left(\frac{(\Delta G_{M2}^o - \Delta G_{M1}^o)}{RT} \right), \quad (35)$$

where $(\Delta G_{M2}^o - \Delta G_{M1}^o)$ relates to the standard state free energy of the exchange reaction between the pure components vapour and condensed phase(s), such as



Because relative entropy changes for gas-liquid or gas-solid reactions are dominated by the (ideal) gas, the quantity $(\Delta G_{M2}^o - \Delta G_{M1}^o)$ is nearly independent of temperature, and exchange reactions become more discriminating (i.e., larger fractionation of $M1$ from $M2$) proportional to $\exp(1/T)$. While the free energy change $(\Delta G_{M2}^o - \Delta G_{M1}^o)$ is readily tabulated from thermodynamic databases (e.g. JANAF), the activity coefficients for many components in silicate melts are uncertain [see *Sossi and Fegley, 2018; Fegley et al., 2023*]. However, divalent metal oxides mix near-ideally in silicate liquids [*O'Neill and Eggins, 2002; Wood and Wade, 2013*], while activity coefficients (γ) for the alkali metal oxides are typically very small but relatively well characterised [*Charles, 1967; Mathieu et al., 2011; Sossi et al., 2019*]. Here, measurements of activity coefficients at a given temperature are extrapolated according to:

$$\frac{\ln \gamma}{\ln \gamma_{ref}} = \frac{T_{ref}}{T}, \quad (37)$$

where γ tends to 1 at infinite temperature. Values of γ_{ref} and T_{ref} are given in Table 5.

Table 5: Thermodynamic properties of evaporation reactions for selected moderately volatile elements of the form eq. 14.

	ΔH^o (kJ/mol)	ΔS^o (kJ/mol.K)	n	γ_{ref}^*	Source
Li	419.0	0.141	1	0.2	[<i>Sossi et al., 2019</i>]
K	236.1	0.122	1	7.3×10^{-5}	[<i>Sossi et al., 2019; Wolf et al., 2023</i>]
Na	267.0	0.121	1	5.0×10^{-4}	[<i>Sossi et al., 2019; Wolf et al., 2023</i>]
Mn	606.3	0.173	2	1	[<i>Kohn and Schofield, 1994</i>]
Mg	666.4	0.186	2	0.20	[<i>Wolf et al., 2023</i>]

* γ_{ref} calculated for the oxide in silicate liquid at a reference temperature of 1673 K.

For a canonical solar nebula gas, the fO_2 is roughly $\Delta IW-6$ during the condensation of most rock-forming elements (Fig. 8). The fO_2 during melting and vaporisation/condensation on planets *after* the dispersal of the nebular gas, reflects the composition of the evaporating/condensing material [e.g., *Visscher and Fegley, 2013*]. The FeO contents of small telluric bodies and oxybarometry of basaltic achondrites imply oxygen fugacities near $\Delta IW-1$ [Fig. 1, Table 1, *Wadhwa, 2008*].

The change in the Mn/Na (Fig. 11a) and K/Li (Fig. 11b) ratios of evaporation residues/partial condensates are computed as a function of the Mn/Mg ratio using eq. 35. The Mn/Na ratio is not only sensitive to fO_2 [*O'Neill and Palme, 2008*], but also to temperature at constant relative fO_2 . For 25 % Mn loss, 70 %, 89 % and 98.5 % of Na is lost at 2500 K, 2000 K and 1500 K, respectively. Therefore, at higher temperatures, the fraction of Na lost approaches that of the Mn lost. That is, evaporation exchange reactions (eq. 35) become less discriminating. Under nebular conditions (1100 K, $\Delta IW-6$), the Na loss is nearly identical to the 1500 K, $\Delta IW-1$ case (98.6 % lost), but the resulting K/Li is 10-fold lower (compare blue and purple curves). The APB has lost ~ 50 % of its Mn, and has Mn/Na of ~ 30 , achievable for single-stage evaporation at $\Delta IW-1$ and 1500 K; conditions also consistent with its K/Li.

By contrast, the Mn/Na and Mn/Mg range of chondrites is explained by mixtures of a volatile-depleted component and CI chondrites (thin black line, Fig. 11a), equivalent to chondrules (volatile-poor) and matrix (volatile-rich) [e.g., Alexander, 2019; Hellmann *et al.*, 2020].

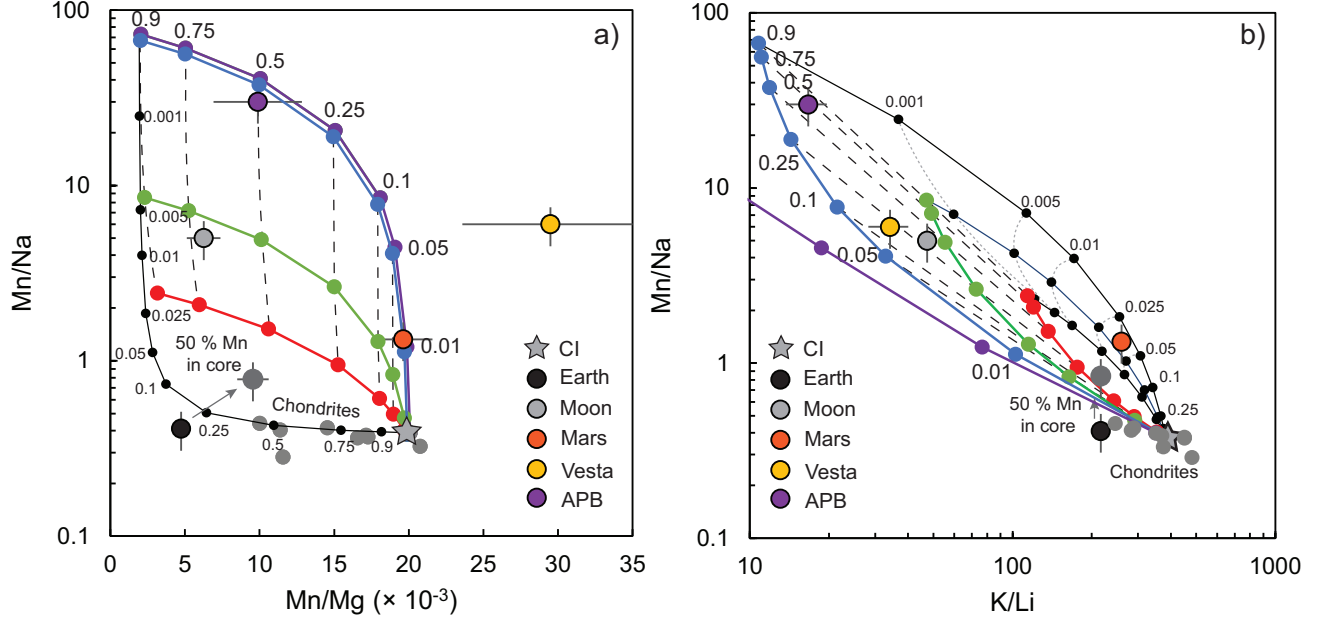


Figure 11: **a)** Mn/Na vs. Mn/Mg and **b)** Mn/Na vs. K/Li ratios among planetary bodies. The coloured curves denote the evolution of the composition of an evaporation residue calculated using eq. 35 at 1100 K (purple), 1500 K (blue), 2000 K (green) and 2500 K (red) at a fixed relative oxygen fugacity ($\Delta IW-1$, except for 1100 K, which was calculated at $\Delta IW-6$, see text), with numbers denoting the fraction of Mn loss undergone by the body. The black dashed lines connect equal degrees of Mn loss at different temperatures. The solid black curves trace a binary mixture of a volatile-depleted end-member with 90 % Mn loss and a CI-like end-member. The small numbers denote the mass fraction of CI in the mixture. On a), only the volatile-depleted end-member at 1500 K is shown due to clarity, whereas in b) the end-members are taken at the three temperatures, and the dotted grey lines connect equal fractions of CI material. The grey point gives the composition of the Earth assuming 50 % of its Mn budget resides in the core [see Siebert *et al.*, 2018]. The grey field denotes the compositional range of chondrites [Wasson and Kallemeyn, 1988; Siebert *et al.*, 2018].

The Earth has Mn/Na – Mn/Mg ratios lower than for any chondrite, its Mn/Na being too low to have been set by evaporation alone. The degree of Na depletion (~ 80 % lost) in the Earth can be used to infer the maximum permitted Mn loss by volatility alone. Roughly 36 % Mn would have been lost at 2500 K, decreasing to 2% for 1500 K or in the solar nebula. This implies between 1/2- to 2/3rds of the Earth’s Mn budget is in the core [see also Drake *et al.*, 1989; Ringwood *et al.*, 1991; Siebert *et al.*, 2018]; a similar result arises when assuming Li is entirely lithophile and is as volatile as Mn.

Compositions of STBs can be reproduced by vapour loss at a single set of temperature- $f\text{O}_2$, favouring relatively ‘high’ temperatures of about 1400 – 1800 K and relatively high $f\text{O}_2$ at $\Delta\text{IW-1}$ compared to conditions in the solar nebula. Vesta is a possible exception (Fig. 11a), perhaps estimates for its mantle Mg content are too low. The fact that the elemental fractionations observed differ empirically from those of chondrites indicates distinct processes were responsible in setting their bulk compositions; that is, evaporation (either in a single-stage or an average of multiple events) for STBs rather than mixing among components as is relevant for chondrites [Alexander, 2019]. This result, coupled with the ancient (< 5 Myr after CAIs) volatile depletion ages implied by the low $^{87}\text{Sr}/^{86}\text{Sr}_i$ [Hans *et al.*, 2013] leads to the conclusion that there must have been localised, ‘oxidised’ domains at the loci of planetesimal formation, even in the presence of the nebular gas.

On the other hand, the compositions of Mars and Earth (see also Section 6.3.2 for Earth) cannot be reconciled with volatile loss at any given temperature. This is because the temperature inferred from Fig. 11a differs from that deduced from 11b. Implicit in these models is the absence of the major volatiles, such as H, C and S, which may modify the stable gas species considered in equations such as eq. 36, that assume monatomic gases. Thermodynamic models indicate the stability of hydroxide- and sulfide-bearing metallic species, in particular [Fegley *et al.*, 2016; Ivanov *et al.*, 2022], yet a systematic investigation of how such differences influence the extent of volatile loss are yet to be undertaken. Nevertheless, within the framework explored here, mixing between volatile-depleted and volatile-rich end-members is required. It is also clear from Fig. 11, however, that these end-members cannot have been identical for Earth and Mars. These observations suggest that more complex, multi-component mixtures of volatile-poor and volatile-rich materials are likely needed to account for the compositions of the Earth and Mars.

6.2 Isotopic fractionation

Partitioning of an element between two phases during cosmo-/geochemical processes is often accompanied by fractionation of its isotopes. The estimated mantle isotopic compositions of planetary objects are determined via analyses of (ultra-)mafic rocks. On Earth, this typically involves peridotites [e.g., Sossi *et al.*, 2016; Savage *et al.*, 2015], or, for (highly) incompatible elements, basalts/komatiites [e.g., Dauphas *et al.*, 2010; Hibbert *et al.*, 2012; Jerram *et al.*, 2020]. For other planetary bodies, we are limited to basaltic samples, as there are no mantle samples. Consequently, particularly for achondrites, the limited number of samples [cf. the angrite parent body, Keil, 2012], and their genetic relationship with their source [cf. geochemical signatures in Martian shergottites, Borg *et al.*, 2002] introduces uncertainty into the assignment of the measured isotopic signature to that of the body. Nonetheless, isotopic bulk compositions determined in this manner are compiled in Table 6.

6.2.1 The major elements Mg, Si and Fe

The estimated Mg, Si and Fe isotope ratios of bulk, differentiated planetary bodies are similar to- or higher than those of the (averages of) carbonaceous, ordinary and enstatite chondrites (Fig. 12a,b; Table 6). Taking hydrothermal alteration for type 1 and 2 carbonaceous chondrites into account [Young *et al.*, 1999; Hin *et al.*, 2017], estimated ratios of Mg, Si and Fe isotopes are higher in the BSE than they are in chondrites. The same applies to the Moon [e.g., Klaver *et al.*, 2024; Armutage *et al.*, 2012; Sossi *et al.*, 2016], whose isotopic composition is indistinguishable from that of the Earth for these elements. Vesta (as estimated largely by eucrites) and Mars (via lherzolitic shergottites), on the other hand, have Fe and Si isotope ratios that overlap with carbonaceous and ordinary chondrites [though heavier than ECs; Fig. 12, Dauphas *et al.*, 2015]. Although these bodies may appear heavier in $\delta^{26/24}\text{Mg}$ (light grey squares) the current estimates should be corrected downward by ~ 0.04 to account for the effect of silicate differentiation [Liu *et al.*, 2022, 2023], which also renders their values similar to chondrites [see also Young *et al.*, 2019, black symbols in Fig 12a].

Table 6: Estimated mean values of the mass-dependent, stable, isotopic compositions of planetary bodies. All values expressed in per mille deviations from the listed standard.

	APB	EPB	Moon	Mars	Earth	CC	OC	EC	References
$\delta^{7/6}\text{Li}_{\text{L-SVEC}}$		3.7	3.8	4.4	3.5	3.2	2.7	1.9	1-3
95% c.i.		0.1	0.8	1.6	0.5	0.6	0.4	0.6	
$\delta^{25/24}\text{Mg}_{\text{DSM-3}}$	-0.079	-0.114	-0.130	-0.113	-0.121	-0.140		-0.134	4-6
95% c.i.	0.010	0.008	0.010	0.006	0.003	0.010		0.004	
$\delta^{30/28}\text{Si}_{\text{NBS-28}}$	-0.21	-0.42	-0.29	-0.48	-0.30	-0.47		-0.69	7,8
95% c.i.	0.03	0.03	0.08	0.03	0.03	0.03		0.05	
$\delta^{41/39}\text{K}_{\text{SRM3141a}}$	-1.70	0.41	-0.04	-0.30	-0.42	-0.25	-0.78	-0.19	9-17
95% c.i.		0.08	0.06	0.03	0.01	0.14	0.34*	0.39*	
$\delta^{53/52}\text{Cr}_{\text{SRM979}}$		-0.220	-0.216	-0.17	-0.124	-0.128	-0.102	-0.050	18-22
95% c.i.		0.030	0.020	0.08*	0.030	0.011	0.006	0.006	
$\delta^{57/54}\text{Fe}_{\text{IRMM014}}$	0.190	0.010	0.08	-0.010	0.050	-0.010			23,24
95% c.i.	0.020	0.010	0.03	0.020	0.010	0.010			
$\delta^{65/63}\text{Cu}_{\text{JMC-Lyon}}$		0.5	0.50		0.70	-0.7	-0.15	-0.25	25-27
95% c.i.		0.5**	0.10		0.010	1.3*	0.5*	0.08	
$\delta^{66/64}\text{Zn}_{\text{JMC-Lyon}}$		1.1	1.39	0.237	0.170	0.36	0.01	0.23	28-35
95% c.i.		2.2**	0.12	0.030	0.011	0.08	0.32	0.07	
$\delta^{71/69}\text{Ga}_{\text{IPGP}}$			0.14		0.000	-0.15	-0.6	-0.23	36-38
95% c.i.					0.016	0.11	0.8*	0.10	
$\delta^{87/85}\text{Rb}_{\text{SRM984}}$	-1.2	1.0	0.03	0.10	-0.13	0.11	-0.12	0.02	39-42
95% c.i.		1.4	0.03	0.03	0.06	0.10	0.20	0.27	

*Uncertainty quoted as 2s instead of 95 percent confidence interval as the data in literature do not pass Wilk's test for a normal distribution around a single population mean.

**Uncertainty quoted as 2s instead of 95 percent confidence interval because of the potential presence of a (unquantifiable) systematic uncertainty (see text).

For Mg, Si and Fe, no OC (and EC for Fe) data are shown, because they have been grouped with CC as their compositions are not statistically different. References: 1-3: *Magna et al.* [2006, 2014]; *von Strandmann et al.* [2011]
4-6: *Hin et al.* [2017]; *Liu et al.* [2023]; *Klaver et al.* [2024]

7,8: *Armstrong et al.* [2011]; *Dauphas et al.* [2015]

9-17: *Tian et al.* [2019, 2020]; *Ku and Jacobsen* [2020]; *Wang et al.* [2016]; *Hu et al.* [2022]; *Bloom et al.* [2020]; *Jiang et al.* [2021]; *Koefoed et al.* [2020]

18-22: *Schoenberg et al.* [2008, 2016]; *Bonnand et al.* [2016]; *Sossi et al.* [2018a]; *Zhu et al.* [2019, 2021]

23,24: *Sossi et al.* [2016]; *Poitras et al.* [2019]

25-27: *Herzog et al.* [2009]; *Savage et al.* [2015]; *Dhaliwal et al.* [2024]

28-35: *Luck et al.* [2005]; *Moynier et al.* [2011]; *Paniello et al.* [2012]; *Sossi et al.* [2018b]; *Paquet et al.* [2023]; *Fang et al.* [2024]

36-38: *Kato and Moynier* [2017]; *Kato et al.* [2017]; *Wimpenny et al.* [2022]

39-42: *Pringle and Moynier* [2017]; *Nie et al.* [2023]; *Wang et al.* [2023, 2024]

K: chondrite data are from observed falls only to avoid potential effects of terrestrial weathering.

Zn: as for K, chondrite data are from observed falls only, with EC data deriving from EH only due to suspected metamorphism effects on the analysed EL6 falls.

The Mg, Si and Fe isotope ratios in bulk planetary objects correlate (Fig. 12a, b), implying a control by the same cosmo-/geochemical fractionation process. Because Mg, Si and Fe are major elements, only reservoir separation involving significant mass fractions of these elements or with large isotope fractionation factors, could have affected their mantle isotopic ratios. This leaves core-mantle-crust separation or vapour-condensed-phase fractionation [Poitrasson *et al.*, 2004; Sossi *et al.*, 2016; Hin *et al.*, 2017; Young *et al.*, 2019]. Silicon and, in particular, Mg are sparingly soluble in metallic Fe during the differentiation of small telluric bodies. This factor, compounded with the fact that the Fe isotope fractionation factor between metal and silicate is small at low pressures [Hin *et al.*, 2012] in the absence of S [Kubik *et al.*, 2022], means that core formation is unlikely to have caused substantial isotopic fractionation of Fe, and, by extension, Mg and Si [although debate is ongoing, see Bourdon *et al.*, 2018; Shahar and Young, 2020]. Despite the fact that the $\Delta\text{Si}_{\text{met-sil}}$ is considerably larger than that for Fe [Shahar *et al.*, 2009; Hin *et al.*, 2014], the observation that the angrite and HED parent bodies, despite both being too oxidised to host Si metal in their cores (Fig. 1), have significantly heavier Si (and Fe in the case of the APB) isotopes than chondrites [cf. Pringle *et al.*, 2014; Liu *et al.*, 2017], casts further doubt over the role of core formation, making vapour-condensed phase fractionation a more likely process.

6.2.2 Cr and the moderately volatile elements

In marked contrast to Mg, Si and Fe, the isotope ratios of Cr in bulk, differentiated planetary bodies are similar to- or lower than those in chondrites. Earth and Mars have $\delta^{53/52}\text{Cr}$ within error of all types of chondrites, while the Moon and Vesta have significantly lower values (Table 6, see section 6.3.1). The isotope ratios of MVEs (the lithophiles Zn, K and Rb, and the siderophiles Cu and Ga) often vary widely compared to those of the major elements and Cr, even within samples from a single parent body, including chondrites [Paniello *et al.*, 2012]. The isotopic ratios of K, Zn, and Rb are similar to chondritic values in the Earth and Mars, but are enriched in heavy isotopes in the Moon and Vesta (Table 6; Fig. 12c,d). This tendency is also seen in the scarcer data on Cu and Ga isotopes, which are chondritic in the Earth, but significantly higher in lunar and vestan rocks [Table 6; Kato and Moynier, 2017; Day *et al.*, 2019; Wimpenny *et al.*, 2022]. The APB, instead, appears to be enriched in light K and Rb isotopes, interpreted as reflecting partial (re)condensation of these elements [Hu *et al.*, 2022; Wang *et al.*, 2024]. Within current measurement precision, no significant variations occur among the Li isotope ratios of the various planetary objects [cf. Tomascak *et al.*, 2016].

None of the isotopic variations in the aforementioned MVEs correlate with those in the major elements, Mg, Si and Fe. As shown in Fig. 12c,d, however, they correlate with one another [see also Wang *et al.*, 2024], again implying that a common process controlled their observed variation. As first pointed out by Day and Moynier [2014] and extended by Tian *et al.* [2021], higher isotopic ratios are found on bodies with lower escape velocities. We show in Fig. 13a that such correlations among the Earth, Mars, the Moon and Vesta occur for the isotopes of K, Cr and Rb (of the MVE isotopic systems with data for these four planetary objects, only Zn does not yield a statistically significant correlation). In the case of K and Rb, data are also available for the APB [Hu *et al.*, 2022; Wang *et al.*, 2024], yet do not follow the trend defined by the other planetary bodies, irrespective of the assumed mass of the APB [Tissot *et al.*, 2022].

Only three isotope systems currently display these correlations, which are based on only four data points per isotopic system, but they seem a worthy endeavour for future investigation. Following normalisation by $\Delta m/m^2$, the variations in Fig. 13a must be caused by either differences in the fractionation factor between vapour and condensed phase(s) or by the extent of mass loss, which is itself proportional to the relative volatilities of the elements. In Fig. 13b, we show that the slopes of the regressions presented in Fig. 13a become steeper for increasingly volatile elements (as quantified by T_c^{50}). As such, differences in K, Cr and Rb isotopic ratios among the different planetary bodies are controlled by the extent of mass loss experienced by the body in volatilisation/condensation event(s), that is, a Rayleigh process with a finite element budget. Because the isotopes of Cr and the MVEs in the Earth and Mars are

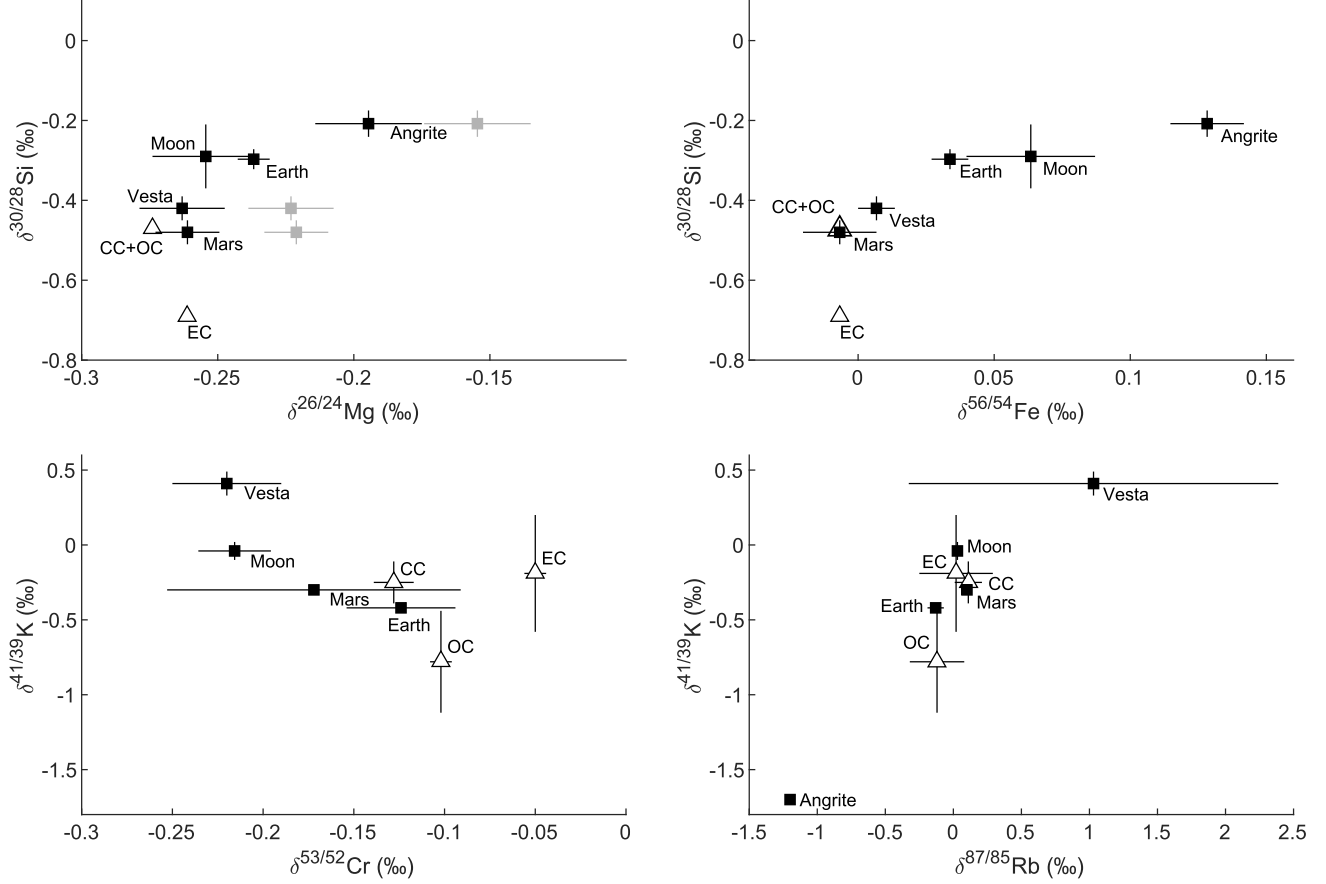


Figure 12: Mass-dependent isotopic variations among bulk differentiated (squares) and undifferentiated (triangles) planetary objects. a) $\delta^{30/28}\text{Si}$ vs. $\delta^{26/24}\text{Mg}$. The grey points correspond to measured values pre-correction (see main text for details). b) $\delta^{30/28}\text{Si}$ vs. $\delta^{56/54}\text{Fe}$. c) $\delta^{41/39}\text{K}$ vs. $\delta^{53/52}\text{Cr}$. d) $\delta^{41/39}\text{K}$ vs. $\delta^{87/85}\text{Rb}$. See Table 6 for data sources.

not fractionated from the range of chondrites, these bodies show no isotopic evidence for vapour loss of these elements of the sort preserved in the STBs, despite the fact that they also have lower MVE abundances than in most chondrites.

6.3 Physical causes of volatile loss

Planetary bodies with magma exposed at their surfaces will develop a vapour atmosphere, with the surface pressure determined by the magma temperature and its composition [e.g., *Wolf et al.*, 2023]. If the atmosphere is no longer hydrostatic, upwards motion can drive atmospheric loss, so-called hydrodynamic escape [Young et al., 2019; Chao et al., 2021]. Whether hydrodynamic escape is efficient or not depends on the competition between thermal energy and gravity. More efficient escape occurs from small, high temperature bodies, as quantified in the parameter λ ,

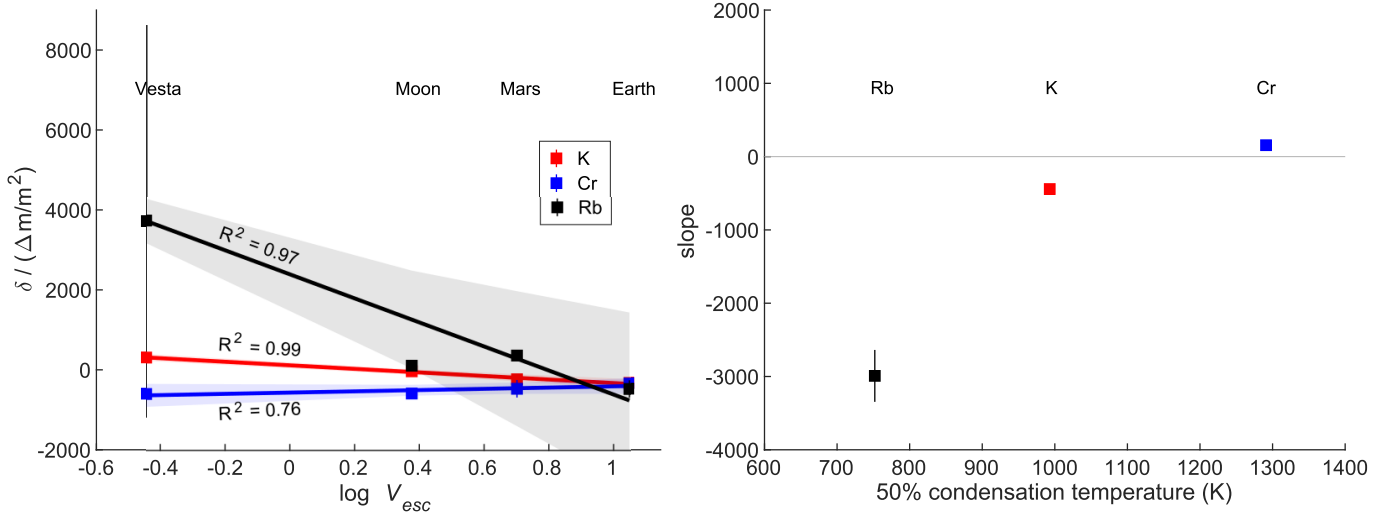


Figure 13: Mass-dependent isotopic fractionation among bulk planetary objects and its relation to the escape velocity of planetary object (a) and their volatility as parameterised by their 50% condensation temperature (b). Isotopic compositions have been normalised to the relative mass differences of the isotopes ($\Delta m/m^2$).

$$\lambda = \frac{GM}{r} \frac{\mu}{RT_s} \quad (38)$$

where G is the gravitational constant, M and r are the mass and radius of the body, μ is the atmospheric mean molar mass, T_s is the surface temperature and R is the gas constant. A large value of λ indicates inefficient escape (gravity wins). For a diatomic gas, the critical value of λ above which hydrodynamic escape shuts off is 2.4-3.6 [Volkov *et al.*, 2011]. For an adiabatic atmosphere, the critical value can be shown to be $\gamma_{ad}/(\gamma_{ad} - 1)$ [Zahnle and Kasting, 1986], where γ_{ad} is the ratio of the specific heat at constant pressure over constant volume. For a diatomic gas this ratio is 7/5, so the critical value of λ in this case is 3.5.

Escape of atmospheres with a $\mu \geq 0.03$ kg/mol (\geq air) is only possible on <1000 km radii bodies (smaller than the Moon; Fig. 14). This limit increases to Mars-sized bodies for $\lambda = 3$ for $\mu = 0.004$ kg/mol at 2000 K. Hydrodynamic escape from the fully-formed Earth is not possible (except possibly for pure hydrogen, and even then only at very high temperatures, ≥ 3500 K). Hydrodynamic escape is impeded relative to that predicted from eq. 38 if the surrounding disk has a non-zero pressure. It is also limited by the thermal energy available: heat is both radiated and advected away from the hot surface, and as the magma cools the vapour pressure drops, reducing the outwards flux of material. This limits the length of time available for escape to occur in the absence of external heat sources. There are two main sources of energy available to drive escape;

- Decay of ^{26}Al . Although this process likely caused melting and differentiation of early-formed solar system bodies, its ability to drive hydrodynamic escape is impeded by the rate at which it supplies thermal energy. A magma body radiating at 700 K [similar to terrestrial lava lakes; Patrick *et al.*, 2016] loses energy at a rate of 14 kW m^{-2} . Conversely, ^{26}Al decay would produce a surface heat flux of 0.5 kW m^{-2} in a 1000 km radius body at t_0 , and less thereafter. As a result, ^{26}Al heating cannot produce significant mass loss in bodies of such size (we note that the contrary finding expressed in Young *et al.* [2019] is due to a numerical error; Young, pers. comm.).

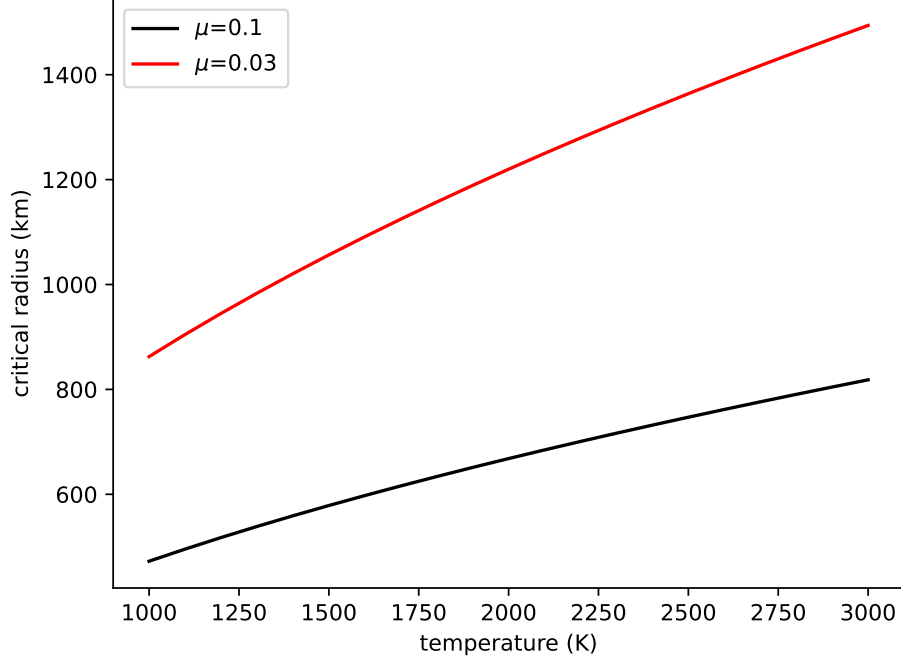


Figure 14: Radius above which hydrodynamic escape is shut off, as a function of surface temperature, for two different molar masses μ in kg/mol. Here, we assume the critical value of λ is to be 3, and a bulk density of 4000 kg m^{-3} .

- Impacts. Sufficiently energetic impacts can cause wide-spread melting and vaporisation [Nakajima *et al.*, 2021]. Hydrodynamic loss is very sensitive to the melt temperature because it determines the surface vapour density, which in turn governs the mass loss rate through the equation:

$$\frac{dN_i}{dt} = 4\pi(r_B)^2 C_s n_i \quad (39)$$

where r_B is the critical radius (i.e. that at which the gas outflow speed equals the sound speed), C_s the sound speed at r_B , and n_i the number density of the vapour. During conventional accretion, impact velocities are typically comparable to the escape velocity of the target body [Safronov, 1969; Agnor *et al.*, 1999], which depends on its mass. Higher impact velocities produce more melting and higher temperatures [Nakajima *et al.*, 2021]. But if impact velocity is controlled by target size, then the high-velocity impacts will typically only take place on large bodies, from which hydrodynamic escape is prohibited (see above). There are several potential ways in which this trade-off can be overcome.

The first is to appeal to some event stirring up the planetesimals so that their impact velocities are higher than would be expected based on the arguments above. For instance, Hin *et al.* [2017] argued that high-velocity impacts

driven by excited bodies on highly eccentric orbits, as induced by gas giant migration [Carter *et al.*, 2015] yield sufficient energy to cause planetesimal melt production and vapour loss. Calogero *et al.* [2025] explored this hypothesis in more detail, focusing on potassium. A second mechanism states that planetary envelopes enriched in rock-forming elements can exchange mass with the ambient nebular gas. As long as the molecular mass is dominated by that of H₂ (0.002 kg/mol), escape from envelopes may be efficient [Steinmeyer *et al.*, 2023]. A third is to consider impact-produced melt that is not contained within the target planet, such as an impact-generated proto-lunar disk. Here, the liquid is hot but the effective gravity of the proto-lunar disk is low, facilitating escape from the Moon, but not from the Earth-Moon system [Charnoz *et al.*, 2021].

While hydrodynamic escape is efficient in engendering mass loss, it does not itself produce large mass fractionation between isotopes in the atmosphere [Hunten *et al.*, 1987]. However, isotopic fractionation can occur at the melt-vapour interface, the magnitude and direction of which depends on two factors that trade off against each other;

- Temperature. Higher temperatures lead to smaller isotopic fractionation factors if occurring at equilibrium (proportional to $1/T^2$).
- Degree of equilibrium. If Langmuir (kinetic) fractionation prevails (i.e., $p_i < p_{i,eq}$), then the fractionation factor, α is $\frac{i}{j}\alpha_{kin} = \sqrt{\frac{m_j}{m_i}}$, where m is the isotopic mass. If equilibrium prevails (i.e., $p_i = p_{i,eq}$), then, in most instances, the gas phase is also enriched in lighter isotopes, but the fractionation factor is closer to unity Young *et al.* [2019]. This is because most rock-forming elements evaporate as monatomic gases [e.g., K⁰, Na⁰, Mg⁰, see Sossi *et al.*, 2019] or as oxide species with a *lower* mean oxidation state than in the condensed phase (e.g., SiO(g) vs. SiO₂(s,l), GeO(g) vs. GeO₂(s,l)).

6.3.1 Volatile loss due to evaporation only

If evaporation mimics a Rayleigh process (see section 6.2.2), then the degree of isotopic fractionation follows:

$$\frac{i/j R_{res}}{i/j R_0} = F^{(i/j \alpha_{gas/cond} - 1)}, \quad (40)$$

where R is the isotopic ratio of the residue (res) and the system (0), respectively and F is the fraction of isotope j remaining in the residue. Here, we examine the correlations between $\frac{i/j R_{res}}{i/j R_0}$ and F fit with values of α , and compare them to those expected from Langmuir (kinetic) and Knudsen (equilibrium) fractionation.

The prime case in which the expected correlation between F and $\frac{i/j R_{res}}{i/j R_0}$ is observed is the Moon. Taking the BSE as $i/j R_0$, $\delta_{Moon} - \delta_{BSE}$ correlates with the degree of depletion, F (Fig. 15). The fitted values of α (for Rb, K, Zn and Cu) are consistent with values of $p_i/p_{i,eq}$ of 0.99, should evaporation have taken place at ~ 2500 K [Nie and Dauphas, 2019], or 1 (i.e., equilibrium) for $T \sim 1300$ K [Tartèse *et al.*, 2021; Dauphas *et al.*, 2022]. Hence, the fitted value of α is degenerate with respect to $p_i/p_{i,eq}$ and temperature. However, Sn and Cr are anomalous, in that they preserve *lighter* isotopic ratios in the Moon than in the bulk silicate Earth [Sossi *et al.*, 2018a; Wang *et al.*, 2019]. Because both Cr and Sn have gas species in which the metal is more strongly bound than in the condensed phase, fractionation at equilibrium can uniquely account for this observation in a vapour-condensed phase system. This interpretation, and the negative slope in Fig. 13 thus support loss of Cr and Sn on STBs at relatively oxidised conditions (\sim IW) [see section 6.1, Zhu *et al.*, 2019].

The propensity for (near-) equilibrium isotopic fractionation to have prevailed reflects; *i*) the fact that vapour phase reactions reach equilibrium in 10^{-9} to 1 s [Fegley Jr *et al.*, 2020]; much shorter than lifetimes of magma oceans

[$\sim 10^2$ – 10^7 yr; *Salvador and Samuel, 2023*] and *ii*) $p_i/p_{i,eq} > 0.95$ when the (far-field) total pressure (P) exceeds $\sim 10^{-8}$ bar [*Young et al., 2019; Tang and Young, 2020*]. In summary, evidence points to near- or at equilibrium values of $p_i/p_{i,eq}$ (> 0.99), at least for the Moon. Such conditions are more readily achieved on planetesimals that are Moon-mass or larger [*Young et al., 2019*], which indicates that volatile loss on the Moon likely occurred when it was close to its present-day mass, though does not require it.

6.3.2 Volatile loss due to evaporation + mixing

Correlations between isotopic fractionation in a given planetary body and its escape velocity (Fig. 13a) could imply that those bodies experienced volatilisation and vapour loss at their (near-)final masses, as posited by *Tian et al. [2021]*. The calculations in section 6.3 and the observations in section 6.3.1 support the idea that Vesta and the Moon [see also *Charnoz et al., 2021*], were able to lose vapour by hydrodynamic escape, even at their present day masses. Conversely, Mars, and in particular the Earth, were barely able to lose any vapour at their current masses. As opposed to the Moon and Vesta, Earth and Mars do not preserve any detectable mass-dependent isotopic fractionation relative to chondrites, yet they are clearly volatile-depleted with respect to CI chondrites (Fig. 15b).

Figure 15b shows that Mg and Si, relative to Ca and EH chondrites ($X/\text{Ca}_{BSE}/X/\text{Ca}_{EH}$), are slightly (32 %) and moderately (59 %) depleted, respectively, in the BSE and are also marginally isotopically heavy [*Hin et al., 2017*]. These figures decrease to 20 % for Mg and 29 % for Si when normalised to Ca and CI chondrites. Therefore, the depletion of Si and Mg observed in the BSE relative to chondrites (both normalised to Ca) is coupled with heavy isotopic enrichment, whereas the elemental depletion in MVEs records no isotopic fractionation compared to chondrites. The simplest explanation for this duality is that the Earth (and Mars) accreted bodies in which MVEs underwent near-complete evaporative loss (or were hardly accreted at all), and mixed with bodies of undepleted, potentially chondritic material [*Hin et al., 2017; Sossi et al., 2022*]. On the Earth’s total mass-basis, this undepleted material is insignificant such that the isotope ratios of the major elements (Mg, Si and Fe) remained essentially unaffected, yet the budgets of the MVEs were entirely overprinted. This implies that there must be at least two populations of smaller bodies, one isotopically heavy and volatile-poor and the other volatile-undepleted and isotopically lighter (i.e., unfractionated relative to chondrites).

To test this idea, output from an N-body model [*Carter et al., 2015*] was analysed to examine the competition between the chemical and isotopic fractionation induced by impact-driven evaporation of K and the mixing of these bodies over time [*Calogero et al., 2025*]. Bodies were assumed to have an initial bulk and isotopic composition identical to that of Mars. Subsequent impacts in some cases caused melting, magma ocean formation and hydrodynamic loss of K. Isotopic fractionation was assumed to occur in such cases with $\alpha=0.999541$. Other collisions did not generate melting and were thus assumed to simply mix the compositions of the two colliding objects.

These simulations show that in general, as predicted by eq. 38, smaller bodies are the most isotopically fractionated (Fig. 16b). However, they are not necessarily the most depleted in K. Indeed, other, larger bodies, which have experienced more impacts, can be *more* depleted in K, but have lower (i.e., more chondritic) $\delta^{41}\text{K}$ values (e.g. bodies I and L in Fig. 16). This arises because the combination of early evaporative loss in small bodies followed by mixing results in larger bodies having isotopically unfractionated signatures (because more isotopically unfractionated material was added). For an Earth-sized body, this process naturally results in broadly chondritic $\delta^{41}\text{K}$ and $\delta^{66}\text{Zn}$ values, because the budget of these elements is entirely dominated by the addition of volatile-rich material that experienced little- to no evaporation. This is the scenario envisaged by *Sossi et al. [2022]*, and states that, all else being equal, the compositions (both chemical and isotopic) of larger bodies will be determined to a greater extent by mixing, and those of smaller bodies by partial evaporation.

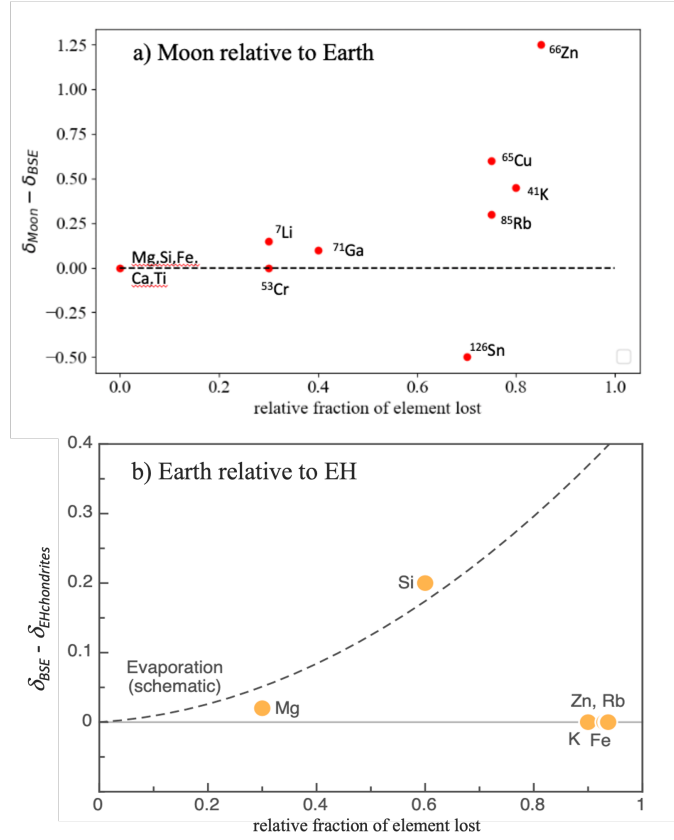


Figure 15: a) The isotopic differences between the bulk silicate Earth and Moon for the isotopes of various elements, against the depletion of those elements in the Moon relative to the bulk silicate Earth. b) Mass-dependent isotopic fractionation in the bulk silicate Earth relative to EH chondrites for selected elements as a function of their elemental depletion (calculated as $X/\text{Ca}_{\text{BSE}}/X/\text{Ca}_{\text{EH}}$, where $X = \text{Mg}$ or Si). The dashed line shows the expected increase in isotopic fractionation for larger degrees of evaporative loss. Despite their greater degrees of depletion, the moderately volatile elements (K, Zn, Rb) do not show any isotopic deviation with respect to EH chondrites. Source data are listed Table 6.

7 Provenance of planet-building materials

The provenance of planetary building materials can be quantified using nucleosynthetic isotope anomalies. These arise through the heterogeneous distribution of presolar material in the solar protoplanetary disk and, as such, allow genetic links among and between meteorites and planets to be examined. The isotope anomalies in a given element are quantified by their part per ten-thousand deviation (ε) from a terrestrial reference standard (in most cases close to but often not identical with the BSE), following internal normalisation to a chosen ratio:

$$\varepsilon^i X = \left(\frac{(^iX/^jX)_{\text{body}}}{(^iX/^jX)_{\text{std}}} - 1 \right) \times 10000 \quad (41)$$

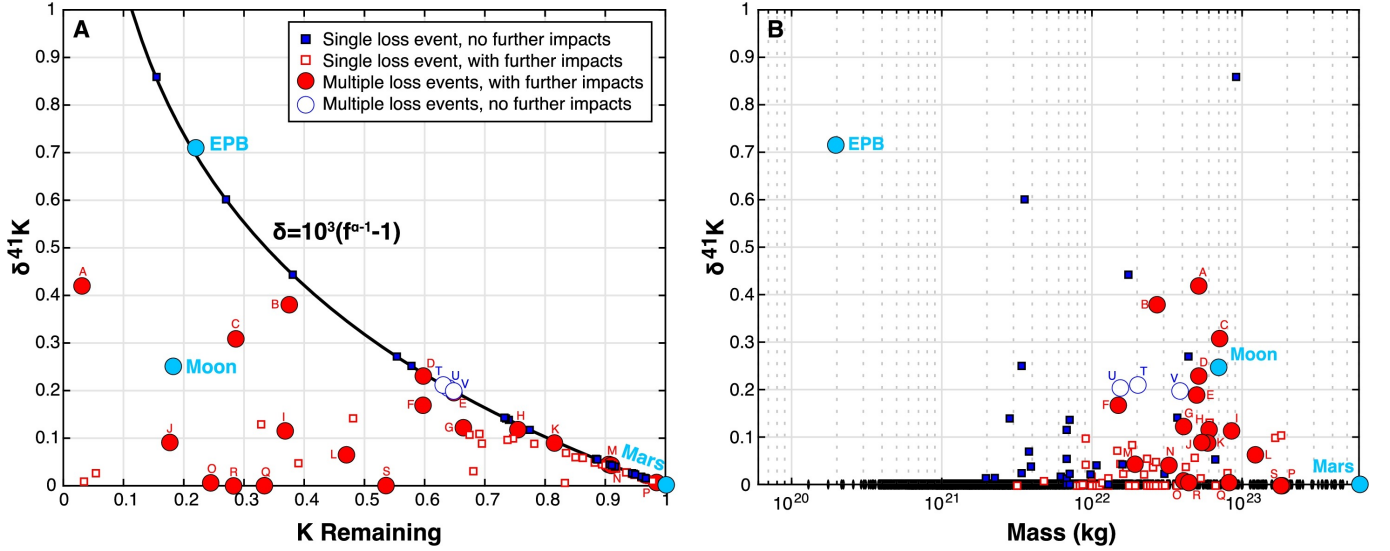


Figure 16: Calculations using output from N-body simulations [Carter *et al.*, 2015] showing the K isotope fractionation (expressed as $\delta^{41}\text{K}$) with respect to the **a)** fraction of K remaining and **b)** the mass of individual planetary bodies, assuming a Mars-like starting composition. Different symbols show whether bodies experienced multiple impact-driven evaporative events. The solid line in **a)** is that for evaporative loss of K governed by the Rayleigh equation with a value of $\alpha = 0.999541$. See Calogero *et al.* [2025] for further details

where i and j are the numerator- and denominator isotope, respectively, and X is the element of interest. Implicit in computing isotope anomalies in this way is the assumption that the chosen internal normalising ratio of all samples is terrestrial. For samples having nucleosynthetic isotope anomalies this is almost certainly not true, and so calculated $\varepsilon^i X$ values may not reflect anomalies on a particular isotope, but rather the combined effects of abundance variations of several isotopes, including those used for the internal normalisation.

A key observation from the nucleosynthetic isotope anomalies, as well as $\Delta^{17}\text{O}$ (whose variations are not nucleosynthetic in origin), is the notion of an isotopic dichotomy between non-carbonaceous (NC) and carbonaceous chondrite (CC) type materials [see Bermingham *et al.*, 2020; Kleine *et al.*, 2020; Kruijer *et al.*, 2020, for recent reviews]. The first indication of what is now known as the NC-CC dichotomy dates back to Trinquier *et al.* [2007], who observed that, for nucleosynthetic isotope anomalies, differentiated meteorites and carbonaceous chondrites define two distinct fields. Warren [2011] then showed that isotope anomalies in O, Ti, Cr, and Ni, meteorites always fall into two distinct clusters, which he termed the non-carbonaceous (NC) and carbonaceous (CC) groups. Since then, the number of elements for which the NC-CC dichotomy has been identified has grown considerably, making it a fundamental characteristic of the early solar system. Importantly, the dichotomy was also identified for isotopes of Mo [Budde *et al.*, 2016; Poole *et al.*, 2017], in which it exists not only for chondrites but also for iron meteorites, which derive from parent bodies that accreted within the first 1 Myr of the solar system [Kruijer *et al.*, 2017]. Thus, together, these observations reveal that the dichotomy was established early, and was maintained for essentially the entire lifetime of the disk.

It is now widely thought that the NC reservoir represents the inner disk, and the CC reservoir the outer disk

[Warren, 2011; Budde *et al.*, 2016; Kruijer *et al.*, 2017]. Below we assess whether or not CC material is the dominant source of *i*) volatile elements to the Earth and *ii*) oxidation relative to the solar nebula among telluric bodies. Owing to their distinct nucleosynthetic heritage, we discuss the iron-peak (section 7.1) and heavier elements (section 7.2) separately.

7.1 Iron-peak elements

The ‘iron-peak’ elements have binding energies per nucleon that are higher than those of the surrounding nuclides, leading to enhanced abundances during stellar nucleosynthesis via the alpha process [Clayton, 2003]. Typically, these elements are Ti, V, Cr, Mn, Fe, Ni, Cu and Zn. Here, we also extend this classification to Si (produced by O burning) and Ca (produced by Si burning), owing to their similar masses and nucleosynthetic heritage.

In a diagram of $\varepsilon^{50}\text{Ti}$ versus $\varepsilon^{54}\text{Cr}$, the composition of the BSE plots within the NC field, albeit as an endmember, with excesses in neutron-rich isotopes compared to other NCs, pointing towards the CC field [Trinquier *et al.*, 2009]. Thus, the composition of the BSE can be produced by mixtures of the extant groups of NC and CC meteorites for these two systems. However, the choice of end-members to represent each group is non-unique. One interpretation (hereinafter hypothesis A) first mooted by Warren [2011], and developed by Schiller *et al.* [2018] states that the isotopic composition of the Earth evolved over time from ureilite-like (i.e., the meteorites defining the lower end of the NC trend) to its present-day composition by the addition of CI-like material. Schiller *et al.* [2018] based their arguments on anomalies in ^{48}Ca , but the correlated nature of the isotope anomalies in Ca, Ti, and Cr among the NC meteorites means that the same argument holds for any of these elements. An alternative hypothesis (B), is built on the observation that, in many isotopic systems, including Cr and Ti, the Earth (and Moon) have compositions similar to those of enstatite chondrites (ECs) [e.g., Warren, 2011; Dauphas, 2017]. In this scenario, the Earth accreted $\sim 95\%$ EC-like material, which could reflect objects with a uniform, EC-like isotopic composition [Dauphas, 2017; Dauphas *et al.*, 2024], but also via accretion of a variety of NC materials with a range of isotopic compositions, whose average is that of the ECs [Burkhardt *et al.*, 2021].

As pointed out by Warren [2011], hypotheses A and B lead to very different CC fractions inferred for the Earth. The CI-derived fraction for each element, X , in the BSE can be computed by mass balance:

$$f_{X,CI} = \frac{\varepsilon^i X_{NC} - \varepsilon^i X_{BSE}}{\varepsilon^i X_{NC} - \varepsilon^i X_{CI}} \quad (42)$$

where NC denotes the isotopic composition of the NC material in Earth, which can either be ureilite- (hypothesis A) or EC-like (hypothesis B). Use of eq. 42 implies identical element concentrations in each reservoir. For identical element concentrations in each reservoir, the CI-derived fraction for an element X is the same as the apparent mass fraction of CI material accreted to the Earth. This is likely to hold for RLEs (e.g., Ti) and potentially the main components (Cr, Si), but may not for volatile (e.g., Zn) and siderophile elements (e.g., Fe, Ni). This is because these elements are depleted in the BSE relative to chondrites as a result of volatile depletion [Steller *et al.*, 2022; Savage *et al.*, 2022] or core formation, respectively [Dauphas, 2017].

In both hypotheses, the apparent fraction of CI-like material is near-constant for Ca, Ti, and Cr, at $\sim 5\%$ for the BSE assuming an EC-like NC end-member, or $\sim 40\%$ for a ureilite-like NC end-member (Fig. 17). As noted above, this constancy of inferred CI fractions in both hypotheses reflects the correlated nature of the isotope anomalies in these elements among the NC meteorites, and the position of Earth on the neutron-rich end of the NC trend.

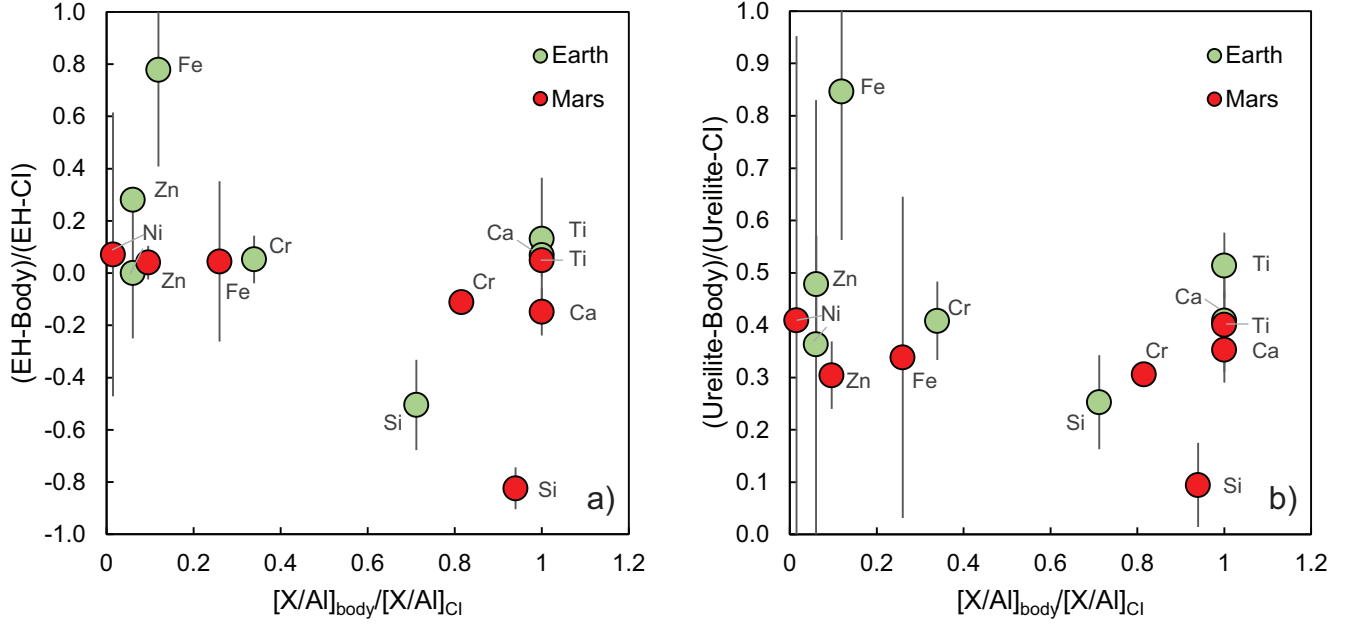


Figure 17: The fraction of each element in the bulk silicate Earth (BSE, green) and bulk silicate Mars (BSM, red) brought by the CI component in mixtures between a) EH-like and CI-like and b) ureilite-like and CI-like isotopic end-members, each with identical concentrations, as a function of their Al, CI-normalised abundances in the BSE and BSM. Note the large uncertainties for Fe and Ni, owing to the relatively small degree of isotopic variation relative to the uncertainty on the analyses. Isotope ratios used are $\mu^{30}\text{Si}$, $\epsilon^{48}\text{Ca}$, $\epsilon^{50}\text{Ti}$, $\epsilon^{54}\text{Cr}$, $\epsilon^{54}\text{Fe}$ and $\epsilon^{62}\text{Ni}$. Data from [Trinquier *et al.*, 2007, 2009; Schiller *et al.*, 2018, 2020; Burkhardt *et al.*, 2021; Steller *et al.*, 2022; Savage *et al.*, 2022; Onyett *et al.*, 2023].

For Ni, using $\epsilon^{62}\text{Ni}$ as in Fig. 17, the inferred CI fractions are similar to those obtained from the three aforementioned elements, but the small Ni isotope variations have larger uncertainties and would also be compatible with a wider range of CI fractions [Steele *et al.*, 2012; Tang and Dauphas, 2014; Nanne *et al.*, 2019]. For example, when using the $\epsilon^{60}\text{Ni}$ anomaly, the BSE and CI chondrites are indistinguishable within error [Spitzer *et al.*, 2024]. For Fe, the $\epsilon^{54}\text{Fe}$ values of CI chondrites and the BSE are indistinguishable, leading to high apparent CI fractions in the BSE (0.79 ± 0.39 and 0.84 ± 0.27 for an EC-CI mixture or Ureilite-CI mixture, respectively; Fig. 17) [Schiller *et al.*, 2020; Hopp *et al.*, 2022b]. However, CI chondrites are unlikely to have significantly contributed to the Fe budget of the BSE because, as noted by Hopp *et al.* [2022b], the isotopic compositions of both Cr (less siderophile) and Ni (more siderophile) in CIs are distinct from the BSE. We note that the apparent contradiction can be resolved by considering that the BSE lies at the neutron-rich (i.e., ^{54}Fe -rich) end of the NC trend, indicating that Fe is entirely consistent with an NC origin [see also Hopp *et al.*, 2022a].

For Si the apparent fractions of CI-like material are systematically lower than that from other elements (and extend to negative values), which indicates that the $\epsilon^{30}\text{Si}_{\text{BSE}}$ is lower ($=0$) than both CI ($\epsilon^{30}\text{Si} = \sim 0.3$) and EC ($\epsilon^{30}\text{Si} = \sim 0.1$) [see Onyett *et al.*, 2023]. On this basis, Onyett *et al.* [2023] argued that EC-CI mixtures are precluded as

proto-Earth source material. However, because ECs are fractionated mass-dependently in $\delta^{30}\text{Si}$, correcting the $\varepsilon^{30}\text{Si}$ for such fractionation yields a revised value of $\varepsilon^{30}\text{Si} = 0.04 \pm 0.03$ [Dauphas *et al.*, 2024] which scarcely differs from that of the BSE and hence is broadly consistent with hypothesis B. Because such a correction is implicit on mass-dependent fractionation occurring at high temperatures, additional data to better resolve any potential differences between ECs and the BSE are essential in discerning between hypotheses A and B.

A key distinction between hypotheses A and B can instead be made using Zn isotopic composition of the BSE [Steller *et al.*, 2022; Savage *et al.*, 2022; Martins *et al.*, 2023]. In hypothesis A, the fraction of CI-derived Zn is 0.48 ± 0.09 (Fig. 17b); indistinguishable from Cr (0.41 ± 0.07) and Ti (0.51 ± 0.06). Hypothesis B yields a higher apparent CI-derived fraction computed from Zn (0.29 ± 0.05) compared to Cr (0.07 ± 0.03) and Ti (0.05 ± 0.09 ; Fig. 17a). In $\varepsilon^{66}\text{Zn}$ versus $\varepsilon^{54}\text{Cr}$ space, using the Zn concentrations of CC meteorites and the BSE, any mixing line between the CC field that passes through the BSE intersects the NC field near the *isotopic* composition of the ECs with an average ~ 35 ppm Zn for the NC material [Kleine *et al.*, 2023; Kleine and Nimmo, 2024, curve ‘B’, Fig. 18]. This implies that the BSE contains ~ 6 % CI-like material by mass in hypothesis B. Notably, this ~ 6 % CI chondrite-like material is identical to the CC *mass* fractions inferred from the isotope anomalies in Ca, Ti, and Cr in Hypothesis B (Fig. 17), meaning Earth would have accreted predominantly from NC material with an EC-like isotopic composition, on average, with a 6 % contribution of CI material, which delivered $\sim 30\%$ of Earth’s Zn budget. Hypothesis A, in contrast to Hypothesis B, would require that the NC (ureilite) and CC (CI) end-members had the same Zn/Cr ratios such that the mixing line passes through the BSE (curve ‘A’, Fig. 18). Indeed, Zn/Cr ratios in ureilites are similar, to within a factor ~ 2 , of those in CI chondrites [Brugier *et al.*, 2019; Zhu *et al.*, 2022]. In this scenario, the apparent CI-like fraction in the BSE inferred from Zn matches those from Ca, Ti and Cr, but, in contrast to hypothesis B, CI chondrites must represent ~ 40 % of the mass of the Earth.

Variations in oxygen isotopes, although not nucleosynthetic in origin, nevertheless provide information on a samples provenance. Ureilites are heterogeneous with respect to $\delta^{17}\text{O}$ and $\delta^{18}\text{O}$ [Clayton and Mayeda, 1996; Kruttsch and Mezger, 2025], yet, unlike other NC bodies, they lie on the Carbonaceous Chondrite Anhydrous Mineral Line (CCAM), which defines a slope of unity in a three-isotope plot [Clayton *et al.*, 1977]. Because CI chondrites also lie on the CCAM with $\delta^{17}\text{O} \sim 9$ ‰ and $\delta^{18}\text{O} \sim 16$ ‰ [Clayton and Mayeda, 1999], any mixture of ureilite-like and CI-like material, even if a specific proportion can produce the $\Delta^{17}\text{O}$ composition of the BSE, does not pass through the BSE composition [$\delta^{17}\text{O} = 2.7$ ‰, $\delta^{18}\text{O} = 5.2$ ‰, Eiler, 2001]. As such, ureilite-CI mixtures appear not to be compatible with the O isotope composition of the BSE.

These distinct interpretations provide a testable hypothesis, namely, which (if either) of the two scenarios is consistent with the volatile element budget of the BSE? Figure 19 shows the abundances of a selection of volatile elements for mixing between a volatile-free proto-Earth and a) 40 %- and b) 6 % by mass of CI chondrites. In the latter case, this is equivalent to ~ 30 % of the Zn budget of the BSE as explained above and posited by Steller *et al.* [2022]; Savage *et al.* [2022] in the framework of hypothesis B. The choice of a volatile-free proto-Earth provides upper limits for the inferred volatile element abundances.

Delivery of 6 % CI to an otherwise volatile-free proto-Earth (hypothesis B) would account for roughly the entire present-day budget of Pb, while the budgets of C, S, Ag, Ge, Tl and Br (\pm Cl, Cd) would be in excess of those observed. Because Ag, Ge, C and S are more siderophile than is Zn, their additional sequestration into the core *after* the delivery of CI material could reconcile their predicted excesses [Mann *et al.*, 2009; Wood *et al.*, 2014; Blanchard *et al.*, 2022]. The same argument cannot be made for Tl, Br, Cl and Cd, whose metal-silicate partition coefficients are similar to [Cd; Wang *et al.*, 2016] or lower than [Br, Cl, Tl; Kuwahara *et al.*, 2017; Yang *et al.*, 2023] those for Zn. The excess halogen problem can be resolved if the CI abundances of [Clay *et al.*, 2017] are adopted. Hence, hypothesis B remains plausible without significant volatile loss post-CI-addition (though additional core formation after CI addition is needed).

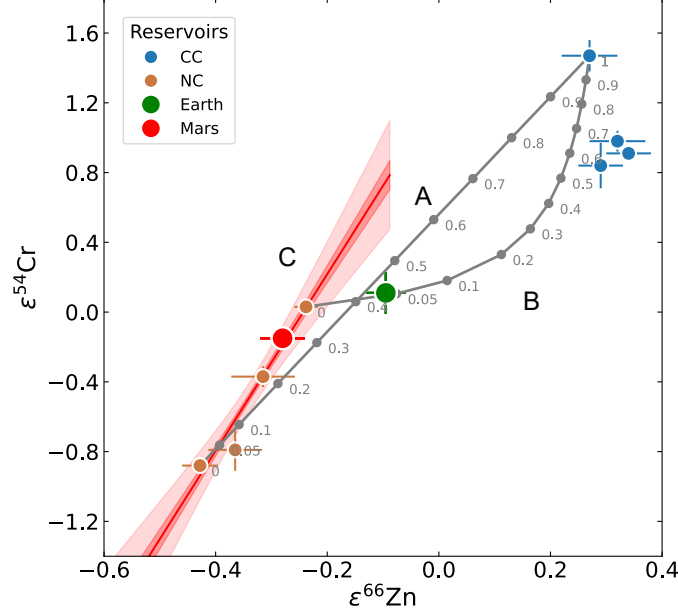


Figure 18: The $\epsilon^{54}\text{Cr}$ - $\epsilon^{66}\text{Zn}$ variation among non-carbonaceous meteorites (NC, orange), carbonaceous meteorites (CC, blue), the bulk silicate Earth (Earth, green), and bulk silicate Mars (Mars, red). The grey curves denote mixing lines between CI chondrites and, A - a ureilite-like end-member with Zn/Cr ratios identical to CI chondrites (0.12) and B - an EC-like end-member with 35 ppm Zn ($\text{Zn}/\text{Cr}_{\text{EC}} = 0.014$). Tick marks show the mass fraction of CI-like material in the mixture. C denotes a fit according to the York method [York *et al.*, 2004] assuming uncorrelated errors in x and y and its associated 1- σ (dark red) and 2- σ (light red) error envelope, yielding $\epsilon^{54}\text{Cr} = (5.06 \pm 1.05)\epsilon^{66}\text{Zn} + 1.23 \pm 0.33$. All data taken from Steller *et al.* [2022] for chondrites and the Earth, and Kleine *et al.* [2023]; Paquet *et al.* [2023] for Mars using $^{67}\text{Zn}/^{64}\text{Zn}$ -normalised values.

The addition of 40 % CI chondrites by mass in hypothesis A, results in an overabundance of all volatile elements, including Zn. Therefore, the BSE must have to have undergone volatile loss *after* the delivery of CI material for hypothesis A to hold, which is very difficult because thermal loss of volatiles (except perhaps hydrogen) is not energetically feasible from a body >10 % of Earth's mass (see section 6.3). Alternatively, the material was only isotopically CI-like, but had similar and BSE-like elemental ratios (such as Cr/Zn), see above. A final possibility states that ureilite- and CI-like material was accreted to the Earth in constant 60:40 proportions, before mixing to form a uniform reservoir, from which a fraction of the Zn budget was lost [Bizzarro *et al.*, 2025]. To this end, sublimation of accreting pebbles in H_2 -rich planetary envelopes was proposed in order to explain the depletion of S relative to more refractory elements [Steinmeyer *et al.*, 2023], but is yet to be tested for a larger suite of elements. Moreover, this volatile loss must not have engendered any perceptible mass-dependent isotopic fractionation [section 6.2.2, Sossi *et al.*, 2022]. Therefore, for hypothesis A to remain valid, it requires any elemental fractionation occurring in the H_2 -rich envelope of the growing Earth to reproduce both its smooth decline in abundances of volatile elements with condensation

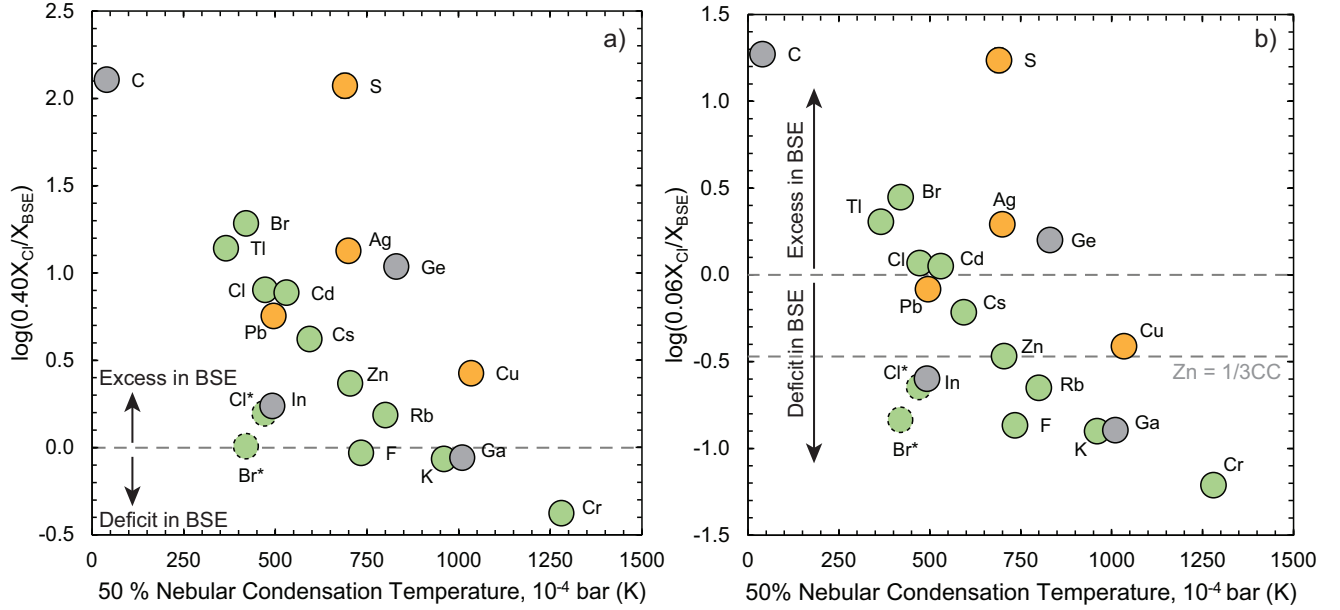


Figure 19: The log₁₀ of the ratio of the concentrations of a selection of moderately- and highly volatile elements for a) 40 % and b) 6 % (by weight) given by addition of CI chondrites to an otherwise volatile-free proto-Earth, normalised by the present-day bulk silicate Earth (BSE) abundances of these elements. Green = lithophile, grey = siderophile, orange = chalcophile. Cl* and Br* refer to the CI chondrite abundances of *Clay et al.* [2017]. Values that exceed 0 indicate that these elements are more abundant in 0.40× (a) or 0.06× (b) CI chondrite than in the BSE.

temperature, and their lack of isotopic fractionation. No such results have yet been demonstrated.

Finally, owing to the relatively few studies conducted on Zn isotopic variations among meteorites [*Steller et al.*, 2022; *Savage et al.*, 2022; *Martins et al.*, 2023], Fig. 18 shows that the BSE is displaced from trend defined by NC bodies and Mars. However, the 2- σ uncertainty is sufficiently large that the BSE falls close to its extension (envelope ‘C’), though more data are required to provide a statistical assessment. Alternatively, the apparent deviation of the BSE from the ⁶⁶Zn-⁵⁴Cr trend might reflect the late-stage addition of volatile-rich NC material having a composition beyond the NC trend (i.e., unsampled NC material). Provided this material is volatile-rich compared to the composition of the proto-Earth, it would exert a stronger control on the BSEs isotope composition for Zn than for Cr, a potential explanation why the BSE appears to diverge from the NC trend for these two elements. This permits the possibility that the Zn and Cr isotopic compositions of the BSE are consistent with those of an NC body that lies to higher $\epsilon^{66}\text{Zn}$ and $\epsilon^{54}\text{Cr}$ than any existing NC meteorite group.

7.2 Heavy elements

These elements, defined as those with $Z > 26$ (Fe), were synthesised by nuclear processes distinct from those of the lighter elements. In brief, nuclides form by neutron capture at different rates; the *s*-process (slow neutron capture) and *r*-process (rapid neutron capture), which produce roughly equal amounts of nuclides, and the less widespread

p-process that gives rise to proton-rich nuclei. The rates of neutron capture (slow or rapid) are determined relative to the β^- -decay rate of the target nuclide, and depend on the nuclide's neutron capture cross section, which is highly temperature-dependent [Schramm and Norman, 1976]. In general, *r*-process nucleosynthesis produces more neutron-rich nuclides of a given element relative to the *s*-process, as well as higher-*Z* elements. Isotopic variations among heavy elements have been reported for, for example, Sr [Moynier et al., 2012; Hans et al., 2013; Schneider et al., 2023], Zr [Akram et al., 2015; Render et al., 2022], Mo [Dauphas et al., 2002; Burkhardt et al., 2011], Ru [Chen et al., 2010; Fischer-Gödde et al., 2015], Nd and Sm [Qin et al., 2011; Boyet and Gannoun, 2013; Burkhardt et al., 2016; Frossard et al., 2022].

The BSE is an end-member among *all* planetary materials in the isotopic compositions observed for heavy elements, as has been shown for Mo [Burkhardt et al., 2011; Budde et al., 2019], Zr [Akram et al., 2015; Render et al., 2022], Nd [Burkhardt et al., 2016], and Ru [Fischer-Gödde and Kleine, 2017]. Importantly, this implies that the BSE composition is inconsistent with any mixture of NC- and CC components currently available, an interpretation that is otherwise permitted from iron-peak elements alone (see section 7.1). Specifically, for isotopic variations between an iron-peak element and a heavy element (e.g., $\epsilon^{50}\text{Ti}$ vs. $\epsilon^{96}\text{Zr}$), the NC trend is transverse to variations among CCs [see Burkhardt et al., 2021; Render et al., 2022; Yap and Tissot, 2023; Kleine and Nimmo, 2024] such that no mixture of a known NC and a (known) CC body passes through the terrestrial composition. Consequently, the processes that lead to variability among NC bodies were distinct from those that gave rise to variation among CC bodies, and the two populations cannot be considered as sampling different portions of a continuum, as in hypothesis A.

Isotopic variations induced by the *r*- and *s*-processes for a given isotopic ratio may often counteract one another, preventing an unequivocal assessment of their nucleosynthetic origin [Schneider et al., 2023]. Molybdenum is an exception, because *r*- and *s*-process variations can be distinguished in ϵ - ϵ including one of the two *p*-process Mo nuclides (i.e., ^{92}Mo or ^{94}Mo) [Burkhardt et al., 2011]. The CC and NC meteorite groups in $\epsilon^{94}\text{Mo}$ - $\epsilon^{95}\text{Mo}$ space [Budde et al., 2016], form two lines, which reflect *s*-process heterogeneities [Budde et al., 2016], while the offset between the two lines reflects a near-constant *r*-process-excess in CC over NC materials (Fig. 20).

Spitzer et al. [2020], based on Mo isotopic data representing 15 different parent bodies, including early- (i.e., iron meteorites, achondrites) and late-formed bodies (i.e., chondrites) found that the NC-line ($\epsilon^{95}\text{Mo} = [0.528 \pm 0.045]\epsilon^{94}\text{Mo} - 0.058 \pm 0.040$) is slightly shallower than the CC-line ($\epsilon^{95}\text{Mo} = [0.596 \pm 0.006]\epsilon^{94}\text{Mo} + 0.264 \pm 0.010$). More recently, Bermingham et al. [2024] argued that the slope of the NC-line is shallower again ($\epsilon^{95}\text{Mo} = [0.517 \pm 0.042]\epsilon^{94}\text{Mo} + 0.01 \pm 0.02$); however, this result is not only based on a lower number of samples (six iron meteorites), but also is influenced by the Mo isotope data for two IAB irons, whose composition differs from that reported in an earlier study [Worsham et al., 2017]. The latest compilation of Spitzer et al. [2025], yields $\epsilon^{95}\text{Mo}_{\text{NC}} = (0.517 \pm 0.028) \times \epsilon^{94}\text{Mo}_{\text{NC}} - 0.045 \pm 0.026$ (95 % confidence interval, Fig. 20) based on data for 41 distinct NC bodies and including available data for IAB irons from different studies with an indistinguishable slope but a lower intercept than that of Bermingham et al. [2024].

Based on Mo isotope data for several terrestrial igneous rocks, Budde et al. [2019] report $\epsilon^{94}\text{Mo} = 0.04 \pm 0.06$ and $\epsilon^{95}\text{Mo} = 0.10 \pm 0.04$ (95 % confidence interval) for the BSE, indicating that in the $\epsilon^{94}\text{Mo}$ - $\epsilon^{95}\text{Mo}$ diagram the BSE plots between the NC- and CC-lines (Fig. 20). From the position of the BSE in this diagram, these authors calculated that 46 ± 15 % of the BSEs Mo derives from the CC reservoir. Budde et al. [2023] showed that there is some uncertainty on the BSEs Mo isotope composition owing to non-exponential isotope fractionation, either intrinsic to the sample, during the measurement, or both, but also argued that this does not affect the fraction of CC material in the BSE, though uncertainties are larger. Conversely, Bermingham et al. [2024], based largely on data for molybdenites, argued that the BSE composition is different from that reported by Budde et al. [2019], and quote $\epsilon^{94}\text{Mo} = -0.07 \pm 0.03$ and

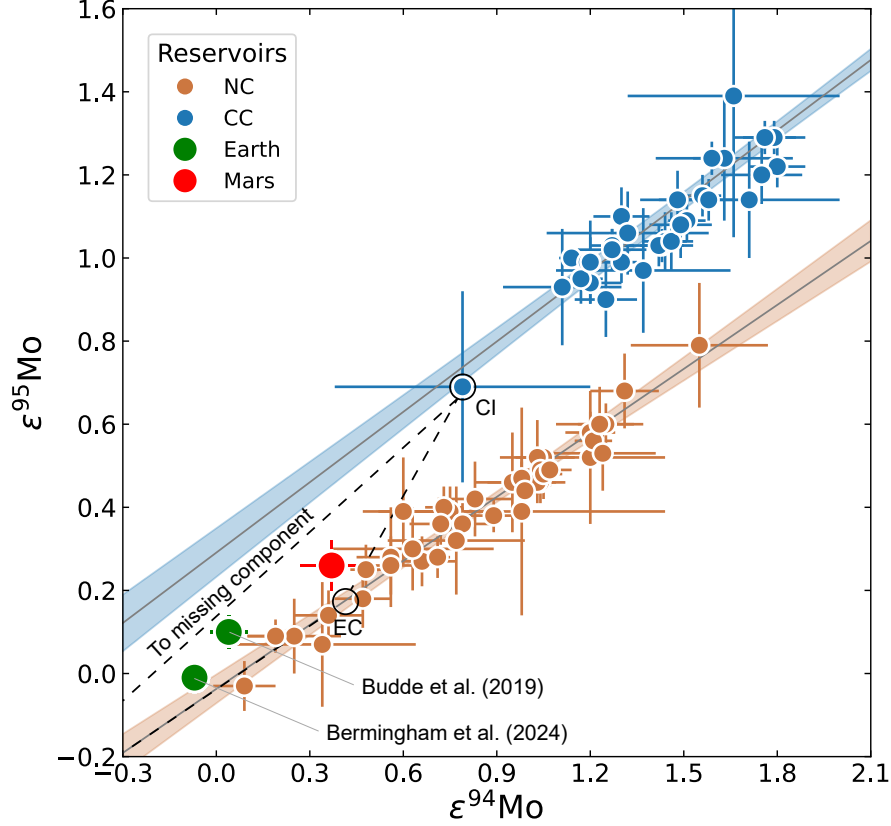


Figure 20: Compositions of CC meteorites (blue circles), NC meteorites (red circles), the Earth (green circle) and Mars (red circle) expressed in terms of their $\epsilon^{94}\text{Mo}$ and $\epsilon^{95}\text{Mo}$ isotopic compositions. Data from *Spitzer et al.* [2025]. The CC and NC trends were fit according to the York method [York et al., 2004] assuming uncorrelated errors in x and y , and yield $\epsilon^{95}\text{Mo}_{\text{NC}} = (0.517 \pm 0.028) \times \epsilon^{94}\text{Mo}_{\text{NC}} - 0.045 \pm 0.026$ and $\epsilon^{95}\text{Mo}_{\text{CC}} = (0.560 \pm 0.023) \times \epsilon^{94}\text{Mo}_{\text{CC}} + 0.298 \pm 0.037$ (all uncertainties 2- σ ; red and blue envelopes). Black circles indicate compositions of end-members in a three-component mixture reproducing the composition of the BSE in hypothesis B, in which the ‘missing component’ has $\epsilon^{94}\text{Mo} = -0.60$ and $\epsilon^{95}\text{Mo} = -0.30$ [Burkhardt et al., 2021]. In this scheme the contributions to the Mo budget of the BSE of *Budde et al.* [2019] can be reproduced by 50 % missing component, 20 % EC and 30 % CI. The BSE value of *Bermingham et al.* [2024] does not require a CC contribution within uncertainty, but does not exclude it.

$\epsilon^{95}\text{Mo} = -0.01 \pm 0.03$. Because this composition overlaps with that of a single IAB iron meteorite and, hence, is on the limit of resolution at 1- σ from the NC line and within uncertainty at 2- σ (Fig. 20), these authors argue for a purely NC origin of the BSEs Mo.

In hypothesis B, the fraction of CC-derived Mo is similar to the 30 % CC-derived Zn in the BSE deduced by *Steller et al.* [2022] and *Savage et al.* [2022]. In this model, given that enstatite chondrites are taken as the NC end-member, the fraction of CC-derived Mo in the BSE can be calculated using $\Delta^{95}\text{Mo}$, which represents a measure

of the position of a sample relative to the NC- and CC-lines. The BSE composition of *Berminham et al.* [2024] results in $\Delta^{95}\text{Mo} = 3 \pm 3$ for the BSE; using $\Delta^{95}\text{Mo} = -7 \pm 4$ for enstatite chondrites and $\Delta^{95}\text{Mo} = 26 \pm 2$ for the CC reservoir then results in $31 \pm 17\%$ CC-derived Mo in the BSE for hypothesis B, whereas using instead the value of *Budde et al.* [2019] yields $41 \pm 17\%$ CC-derived Mo in the BSE [see *Nimmo et al.*, 2024]. Therefore, hypothesis B indicates some of the BSE’s Mo derived from CC material. In this model, because Mo (siderophile) and Zn (volatile) are depleted in the BSE with respect to RLEs, their isotopic compositions do not reflect the bulk CC fraction in the Earth, but rather the late-stage addition of volatile-rich, CC material to the Earth [*Kleine and Nimmo*, 2024; *Nimmo et al.*, 2024]. In hypothesis B, the BSE’s Mo isotopic composition is reconciled by a three-component mixture of CI, EC and *s*-process-enriched NC material [the missing component, see Fig. 20, *Burkhardt et al.*, 2021; *Budde et al.*, 2019].

On the other hand, if the Mo BSE interpretation of *Berminham et al.* [2024] is correct, and if the isotopic composition of Zn is also taken to be consistent with that of an NC body, then this leads to a third hypothesis (C) in which the isotopic composition of the BSE is an entirely NC body whose composition is related to, but more extreme than other NC bodies. It should be noted that, converting the fraction of the CC-derived Mo in the BSE from hypothesis B into an actual mass of CC bodies accreted by Earth is difficult, mainly because the Mo isotopic composition of the missing component in hypothesis B is not known precisely, and, since almost all the Mo of a body might be expected to reside in its metallic core, only a fraction of this Mo may now be recorded in the BSE. Thus, hypotheses B and C may eventually be reconciled if the mass fraction of the CC contribution to the BSE is small (i.e., within uncertainty). Hypothesis C naturally resolves the apparent contradiction in the CI-like Fe isotopic composition of the BSE (see section 7.1) as well as the *s*-process excesses observed in nuclides of heavy elements such as Zr, because, in both cases, the BSE is consistent with a linear extension of the NC trend [see also *Render et al.*, 2022]. These ideas remain to be thoroughly tested.

7.3 Implications for the astrophysical setting and redox state of the Earth and planets

It is clear that hypothesis A requires considerable quantities of outer solar system material ($\sim 40\%$), hypothesis B requires a small fraction ($\sim 6\%$), while hypothesis C states that there is essentially none within some as yet undefined uncertainty ($\sim 0\%$). A schematic illustration as to how these scenarios could have played out spatio-temporally is shown in Fig. 21.

The initial conditions (t_1 , Fig. 21) for all models invoke inner (NC) or outer (CC) solar system provenance, the approximate boundary between which is the present-day asteroid belt [*Kruijer et al.*, 2017]. Physical isolation of these two reservoirs is grounded in the observation that, isotopically, there is a dearth of planetary materials that show compositions intermediate to these groups. Isotopic variations in CIs, particularly in Fe as well as Cr [*Schiller et al.*, 2020; *Hopp et al.*, 2022b; *van Kooten et al.*, 2024], have been used as a basis for the existence of a third reservoir [*Yap and Tissot*, 2023; *Dauphas et al.*, 2024]. Nevertheless, the CI reservoir is thought, initially, to have resided in the outer solar system.

The interpretations diverge at t_2 (cf. Fig. 21), where hypothesis A indicates significant inflow of CC material to the inner disk, which was initially sporadic to explain the compositions of early-formed NC planetesimals [ureilite parent body, angrite parent body, *Schiller et al.*, 2018] but ramped up over time, resulting in $\sim 40\%$ CC in the fully-formed Earth. In hypothesis A, this reflects the inward drift of CI-like pebbles [e.g., *Johansen et al.*, 2023]. In hypotheses B and C, the contribution of CC material was either limited and occurred late during the accretion of the Earth (t_3 , B) or was absent altogether (t_3 , C). One mechanism for arresting inward drift would have been upon cooling of the disk and the formation of rings associated with pressure bumps [section 3, *Whipple*, 1972; *Carrera et al.*, 2021], compounded by the subsequent formation of giant planets [*Lau et al.*, 2024] that hindered transport of condensing grains outside of heliocentrically restricted zones (Fig. 21, t_2). In this way, the rings could have evolved locally in terms of chemical

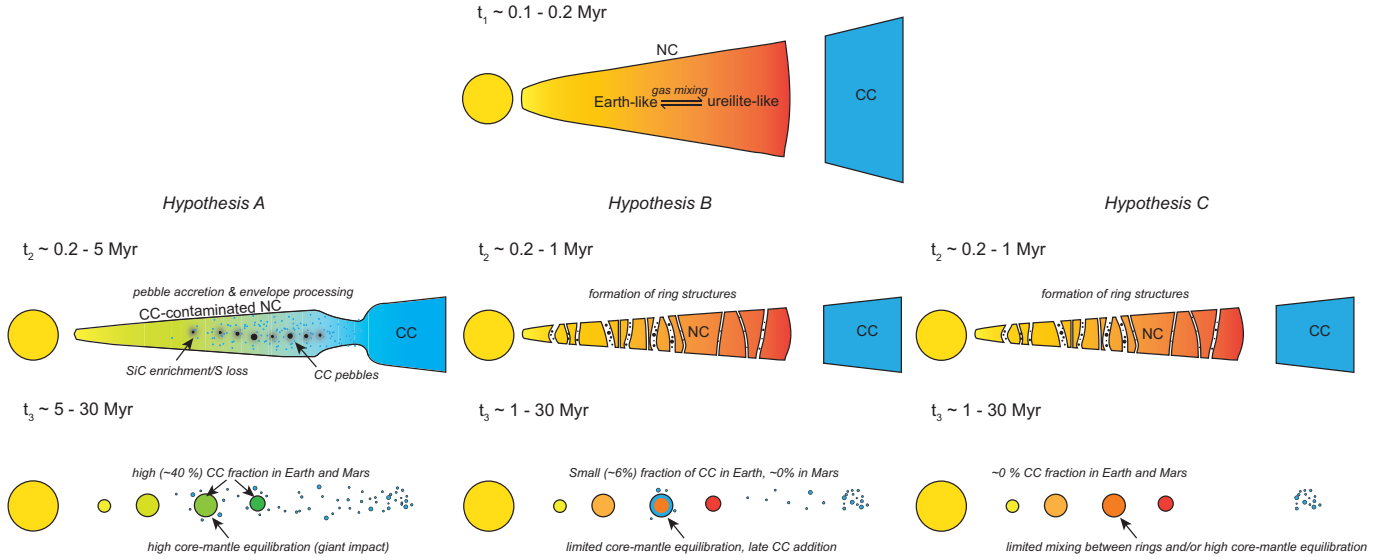


Figure 21: Schematic illustration of the astrophysical setting of planetary accretion through time.

compositions through ^{26}Al heating and collisions within the rings, but would have undergone little mixing outside of these zones, consistent with the preservation of bodies in the NC trend with distinct isotopic compositions.

Mars does not show strong evidence for heterogeneous accretion [in that its isotopic composition lies between EC and OC for most systems, see *Dauphas et al.*, 2024; *Bizzarro et al.*, 2025; *Liebske et al.*, 2025] and also contains *less* CC material than does the Earth [see *Paquet et al.*, 2023; *Kleine et al.*, 2023, at least for hypotheses A and B], despite its more proximal location to the presumed CC reservoir in the outer solar system. This poses a dynamical challenge, particularly because Mars formed earlier than did the Earth [*Dauphas and Pourmand*, 2011] and would have therefore been able to accrete any CC material scattered inwards during the early growth and migration of Jupiter [see *Kleine and Nimmo*, 2024, for a discussion]. As a result, pebble accretion is hard to reconcile with the CC-poor nature of Mars. The observations can, however, be explained if Earth but not Mars received a late CC-embryo impact, as discussed in *Nimmo et al.* [2024]. Recent dynamical simulations [*Branco et al.*, 2025] support this argument.

Hypothesis C states that Mars and Earth are equally (and essentially entirely) NC, and that the Earth either i) accreted material of, on average, uniform provenance through time and/or ii) any pre-existing signature of heterogeneous accretion in the BSE was reset by perfect core-mantle equilibration, in which the isotopic composition of the mantle exchanges completely with that of the underlying core at the completion of Earth's accretion. Homogeneous accretion with respect to chemical composition is unlikely on the basis that increasing $f\text{O}_2$ during terrestrial core formation appears to be required by *Rubie et al.* [2015, 2025], [see discussion in section 5.2, *Siebert et al.*, 2013]. Although this does not *per se* mandate a difference in the nucleosynthetic origin of such material, it would seem logical that chemical differences, especially in oxidation state, are linked to nucleosynthetic variations. On the other hand, $f\text{O}_2$ changes accompany changing $P - T$ conditions of chemically identical material (Sect. 5.2), such that this process cannot be used as an argument for accretion of compositionally or isotopically heterogeneous material. Therefore, while hypothesis B is consistent with many observations, hypothesis C, though promising, will require further investigation, in particular for the Zn and Mo isotope signatures of the BSE, and its ability to reproduce the BSEs depletion in

siderophile elements with homogeneous accretion.

Importantly, hypothesis A appeals to CI material to oxidise the inner disk. Taking the bulk composition of CI chondrites, and assuming that all H associated with H_2O is lost while O remains behind, mixtures between an NC body (here EH) and CI chondrites are used to compute Fe/O ratios. For an Fe/O of 1.04 for EH and 0.40 for CI by mass [Wasson and Kallemeyn, 1988], addition of 6 % CI material gives a bulk Earth Fe/O ratio of 0.97, whereas 40 % results in 0.70. The best estimate for the bulk Earth yields 1.07 (Table 4), suggesting O must be lost, too, in hypothesis A to reproduce the composition of the Earth. This would imply mass loss of O-bearing rocky materials (e.g., the Earth’s mantle), as the amount of O that binds with nominally volatile components (e.g., CO_2) is insignificant with respect to that stored in the mantle. Hypothesis C provides no information as to the oxidation state of the Earth, other than to imply that it must be intrinsic to the material of the inner solar system.

8 Summary, future directions and extension to other planets

Here we summarise some of the key findings from this work, and highlight possible future directions to understand terrestrial planet formation in our Solar System.

- The major telluric bodies, in terms of their core-mantle ratios, are slightly- (Earth) to strongly (Moon, Mercury) non-chondritic, while small telluric bodies are more oxidised (i.e., have more Fe as FeO) than any chondrite. Consequently, the Mg and Fe concentrations of the Earth, Moon and Mercury cannot be explained by any mixture of condensed materials from a canonical solar nebula. Other processes, such as a non-solar bulk composition, physical sorting of metal/silicate grains and/or collisional erosion are required.
- Disk viscosities are much higher than those controlled by internal (molecular) viscosities in order to match the observed mass accretion rate of T-Tauri stars. The Sun must have lost angular momentum to the planets via early, likely magnetised outflows. The modern thinking on disks therefore states that they probably transitioned from hot and rapidly radially expanding (> 1000 K inward of 1 AU) to cold and accreting very early on in their history (within a few 100 kyr). In the cold phase the snow line was inwards of 1 AU.
- Equilibrium and non-equilibrium condensation of the solar nebula effectively discriminates between elements according to their volatilities, owing to the limited range of temperatures over which the budget of a given element condenses (50–100 K). The compositions of small telluric bodies *do* adhere to this expectation. However, the terrestrial planets do not exhibit the step-pattern expected for condensation/evaporation at a single temperature, indicating they accreted from a mixture of materials that experienced different thermal histories.
- Equilibrium condensation of the solar nebula predicts that there should be a correlation between the moderately volatile element content of the condensed grains and their oxygen content. This results from the condensation of S into FeS and additional O into FeO at similar temperatures (starting at ~ 700 K and ~ 550 K, respectively, independent of pressure). Because O condenses after S, this predicts that small telluric bodies and many iron meteorite parent bodies, which are almost exclusively oxidised (i.e., inferred mantle FeO contents > 10 wt. %), should have their full complement of moderately volatile elements, which is not observed. Instead, this suggests either *i*) alternative mechanisms for their oxidation and/or *ii*) subsequent loss of highly volatile (H, C) and moderately volatile (S, Zn, etc.) elements at conditions distinct from those of the solar nebula.
- The mantle FeO content of the Earth can be produced from initially reduced materials (all Fe as Fe^0), provided core-mantle equilibration occurred at mean conditions of ~ 40 GPa and ~ 3150 K, but requires higher Fe/O ratios (~ 1.06) than found in chondrites (0.4, CI to 1.04, EH) or in mixtures of equilibrium condensates (~ 0.81 to 0.93).

- Enrichment in heavy isotopes of moderately volatile elements (except for Cr, which tends to lighter values) on small telluric bodies is correlated to the extent of their elemental depletion, implying a Rayleigh process governing their loss. A correlation also exists between the isotopic fractionation and the present-day escape velocities of bodies over a range of masses (from Vesta to Earth). Evaporative loss is generally expected to result in the residues (planets) being enriched in heavier isotopes, but is not effective for bodies of Moon-mass or greater unless their atmospheres were H₂-dominated.
- The inferred fractionation factors of mass-dependent stable isotope fractionation, together with the light isotope enrichment of Cr in small telluric bodies (Moon, Vesta, but not the angrite parent body) are indicative of the attainment of near-equilibrium between vapour- and condensed phase(s) during their separation. This high degree of equilibration implies that there is no means of discriminating between evaporation or condensation.
- Volatile depletion from small telluric bodies (except the Moon) must have occurred within a few million years after the condensation of the first solids, and therefore likely in the presence of the nebular gas. Nevertheless, the ratios of moderately volatile elements (Mn/Na, K/Li, Mn/Mg) show evidence for evaporation under more oxidised conditions ($\Delta IW-1$) and at higher temperatures ($\sim 1400-1800$ K) than in a canonical solar nebula.
- The growth of planets is consistent with mixing of small bodies of variable composition through collisions to produce increasingly more massive bodies. This process reconciles the observation that small telluric bodies have step function-like abundance patterns together with isotopically heavy moderately volatile element stable isotope ratios, while more massive bodies have increasingly smooth abundance patterns, are more volatile-rich, and have chondritic stable isotope compositions.
- A ureilite-like proto-Earth for Cr- and Ti isotopes implies 40 % by mass CI chondrites to match the composition of the Earth. This delivers too many volatile elements with respect to the present-day Earth's mantle and would therefore require volatile loss thereafter. Furthermore, this loss would have had to have happened without significant fractionation of mass-dependent stable isotope compositions and the preferential loss of *s*-process depleted material to satisfy the Mo isotope composition of the BSE. Further work on volatile loss mechanisms from a protoplanet embedded in an H₂-rich disk is required to assess this hypothesis.
- An enstatite chondrite-like proto-Earth requires only 6 % by mass CI chondrite addition, broadly in-line with the present-day abundances of the volatile elements in the BSE. So that this 6 % of CI material delivers the $\sim 30-40$ % of the Mo and Zn budgets, the proto-Earth's mantle would have had to have had sub-CI Mo and Zn abundances (e.g. by core formation and volatile loss, respectively). This hypothesis implies the Earth accreted heterogeneously with respect to early-accreted inner (NC) material and late-accreted (CC) material. Because the BSE is an end-member with respect to the compositions of heavy elements (Zr, Mo and Ru), the NC component must contain a mixture of on average enstatite chondrite-like material and a missing component not preserved in the meteorite collection.
- The evidence for a minor contribution of CC material to an otherwise NC Earth (hypothesis B) is based entirely on the BSEs Zn and Mo isotope composition. For both some uncertainty exists in the estimated CC fractions, which is mostly related to uncertainties in the isotopic composition of the missing component accreted by Earth. Provided the CC fractions for these two elements are even smaller than currently estimated, as permitted by their uncertainties, the Earth may be considered an essentially pure NC body whose composition is more extreme than other NC bodies uniformly across all elements (hypothesis C).
- There must have been a population of oxidised, volatile-depleted bodies in the inner solar system, given that the Earth represents nearly 50 % of its mass and is markedly poorer in both highly- and moderately volatile

elements than chondrites. The oxidation states of these bodies must have been somewhat elevated (ΔIW -1 to -2) with respect to the solar nebula (ΔIW -6). The Earth and Mars obtained their moderately volatile element budgets largely (~ 60 – 100 %, Earth) or almost entirely (Mars) from NC bodies, implying that oxidised, MVE-rich bodies were endemic to the inner disk.

- One mechanism to prevent ingress of CC material into the inner disk is through trapping at pressure bumps and/or giant planet growth. However, cooling of a solar composition gas to completion should still result in CI-like abundances of volatile elements, which are not observed in the terrestrial planets. As such, it may imply that relatively high temperatures were sustained in the inner disk until the dispersal of gas and/or this dispersal occurred earlier than it did in the CC-forming region.
- Evidence for a clear heliocentric gradient in composition preserved in the planets is incomplete, despite a decrease in core/mantle ratio with distance from the Sun. The composition of Mercury will be key to constraining the extent to which volatile elements were able to condense at small heliocentric distances. Additional constraints on its moment of inertia and core density will be instrumental to facilitate better estimates of its composition.

Acknowledgements

We thank the handling editor, Dominik Hezel, for his patience and persistence in helping us see this contribution over the finish line, and to two anonymous reviewers, who highlighted the role of dust transport, envelope processing, oxygen isotope constraints, and other factors in the cosmochemical evolution of the early solar system. This contribution was the fruit of an ISSI Meeting held in Bern in July, 2023, a follow-up held at ETH Zürich in October, 2023 and finally in IPG Paris in May, 2024. PAS is grateful to the Swiss National Science Foundation (SNSF) via an Eccellenza Professorship (203668) and the Swiss State Secretariat for Education, Research and Innovation (SERI) under contract number MB22.00033, a SERI-funded ERC Starting Grant “2ATMO”. FN acknowledges support from NSF-CSEDI-2054876 and NASA-EW-80NSSC18K0594. RCH acknowledges support from the European Research Council (ERC-STG-2020 grant 949417 - VapLoss) and the Italian Ministry of University and Research (NRRP M4C2 Investment 1.2 Young Researchers grant ERC-PI_0000002 - VapourTime).

Conflict of interest statement

Not applicable.

References

- Agnor, C. B., R. M. Canup, and H. F. Levison, On the character and consequences of large impacts in the late stage of terrestrial planet formation, *Icarus*, 142(1), 219–237, 1999.
- Akram, W., M. Schönbachler, S. Bisterzo, and R. Gallino, Zirconium isotope evidence for the heterogeneous distribution of s-process materials in the solar system, *Geochimica et Cosmochimica Acta*, 165, 484–500, 2015.
- Alexander, C. M., Quantitative models for the elemental and isotopic fractionations in chondrites: The carbonaceous chondrites, *Geochimica et Cosmochimica Acta*, 254, 277–309, 2019.
- Alexander, R. D., C. Clarke, and J. Pringle, Photoevaporation of protoplanetary discs—ii. evolutionary models and observable properties, *Monthly Notices of the Royal Astronomical Society*, 369(1), 229–239, 2006.
- Amelin, Y., A. N. Krot, I. D. Hutcheon, and A. A. Ulyanov, Lead isotopic ages of chondrules and calcium-aluminum-rich inclusions, *Science*, 297(5587), 1678–1683, 2002.

- Andrault, D., N. Bolfan-Casanova, G. L. Nigro, M. A. Bouhifd, G. Garbarino, and M. Mezouar, Solidus and liquidus profiles of chondritic mantle: Implication for melting of the earth across its history, *Earth and planetary science letters*, 304(1-2), 251–259, 2011.
- Armitage, P. J., C. J. Clarke, and F. Palla, Dispersion in the lifetime and accretion rate of t tauri discs, *Monthly Notices of the Royal Astronomical Society*, 342(4), 1139–1146, 2003.
- Armstrong, R., R. Georg, P. Savage, H. Williams, and A. Halliday, Silicon isotopes in meteorites and planetary core formation, *Geochimica et Cosmochimica Acta*, 75(13), 3662–3676, 2011.
- Armstrong, R., R. Georg, H. Williams, and A. Halliday, Silicon isotopes in lunar rocks: Implications for the moons formation and the early history of the earth, *Geochimica et Cosmochimica Acta*, 77, 504–514, 2012.
- Aston, F., The rarity of the inert gases on the earth, *Nature*, 114(2874), 786–786, 1924.
- Badro, J., A. S. Côté, and J. P. Brodholt, A seismologically consistent compositional model of earths core, *Proceedings of the National Academy of Sciences*, 111(21), 7542–7545, 2014.
- Bai, X.-N., and J. M. Stone, Local study of accretion disks with a strong vertical magnetic field: Magnetorotational instability and disk outflow, *The Astrophysical Journal*, 767(1), 30, 2013.
- Balbus, S. A., and J. F. Hawley, Instability, turbulence, and enhanced transport in accretion disks, *Rev. Mod. Phys.*, 70, 1–53, 1998.
- Batygin, K., and A. Morbidelli, Self-consistent model for dust-gas coupling in protoplanetary disks, *Astronomy & Astrophysics*, 666, A19, 2022.
- Bercovici, H. L., L. T. Elkins-Tanton, J. G. O’Rourke, and L. Schaefer, The effects of bulk composition on planetesimal core sulfur content and size, *Icarus*, 380, 114,976, 2022.
- Bermingham, K., H. Tornabene, R. Walker, L. Godfrey, B. Meyer, P. Piccoli, and S. Mojzsis, The non-carbonaceous nature of earths late-stage accretion, *Geochimica et Cosmochimica Acta*, 2024.
- Bermingham, K. R., E. Füri, K. Lodders, and B. Marty, The nc-cc isotope dichotomy: Implications for the chemical and isotopic evolution of the early solar system, *Space science reviews*, 216, 1–29, 2020.
- Bitsch, B., A. Morbidelli, E. Lega, and A. Crida, Stellar irradiated discs and implications on migration of embedded planets-ii. accreting-discs, *Astronomy & Astrophysics*, 564, A135, 2014.
- Bitsch, B., A. Johansen, M. Lambrechts, and A. Morbidelli, The structure of protoplanetary discs around evolving young stars, *Astronomy & Astrophysics*, 575, A28, 2015.
- Bizzarro, M., A. Johansen, and C. Dorn, The cosmochemistry of planetary systems, *Nature Reviews Chemistry*, pp. 1–19, 2025.
- Blanchard, I., D. C. Rubie, E. S. Jennings, I. A. Franchi, X. Zhao, S. Petitgirard, N. Miyajima, S. A. Jacobson, and A. Morbidelli, The metal–silicate partitioning of carbon during earth’s accretion and its distribution in the early solar system, *Earth and Planetary Science Letters*, 580, 117,374, 2022.
- Bloom, H., K. Lodders, H. Chen, C. Zhao, Z. Tian, P. Koefoed, M. K. Pető, Y. Jiang, and K. Wang, Potassium isotope compositions of carbonaceous and ordinary chondrites: Implications on the origin of volatile depletion in the early solar system, *Geochimica et Cosmochimica Acta*, 277, 111–131, 2020.

- Bollard, J., J. N. Connelly, M. J. Whitehouse, E. A. Pringle, L. Bonal, J. K. Jørgensen, Å. Nordlund, F. Moynier, and M. Bizzarro, Early formation of planetary building blocks inferred from pb isotopic ages of chondrules, *Science Advances*, 3(8), e1700407, 2017.
- Bonnand, P., H. Williams, I. Parkinson, B. Wood, and A. Halliday, Stable chromium isotopic composition of meteorites and metal–silicate experiments: Implications for fractionation during core formation, *Earth and Planetary Science Letters*, 435, 14–21, 2016.
- Borg, L. E., L. E. Nyquist, H. Wiesmann, and Y. Reese, Constraints on the petrogenesis of martian meteorites from the rb-sr and sm-nd isotopic systematics of the lherzolitic shergottites alh77005 and lew88516, *Geochimica et Cosmochimica Acta*, 66(11), 2037–2053, 2002.
- Bouhifd, M. A., and A. P. Jephcoat, The effect of pressure on partitioning of ni and co between silicate and iron-rich metal liquids: a diamond-anvil cell study, *Earth and Planetary Science Letters*, 209(1-2), 245–255, 2003.
- Bourdon, B., M. Roskosz, and R. C. Hin, Isotope tracers of core formation, *Earth-Science Reviews*, 181, 61–81, 2018.
- Boyce, J. W., F. M. McCubbin, N. Lunning, and T. Anderson, Large carbonaceous chondrite parent bodies favored by abundance–volatility modeling: A possible chemical signature of pebble accretion, *The Planetary Science Journal*, 5(2), 53, 2024.
- Boyet, M., and A. Gannoun, Nucleosynthetic nd isotope anomalies in primitive enstatite chondrites, *Geochimica et Cosmochimica Acta*, 121, 652–666, 2013.
- Branco, D., P. Machado, and S. N. Raymond, Dynamical origin of theia, the last giant impactor on earth, *Icarus*, p. 116724, 2025.
- Brasser, R., and S. J. Mojzsis, The partitioning of the inner and outer solar system by a structured protoplanetary disk, *Nature Astronomy*, 4, 492–499, 2020.
- Braukmüller, N., F. Wombacher, D. C. Hezel, R. Escoube, and C. Münker, The chemical composition of carbonaceous chondrites: Implications for volatile element depletion, complementarity and alteration, *Geochimica et Cosmochimica Acta*, 239, 17–48, 2018.
- Brugier, Y.-A., J.-A. Barrat, B. Gueguen, A. Agranier, A. Yamaguchi, and A. Bischoff, Zinc isotopic variations in ureilites, *Geochimica et Cosmochimica Acta*, 246, 450–460, 2019.
- Budde, G., C. Burkhardt, G. A. Brenneka, M. Fischer-Gödde, T. S. Kruijer, and T. Kleine, Molybdenum isotopic evidence for the origin of chondrules and a distinct genetic heritage of carbonaceous and non-carbonaceous meteorites, *Earth and Planetary Science Letters*, 454, 293–303, 2016.
- Budde, G., C. Burkhardt, and T. Kleine, Molybdenum isotopic evidence for the late accretion of outer solar system material to earth, *Nature Astronomy*, 3(8), 736–741, 2019.
- Budde, G., F. L. Tissot, T. Kleine, and R. T. Marquez, Spurious molybdenum isotope anomalies resulting from non-exponential mass fractionation, *Geochemistry*, 83(3), 126,007, 2023.
- Burkhardt, C., T. Kleine, F. Oberli, A. Pack, B. Bourdon, and R. Wieler, Molybdenum isotope anomalies in meteorites: Constraints on solar nebula evolution and origin of the earth, *Earth and Planetary Science Letters*, 312(3-4), 390–400, 2011.

- Burkhardt, C., L. Borg, G. Brennecke, Q. Shollenberger, N. Dauphas, and T. Kleine, A nucleosynthetic origin for the earths anomalous 142nd composition, *Nature*, 537(7620), 394–398, 2016.
- Burkhardt, C., F. Spitzer, A. Morbidelli, G. Budde, J. H. Render, T. S. Kruijer, and T. Kleine, Terrestrial planet formation from lost inner solar system material, *Science advances*, 7(52), eabj7601, 2021.
- BVSP, *Basaltic Volcanism on the Terrestrial Planets*, 1286 pp., Pergamon Press, Inc., 1981.
- Béthune, W., G. Lesur, and J. Ferreira, Global simulations of protoplanetary disks with net magnetic flux - i. non-ideal mhd case, *A&A*, 600, A75, 2017.
- Calogero, M. A., F. Nimmo, and R. C. Hin, Can impact-induced heating drive moderately volatile element loss?, *Earth and Planetary Science Letters*, 669, 119,580, 2025.
- Campbell, I. H., and H. S. C. O'Neill, Evidence against a chondritic earth, *Nature*, 483(7391), 553–558, 2012.
- Carrera, D., J. B. Simon, R. Li, K. A. Kretke, and H. Klahr, Protoplanetary disk rings as sites for planetesimal formation, *The Astronomical Journal*, 161(2), 96, 2021.
- Carter, P. J., Z. M. Leinhardt, T. Elliott, M. J. Walter, and S. T. Stewart, Compositional evolution during rocky protoplanet accretion, *The Astrophysical Journal*, 813(1), 72, 2015.
- Carter, P. J., Z. M. Leinhardt, T. Elliott, S. T. Stewart, and M. J. Walter, Collisional stripping of planetary crusts, *Earth and Planetary Science Letters*, 484, 276–286, 2018.
- Cartier, C., L. Llado, H. Pirotte, L. Tissandier, O. Namur, M. Collinet, S.-J. Wang, and B. Charlier, Partitioning of nickel and cobalt between metal and silicate melts: Expanding the oxy-barometer to reducing conditions, *Geochimica et Cosmochimica Acta*, 367, 142–164, 2024.
- Cassen, P., Nebular thermal evolution and the properties of primitive planetary materials, *Meteoritics & Planetary Science*, 36(5), 671–700, 2001.
- Cassen, P., *Protostellar disks and planet formation*, p. 369448, Springer-Verlag Berlin Heidelberg, 2006.
- Chao, K.-H., R. deGraffenried, M. Lach, W. Nelson, K. Truax, and E. Gaidos, Lava worlds: From early earth to exoplanets, *Geochemistry*, 81(2), 125,735, 2021.
- Charles, R., Activities in li₂o-, na₂o, and k₂o-sio₂ solutions, *Journal of the American Ceramic Society*, 50(12), 631–641, 1967.
- Charnoz, S., A. Jérôme, M. Chaussidon, P. A. Sossi, Y. Marrocchi, and P. Franco, Forming the first solids precursors in the solar system through kinetic condensation, *Tech. rep.*, Copernicus Meetings, 2025.
- Charnoz, S., et al., Tidal pull of the earth strips the proto-moon of its volatiles, *Icarus*, 364, 114,451, 2021.
- Chen, J., D. Papanastassiou, and G. Wasserburg, Ruthenium endemic isotope effects in chondrites and differentiated meteorites, *Geochimica et Cosmochimica Acta*, 74(13), 3851–3862, 2010.
- Chiang, E., and A. Youdin, Forming planetesimals in solar and extrasolar nebulae, *Annual Review of Earth and Planetary Sciences*, 38(Volume 38, 2010), 493–522, doi:<https://doi.org/10.1146/annurev-earth-040809-152513>, 2010.

- Ciesla, F. J., and J. N. Cuzzi, The evolution of the water distribution in a viscous protoplanetary disk, *Icarus*, 181(1), 178–204, 2006.
- Clay, P. L., R. Burgess, H. Busemann, L. Ruzié-Hamilton, B. Joachim, J. M. Day, and C. J. Ballentine, Halogens in chondritic meteorites and terrestrial accretion, *Nature*, 551(7682), 614–618, 2017.
- Clayton, D., *Handbook of Isotopes in the Cosmos*, 2003.
- Clayton, R. N., and T. K. Mayeda, Oxygen isotope studies of achondrites, *Geochimica et Cosmochimica Acta*, 60(11), 1999–2017, 1996.
- Clayton, R. N., and T. K. Mayeda, Oxygen isotope studies of carbonaceous chondrites, *Geochimica et Cosmochimica Acta*, 63(13-14), 2089–2104, 1999.
- Clayton, R. N., N. Onuma, L. Grossman, and T. K. Mayeda, Distribution of the pre-solar component in allende and other carbonaceous chondrites, *Earth and Planetary Science Letters*, 34(2), 209–224, 1977.
- Connelly, J. N., M. Bizzarro, A. N. Krot, Å. Nordlund, D. Wielandt, and M. A. Ivanova, The absolute chronology and thermal processing of solids in the solar protoplanetary disk, *Science*, 338(6107), 651–655, 2012.
- Dauphas, N., The isotopic nature of the earths accreting material through time, *Nature*, 541(7638), 521–524, 2017.
- Dauphas, N., and A. Pourmand, Hf–w–th evidence for rapid growth of mars and its status as a planetary embryo, *Nature*, 473(7348), 489–492, 2011.
- Dauphas, N., B. Marty, and L. Reisberg, Molybdenum nucleosynthetic dichotomy revealed in primitive meteorites, *The Astrophysical Journal*, 569(2), L139, 2002.
- Dauphas, N., F.-Z. Teng, and N. T. Arndt, Magnesium and iron isotopes in 2.7 ga alexo komatiites: Mantle signatures, no evidence for soret diffusion, and identification of diffusive transport in zoned olivine, *Geochimica et Cosmochimica Acta*, 74(11), 3274–3291, 2010.
- Dauphas, N., F. Poitrasson, C. Burkhardt, H. Kobayashi, and K. Kurosawa, Planetary and meteoritic mg/si and $\delta^{30}\text{si}$ variations inherited from solar nebula chemistry, *Earth and Planetary Science Letters*, 427, 236–248, 2015.
- Dauphas, N., T. Hopp, and D. Nesvorný, Bayesian inference on the isotopic building blocks of mars and earth, *Icarus*, 408, 115,805, 2024.
- Dauphas, N., et al., The extent, nature, and origin of k and rb depletions and isotopic fractionations in earth, the moon, and other planetary bodies, *The Planetary Science Journal*, 3(2), 29, 2022.
- Day, J. M., and F. Moynier, Evaporative fractionation of volatile stable isotopes and their bearing on the origin of the moon, *Philosophical Transactions of the Royal Society A: Mathematical, Physical and Engineering Sciences*, 372(2024), 20130,259, 2014.
- Day, J. M., P. A. Sossi, C. K. Shearer, and F. Moynier, Volatile distributions in and on the moon revealed by cu and fe isotopes in the rusty rock66095, *Geochimica et Cosmochimica Acta*, 266, 131–143, 2019.
- Desch, S., M. Morris, H. Connolly, and A. P. Boss, A critical examination of the x-wind model for chondrule and calcium-rich, aluminum-rich inclusion formation and radionuclide production, *The Astrophysical Journal*, 725(1), 692, 2010.

- Dhaliwal, J. K., J. M. Day, J. B. Creech, and F. Moynier, Copper and zinc isotope compositions of pristine eucrites as analogues for differentiated planetary feedstocks, *Earth and Planetary Science Letters*, 637, 118,740, 2024.
- Drake, M. J., and K. Righter, Determining the composition of the earth, *Nature*, 416(6876), 39–44, 2002.
- Drake, M. J., H. E. Newsom, and C. J. Capobianco, V, cr, and mn in the earth, moon, epb, and spb and the origin of the moon: Experimental studies, *Geochimica et Cosmochimica Acta*, 53(8), 2101–2111, 1989.
- Dreibus, G., and H. Palme, Cosmochemical constraints on the sulfur content in the earth’s core, *Geochimica et Cosmochimica Acta*, 60(7), 1125–1130, 1996.
- Dullemond, C. P., *Theoretical Models of the Structure of Protoplanetary Disks*, ecole Doctorale des Houches, Chronology of solar system formation V: the first solids and the first planetesimals, February 10, 2013 - February 15, 2013.
- Dunham, E., A. Sheikh, D. Opara, N. Matsuda, M.-C. Liu, and K. McKeegan, Calcium–aluminum-rich inclusions in non-carbonaceous chondrites: Abundances, sizes, and mineralogy, *Meteoritics & Planetary Science*, 58(5), 643–671, 2023.
- Ebel, D. S., Condensation calculations in planetary science and cosmochemistry, *arXiv preprint arXiv:2306.12645*, 2023.
- Ebel, D. S., and L. Grossman, Condensation in dust-enriched systems, *Geochimica et Cosmochimica Acta*, 64(2), 339–366, 2000.
- Ebel, D. S., C. M. O. Alexander, and G. Libourel, *VaporMelt Exchange: Constraints on Chondrite Formation Conditions and Processes*, p. 151174, Cambridge Planetary Science, Cambridge University Press, 2018.
- Ebel, D. S., M. E. Gemma, S. P. Alpert, J. Bayron, A. H. Lobo, and M. K. Weisberg, Abundance, sizes, and major element compositions of components in cr and ll chondrites: Formation from single reservoirs, *Meteoritics & Planetary Science*, 59(9), 2276–2295, 2024.
- Eiler, J. M., Oxygen isotope variations of basaltic lavas and upper mantle rocks, *Reviews in mineralogy and geochemistry*, 43(1), 319–364, 2001.
- Fang, L., F. Moynier, J.-A. Barrat, A. Yamaguchi, M. Paquet, and M. Chaussidon, The origin of 4-vestas volatile depletion revealed by the zinc isotopic composition of diogenites, *Science Advances*, 10(33), ead11007, 2024.
- Fegley, B., Kinetics of gas-grain reactions in the solar nebula, *Space Science Reviews*, 92, 177–200, 2000.
- Fegley, B., and A. Cameron, A vaporization model for iron/silicate fractionation in the mercury protoplanet, *Earth and Planetary Science Letters*, 82(3-4), 207–222, 1987.
- Fegley, B., N. S. Jacobson, K. Williams, J. Plane, L. Schaefer, and K. Lodders, Solubility of rock in steam atmospheres of planets, *The Astrophysical Journal*, 824(2), 103, 2016.
- Fegley, B., K. Lodders, and N. S. Jacobson, Chemical equilibrium calculations for bulk silicate earth material at high temperatures, *Geochemistry*, 83(2), 125,961, 2023.
- Fegley Jr, B., Cosmochemical trends of volatile elements in the solar system, in *Origins of Solar Systems*, 1988.

- Fegley Jr, B., and H. Palme, Evidence for oxidizing conditions in the solar nebula from mo and w depletions in refractory inclusions in carbonaceous chondrites, *Earth and Planetary Science Letters*, 72(4), 311–326, 1985.
- Fegley Jr, B., K. Lodders, and N. S. Jacobson, Volatile element chemistry during accretion of the earth, *Geochemistry*, 80(1), 125,594, 2020.
- Feigelson, E. D., and T. Montmerle, High-energy processes in young stellar objects, *Annual Review of Astronomy and Astrophysics*, 37(1), 363–408, 1999.
- Fischer, R. A., and W. F. McDonough, Earth’s core composition and core formation, *Treatise of Geochemistry*, 3rd edition, 1, 17–71, 2025.
- Fischer, R. A., Y. Nakajima, A. J. Campbell, D. J. Frost, D. Harries, F. Langenhorst, N. Miyajima, K. Pollok, and D. C. Rubie, High pressure metal–silicate partitioning of ni, co, v, cr, si, and o, *Geochimica et Cosmochimica Acta*, 167, 177–194, 2015.
- Fischer, R. A., E. Cottrell, E. Hauri, K. K. Lee, and M. Le Voyer, The carbon content of earth and its core, *Proceedings of the National Academy of Sciences*, 117(16), 8743–8749, 2020.
- Fischer-Gödde, M., and T. Kleine, Ruthenium isotopic evidence for an inner solar system origin of the late veneer, *Nature*, 541(7638), 525–527, 2017.
- Fischer-Gödde, M., C. Burkhardt, T. S. Kruijer, and T. Kleine, Ru isotope heterogeneity in the solar protoplanetary disk, *Geochimica et Cosmochimica Acta*, 168, 151–171, 2015.
- Flock, M., S. Fromang, N. J. Turner, and M. Benisty, 3d radiation nonideal magnetohydrodynamical simulations of the inner rim in protoplanetary disks, *The Astrophysical Journal*, 835(2), 230, 2017.
- Frossard, P., C. Israel, A. Bouvier, and M. Boyet, Earths composition was modified by collisional erosion, *Science*, 377(6614), 1529–1532, 2022.
- Frost, D., U. Mann, Y. Asahara, and D. Rubie, The redox state of the mantle during and just after core formation, *Philosophical Transactions of the Royal Society A: Mathematical, Physical and Engineering Sciences*, 366(1883), 4315–4337, 2008.
- Frost, D. J., and C. A. McCammon, The redox state of earth’s mantle, *Annu. Rev. Earth Planet. Sci.*, 36, 389–420, 2008.
- Fu, R. R., M. W. Volk, D. Bilardello, G. Libourel, G. R. Lesur, and O. Ben Dor, The fine-scale magnetic history of the allende meteorite: Implications for the structure of the solar nebula, *Agu Advances*, 2(3), e2021AV000,486, 2021.
- Gessmann, C., B. Wood, D. Rubie, and M. Kilburn, Solubility of silicon in liquid metal at high pressure: implications for the composition of the earths core, *Earth and Planetary Science Letters*, 184(2), 367–376, 2001.
- Goodrich, C. A., J. A. Van Orman, and L. Wilson, Fractional melting and smelting on the ureilite parent body, *Geochimica et Cosmochimica Acta*, 71(11), 2876–2895, 2007.
- Gounelle, M., F. H. Shu, H. Shang, A. Glassgold, K. Rehm, and T. Lee, Extinct radioactivities and protosolar cosmic rays: Self-shielding and lightelements, *The Astrophysical Journal*, 548(2), 1051, 2001.
- Gressel, O., N. J. Turner, R. P. Nelson, and C. P. McNally, Global simulations of protoplanetary disks with ohmic resistivity and ambipolar diffusion, *The Astrophysical Journal*, 801(2), 84, 2015.

- Grewal, D. S., N. X. Nie, B. Zhang, A. Izidoro, and P. D. Asimow, Accretion of the earliest inner solar system planetesimals beyond the water snowline, *Nature Astronomy*, 8(3), 290–297, 2024.
- Grossman, L., Condensation in the primitive solar nebula, *Geochimica et Cosmochimica Acta*, 36(5), 597–619, 1972.
- Grossman, L., and J. W. Larimer, Early chemical history of the solar system, *Reviews of Geophysics*, 12(1), 71–101, 1974.
- Grossman, L., J. R. Beckett, A. V. Fedkin, S. B. Simon, and F. J. Ciesla, Redox conditions in the solar nebula: Observational, experimental, and theoretical constraints, *Reviews in Mineralogy and Geochemistry*, 68(1), 93–140, 2008.
- Grossman, L., A. V. Fedkin, and S. B. Simon, Formation of the first oxidized iron in the solar system, *Meteoritics & Planetary Science*, 47(12), 2160–2169, 2012.
- Halliday, A., and D. Porcelli, In search of lost planets—the paleocosmochemistry of the inner solar system, *Earth and Planetary Science Letters*, 192(4), 545–559, 2001.
- Hans, U., T. Kleine, and B. Bourdon, Rb-sr chronology of volatile depletion in differentiated protoplanets: Babi, ador and all revisited, *Earth and Planetary Science Letters*, 374, 204–214, 2013.
- Hartmann, L., N. Calvet, E. Gullbring, and P. D’Alessio, Accretion and the evolution of t tauri disks, *The Astrophysical Journal*, 495(1), 385, 1998.
- Hauck, S. A., et al., The curious case of mercury’s internal structure, *Journal of Geophysical Research: Planets*, 118(6), 1204–1220, 2013.
- Haugbølle, T., P. Weber, D. P. Wielandt, P. Benítez-Llambay, M. Bizzarro, O. Gressel, and M. E. Pessah, Probing the protosolar disk using dust filtering at gaps in the early solar system, *The Astronomical Journal*, 158(2), 55, 2019.
- Helbert, J., A. Maturilli, M. Dyar, and G. Alemanno, Deriving iron contents from past and future venus surface spectra with new high-temperature laboratory emissivity data, *Science Advances*, 7(3), eaba9428, 2021.
- Hellmann, J. L., T. Hopp, C. Burkhardt, and T. Kleine, Origin of volatile element depletion among carbonaceous chondrites, *Earth and Planetary Science Letters*, 549, 116,508, 2020.
- Herzog, G., F. Moynier, F. Albarède, and A. Berezhnoy, Isotopic and elemental abundances of copper and zinc in lunar samples, zagami, peles hairs, and a terrestrial basalt, *Geochimica et Cosmochimica Acta*, 73(19), 5884–5904, 2009.
- Hewins, R., H. Connolly, G. Lofgren Jr, and G. Libourel, Experimental constraints on chondrule formation, in *Chondrites and the protoplanetary disk*, vol. 341, p. 286, 2005.
- Hezel, D. C., S. S. Russell, A. J. Ross, and A. T. Kearsley, Modal abundances of cais: Implications for bulk chondrite element abundances and fractionations, *Meteoritics & Planetary Science*, 43(11), 1879–1894, 2008.
- Hibbert, K. E., H. Williams, A. C. Kerr, and I. Puchtel, Iron isotopes in ancient and modern komatiites: evidence in support of an oxidised mantle from archaean to present, *Earth and Planetary Science Letters*, 321, 198–207, 2012.
- Hillenbrand, L. A., *Observational constraints on dust disk lifetimes: Implications for planet formation*, p. 84105, Space Telescope Science Institute Symposium Series, Cambridge University Press, 2008.

- Hin, R. C., M. W. Schmidt, and B. Bourdon, Experimental evidence for the absence of iron isotope fractionation between metal and silicate liquids at 1 gpa and 1250–1300 c and its cosmochemical consequences, *Geochimica et Cosmochimica Acta*, *93*, 164–181, 2012.
- Hin, R. C., C. Fitoussi, M. W. Schmidt, and B. Bourdon, Experimental determination of the si isotope fractionation factor between liquid metal and liquid silicate, *Earth and Planetary Science Letters*, *387*, 55–66, 2014.
- Hin, R. C., et al., Magnesium isotope evidence that accretional vapour loss shapes planetary compositions, *Nature*, *549*(7673), 511–515, 2017.
- Hirose, K., B. Wood, and L. Vočadlo, Light elements in the earths core, *Nature Reviews Earth & Environment*, *2*(9), 645–658, 2021.
- Hirschmann, M. M., E. A. Bergin, G. A. Blake, F. J. Ciesla, and J. Li, Early volatile depletion on planetesimals inferred from c–s systematics of iron meteorite parent bodies, *Proceedings of the National Academy of Sciences*, *118*(13), e2026779, 118, 2021.
- Hong, Y., and B. Fegley Jr, Experimental studies of magnetite formation in the solar nebula, *Meteoritics & Planetary Science*, *33*(5), 1101–1112, 1998.
- Hopp, T., N. Dauphas, F. Spitzer, C. Burkhardt, and T. Kleine, Earth’s accretion inferred from iron isotopic anomalies of supernova nuclear statistical equilibrium origin, *Earth and Planetary Science Letters*, *577*, 117, 245, 2022a.
- Hopp, T., et al., Ryugus nucleosynthetic heritage from the outskirts of the solar system, *Science advances*, *8*(46), eadd8141, 2022b.
- Hu, Y., F. Moynier, and M. Bizzarro, Potassium isotope heterogeneity in the early solar system controlled by extensive evaporation and partial recondensation, *Nature Communications*, *13*(1), 7669, 2022.
- Huang, D., and J. Badro, Fe-ni ideality during core formation on earth, *American Mineralogist*, *103*(10), 1707–1710, 2018.
- Huang, D., J. Siebert, and J. Badro, High pressure partitioning behavior of mo and w and late sulfur delivery during earths core formation, *Geochimica et Cosmochimica Acta*, *310*, 19–31, 2021.
- Huang, S., J. Lu, M. Prinz, M. K. Weisberg, P. H. Benoit, and D. W. Sears, Chondrules: Their diversity and the role of open-system processes during their formation, *Icarus*, *122*(2), 316–346, 1996.
- Hueso, R., and T. Guillot, Evolution of protoplanetary disks: constraints from dm tauri and gm aurigae, *A&A*, *442*(2), 703–725, 2005.
- Humayun, M., and P. Cassen, Processes determining the volatile abundances of the meteorites and terrestrial planets, *Origin of the Earth and Moon*, *1*, 3–23, 2000.
- Hunten, D. M., R. O. Pepin, and J. C. Walker, Mass fractionation in hydrodynamic escape, *Icarus*, *69*(3), 532–549, 1987.
- Ivanov, D., C. Fitoussi, and B. Bourdon, Trace element volatility and the conditions of liquid-vapor separation in the proto-lunar disk, *Icarus*, *386*, 115, 143, 2022.
- Izidoro, A., R. Dasgupta, S. N. Raymond, R. Deienno, B. Bitsch, and A. Isella, Planetesimal rings as the cause of the solar systems planetary architecture, *Nature Astronomy*, *6*(3), 357–366, 2022.

- Jacquet, E., C. Dullemond, J. Drażkowska, and S. Desch, The early solar system and its meteoritical witnesses, *Space Science Reviews*, 220(7), 78, 2024.
- Javoy, M., The integral enstatite chondrite model of the earth, *Geophysical Research Letters*, 22(16), 2219–2222, 1995.
- Jerram, M., P. Bonnard, A. C. Kerr, E. G. Nisbet, I. S. Puchtel, and A. N. Halliday, The $\delta^{53}\text{Cr}$ isotope composition of komatiite flows and implications for the composition of the bulk silicate earth, *Chemical Geology*, 551, 119,761, 2020.
- Jiang, Y., P. Koefoed, O. Pravdivtseva, H. Chen, C.-H. Li, F. Huang, L.-P. Qin, J. Liu, and K. Wang, Early solar system aqueous activity: K isotope evidence from allende, *Meteoritics & Planetary Science*, 56(1), 61–76, 2021.
- Johansen, A., T. Ronnet, M. Schiller, Z. Deng, and M. Bizzarro, Anatomy of rocky planets formed by rapid pebble accretion-i. how icy pebbles determine the core fraction and FeO contents, *Astronomy & Astrophysics*, 671, A74, 2023.
- Joos, M., P. Hennebelle, and A. Ciardi, Protostellar disk formation and transport of angular momentum during magnetized core collapse, *Astronomy & Astrophysics*, 543, A128, 2012.
- Kalyaan, A., P. Pinilla, S. Krijt, A. Banzatti, G. Rosotti, G. D. Mulders, M. Lambrechts, F. Long, and G. J. Herczeg, The effect of dust evolution and traps on inner disk water enrichment, *The Astrophysical Journal*, 954(1), 66, 2023.
- Kato, C., and F. Moynier, Gallium isotopic evidence for extensive volatile loss from the moon during its formation, *Science advances*, 3(7), e1700,571, 2017.
- Kato, C., F. Moynier, J. Foriel, F.-Z. Teng, and I. S. Puchtel, The gallium isotopic composition of the bulk silicate earth, *Chemical Geology*, 448, 164–172, 2017.
- Kegler, P., A. Holzheid, D. Frost, D. Rubie, R. Dohmen, and H. Palme, New Ni and Co metal-silicate partitioning data and their relevance for an early terrestrial magma ocean, *Earth and Planetary Science Letters*, 268(1-2), 28–40, 2008.
- Keil, K., Angrites, a small but diverse suite of ancient, silica-undersaturated volcanic-plutonic mafic meteorites, and the history of their parent asteroid, *Geochemistry*, 72(3), 191–218, 2012.
- Khan, A., P. A. Sossi, C. Liebske, A. Rivoldini, and D. Giardini, Geophysical and cosmochemical evidence for a volatile-rich Mars, *Earth and Planetary Science Letters*, 578, 117,330, 2022.
- Khan, A., D. Huang, C. Durán, P. A. Sossi, D. Giardini, and M. Murakami, Evidence for a liquid silicate layer atop the martian core, *Nature*, 622(7984), 718–723, 2023.
- Klahr, H., and A. Hubbard, Convective overstability in radially stratified accretion disks under thermal relaxation, *The Astrophysical Journal*, 788(1), 21, 2014.
- Klaver, M., S. Klemme, X.-N. Liu, R. C. Hin, C. D. Coath, M. Anand, C. J. Lissenberg, J. Berndt, and T. Elliott, Titanium-rich basaltic melts on the moon modulated by reactive flow processes, *Nature Geoscience*, pp. 1–6, 2024.
- Kleine, T., and F. Nimmo, *Origin of the Earth*, vol. 5, pp. 1–57, Elsevier, 2024.
- Kleine, T., and R. J. Walker, Tungsten isotopes in planets, *Annual review of earth and planetary sciences*, 45, 389–417, 2017.

- Kleine, T., G. Budde, C. Burkhardt, T. Kruijer, E. Worsham, A. Morbidelli, and F. Nimmo, The non-carbonaceous–carbonaceous meteorite dichotomy, *Space Science Reviews*, 216, 1–27, 2020.
- Kleine, T., T. Steller, C. Burkhardt, and F. Nimmo, An inner solar system origin of volatile elements in mars, *Icarus*, 397, 115–119, 2023.
- Koefoed, P., O. Pravdivtseva, H. Chen, C. Gerritzen, M. M. Thiemens, and K. Wang, Potassium isotope systematics of the 114 chondrite hamlet: Implications for chondrule formation and alteration, *Meteoritics & Planetary Science*, 55(8), 2020.
- Kohn, S. C., and P. F. Schofield, The importance of melt composition in controlling trace-element behaviour: an experimental study of mn and zn partitioning between forsterite and silicate melts, *Chemical Geology*, 117(1–4), 73–87, 1994.
- Kreutzberger, M. E., M. J. Drake, and J. H. Jones, Origin of the earth’s moon: Constraints from alkali volatile trace elements, *Geochimica et Cosmochimica Acta*, 50(1), 91–98, 1986.
- Kruijer, T. S., C. Burkhardt, G. Budde, and T. Kleine, Age of jupiter inferred from the distinct genetics and formation times of meteorites, *Proceedings of the National Academy of Sciences*, 114(26), 6712–6716, 2017.
- Kruijer, T. S., T. Kleine, and L. E. Borg, The great isotopic dichotomy of the early solar system, *Nature Astronomy*, 4(1), 32–40, 2020.
- Krumholz, M. R., and C. Federrath, The role of magnetic fields in setting the star formation rate and the initial mass function, *Frontiers in Astronomy and Space Sciences*, 6, 7, 2019.
- Kruttasch, P. M., and K. Mezger, Time of proto-earth reservoir formation and volatile element depletion from 53mn–53cr chronometry, *Science Advances*, 11(31), eadw1280, 2025.
- Ku, Y., and S. Jacobsen, Potassium isotope anomalies in meteorites inherited from the protosolar molecular cloud, *Science Advances*, 6(41), eabd0511, 2020.
- Kubik, E., P. A. Sossi, J. Siebert, E. Inglis, M. Roskosz, E. S. Rego, N. Wehr, and F. Moynier, The absence of an effect of nickel on iron isotope fractionation during core formation, *Geochimica et Cosmochimica Acta*, 327, 186–199, 2022.
- Kuwahara, H., H. Gotou, T. Shinmei, N. Ogawa, A. Yamaguchi, N. Takahata, Y. Sano, T. Yagi, and S. Sugita, High pressure experiments on metal-silicate partitioning of chlorine in a magma ocean: Implications for terrestrial chlorine depletion, *Geochemistry, Geophysics, Geosystems*, 18(11), 3929–3945, 2017.
- Kuznetsova, A., J. Bae, L. Hartmann, and M.-M. M. Low, Anisotropic infall and substructure formation in embedded disks, *The Astrophysical Journal*, 928(1), 92, 2022.
- Larimer, J., and E. Anders, Chemical fractionations in meteoritesiii. major element fractionations in chondrites, *Geochimica et Cosmochimica Acta*, 34(3), 367–387, 1970.
- Larimer, J. W., Chemical fractionations in meteoritesi. condensation of the elements, *Geochimica et Cosmochimica Acta*, 31(8), 1215–1238, 1967.
- Larimer, J. W., and M. Bartholomay, The role of carbon and oxygen in cosmic gases: some applications to the chemistry and mineralogy of enstatite chondrites, *Geochimica et Cosmochimica Acta*, 43(9), 1455–1466, 1979.

- Latter, H. N., S. Fromang, and O. Gressel, MRI channel flows in vertically stratified models of accretion discs, *Monthly Notices of the Royal Astronomical Society*, 406(2), 848–862, 2010.
- Lau, T. C. H., T. Birnstiel, J. Drażkowska, and S. M. Stammer, Sequential giant planet formation initiated by disc substructure, *Astronomy & Astrophysics*, 688, A22, 2024.
- Lesur, G., et al., Hydro-, magnetohydro-, and dust-gas dynamics of protoplanetary disks, in *Protostars and Planets VII*, vol. 534, edited by S. Inutsuka, Y. Aikawa, T. Muto, K. Tomida, and M. Tamura, pp. 465–500, Astronomical Society of the Pacific, 2023.
- Lesur, G. R. J., Magnetohydrodynamics of protoplanetary discs, *Journal of Plasma Physics*, 87(1), 205870,101, doi: 10.1017/S0022377820001002, 2021.
- Lewis, J. S., Low temperature condensation from the solar nebula, *Icarus*, 16(2), 241–252, 1972.
- Li, J., and C. B. Agee, Geochemistry of mantle–core differentiation at high pressure, *Nature*, 381(6584), 686–689, 1996.
- Li, M., S. Huang, Z. Zhu, M. I. Petaev, and J. H. Steffen, Maximum temperatures in evolving protoplanetary discs and composition of planetary building blocks, *Monthly Notices of the Royal Astronomical Society*, 503(4), 5254–5262, doi:10.1093/mnras/stab837, 2021.
- Li, Y., L. Vočadlo, T. Sun, and J. P. Brodholt, The earths core as a reservoir of water, *Nature Geoscience*, 13(6), 453–458, 2020.
- Lichtenberg, T., J. Drażkowska, M. Schönbachler, G. J. Golabek, and T. O. Hands, Bifurcation of planetary building blocks during solar system formation, *Science*, 371(6527), 365–370, 2021.
- Liebske, C., A. Khan, S. M. McLennan, and P. A. Sossi, What is mars (not) made of? a joint isotopic, geochemical and geophysical analysis, *Icarus*, p. 116666, 2025.
- Liu, J., et al., Iron isotopic fractionation between silicate mantle and metallic core at high pressure, *Nature Communications*, 8(1), 14,377, 2017.
- Liu, X., R. C. Hin, C. D. Coath, M. van Soest, E. Mekekhova, and T. Elliott, Equilibrium olivine-melt mg isotopic fractionation explains high $\delta^{26}\text{Mg}$ values in arc lavas, *Geochemical Perspectives Letters*, 22, 42–47, 2022.
- Liu, X.-N., R. C. Hin, C. D. Coath, M. Bizimis, L. Su, D. A. Ionov, E. Takazawa, R. Brooker, and T. Elliott, The magnesium isotopic composition of the mantle, *Geochimica et Cosmochimica Acta*, 358, 12–26, 2023.
- Lodders, K., Solar system abundances and condensation temperatures of the elements, *The Astrophysical Journal*, 591(2), 1220, 2003.
- Lodders, K., Solar system abundances of the elements, in *Principles and Perspectives in Cosmochemistry: Lecture Notes of the Kodai School on 'Synthesis of Elements in Stars' held at Kodaikanal Observatory, India, April 29-May 13, 2008*, pp. 379–417, Springer, 2010.
- Longhi, J., Phase equilibrium constraints on angrite petrogenesis, *Geochimica et Cosmochimica Acta*, 63(3-4), 573–585, 1999.
- Luck, J.-M., D. B. Othman, and F. Albarède, Zn and cu isotopic variations in chondrites and iron meteorites: early solar nebula reservoirs and parent-body processes, *Geochimica et Cosmochimica Acta*, 69(22), 5351–5363, 2005.

- Lynden-Bell, D., and J. E. Pringle, The evolution of viscous discs and the origin of the nebular variables, *Monthly Notices of the Royal Astronomical Society*, 168(3), 603–637, 1974.
- MacPherson, G. J., Calcium-aluminum-rich inclusions in chondritic meteorites, *Meteorites and Cosmochemical Processes, Volume 1 of Treatise on Geochemistry (Second Edition)*, 1, 139–179, 2006.
- Magna, T., U. Wiechert, and A. N. Halliday, New constraints on the lithium isotope compositions of the moon and terrestrial planets, *Earth and Planetary Science Letters*, 243(3–4), 336–353, 2006.
- Magna, T., M. Šimčíková, and F. Moynier, Lithium systematics in howardite–eucrite–diogenite meteorites: Implications for crust–mantle evolution of planetary embryos, *Geochimica et Cosmochimica Acta*, 125, 131–145, 2014.
- Mah, J., and R. Brasser, Isotopically distinct terrestrial planets via local accretion, *Icarus*, 354, 114,052, 2021.
- Mah, J., R. Brasser, J. Woo, A. Bouvier, and S. Mojzsis, Evidence of a primordial isotopic gradient in the inner region of the solar protoplanetary disc, *Astronomy & Astrophysics*, 660, A36, 2022.
- Manara, C. F., A. Morbidelli, and T. Guillot, Why do protoplanetary disks appear not massive enough to form the known exoplanet population?, *A&A*, 618, L3, 2018.
- Manara, C. F., et al., Evidence for a correlation between mass accretion rates onto young stars and the mass of their protoplanetary disks, *A&A*, 591, L3, 2016.
- Mann, U., D. J. Frost, and D. C. Rubie, Evidence for high-pressure core-mantle differentiation from the metal–silicate partitioning of lithophile and weakly-siderophile elements, *Geochimica et Cosmochimica Acta*, 73(24), 7360–7386, 2009.
- Margot, J.-L., D. B. Campbell, J. D. Giorgini, J. S. Jao, L. G. Snedeker, F. D. Ghigo, and A. Bonsall, Spin state and moment of inertia of venus, *Nature Astronomy*, 5(7), 676–683, 2021.
- Marrocchi, Y., J. Villeneuve, E. Jacquet, M. Piralla, and M. Chaussidon, Rapid condensation of the first solar system solids, *Proceedings of the National Academy of Sciences*, 116(47), 23,461–23,466, 2019.
- Marschall, R., and A. Morbidelli, An inflationary disk phase to explain extended protoplanetary dust disks, *A&A*, 677, A136, 2023.
- Martins, R., S. Kuthning, B. J. Coles, K. Kreissig, and M. Rehkämper, Nucleosynthetic isotope anomalies of zinc in meteorites constrain the origin of earths volatiles, *Science*, 379(6630), 369–372, 2023.
- Mathieu, R., G. Libourel, E. Deloule, L. Tissandier, C. Rapin, and R. Podor, Na₂O solubility in cao–mgo–sio₂ melts, *Geochimica et Cosmochimica Acta*, 75(2), 608–628, 2011.
- Matsumoto, T., and K. Tomisaka, Directions of outflows, disks, magnetic fields, and rotation of young stellar objects in collapsing molecular cloud cores, *The Astrophysical Journal*, 616(1), 266, 2004.
- McCubbin, F. M., and J. J. Barnes, Origin and abundances of h₂o in the terrestrial planets, moon, and asteroids, *Earth and Planetary Science Letters*, 526, 115,771, 2019.
- McKibbin, S. J., and H. S. C. O’Neill, Petrogenesis of d’origny-like angrite meteorites and the role of spinel in the angrite source, *Meteoritics & Planetary Science*, 53(2), 306–325, 2018.

- Mezger, K., A. Maltese, and H. Vollstaedt, Accretion and differentiation of early planetary bodies as recorded in the composition of the silicate earth, *Icarus*, 365, 114,497, 2021.
- Mokhtari, M., and B. Bourdon, Condensation of major and trace elements in dust-rich environments, *Icarus*, p. 116801, 2025.
- Montmerle, T., J.-C. Augereau, M. Chaussidon, M. Gounelle, B. Marty, and A. Morbidelli, 3. solar system formation and early evolution: the first 100 million years, *Earth, Moon, and Planets*, 98, 39–95, 2006.
- Morbidelli, A., M. Lambrechts, S. Jacobson, and B. Bitsch, The great dichotomy of the solar system: Small terrestrial embryos and massive giant planet cores, *Icarus*, 258, 418–429, 2015.
- Morbidelli, A., K. Baillié, K. Batygin, S. Charnoz, T. Guillot, D. Rubie, and T. Kleine, Contemporary formation of early solar system planetesimals at two distinct radial locations, *Nature Astronomy*, 6(1), 72–79, 2022.
- Mori, S., X.-N. Bai, and S. Okuzumi, Temperature structure in the inner regions of protoplanetary disks: Inefficient accretion heating controlled by nonideal magnetohydrodynamics, *The Astrophysical Journal*, 872(1), 98, 2019.
- Moynier, F., R. C. Paniello, M. Gounelle, F. Albarède, P. Beck, F. Podosek, and B. Zanda, Nature of volatile depletion and genetic relationships in enstatite chondrites and aubrites inferred from zn isotopes, *Geochimica et Cosmochimica Acta*, 75(1), 297–307, 2011.
- Moynier, F., J. M. Day, W. Okui, T. Yokoyama, A. Bouvier, R. J. Walker, and F. A. Podosek, Planetary-scale strontium isotopic heterogeneity and the age of volatile depletion of early solar system materials, *The Astrophysical Journal*, 758(1), 45, 2012.
- Nakajima, M., G. J. Golabek, K. Wünnemann, D. C. Rubie, C. Burger, H. J. Melosh, S. A. Jacobson, L. Manske, and S. D. Hull, Scaling laws for the geometry of an impact-induced magma ocean, *Earth and Planetary Science Letters*, 568, 116,983, 2021.
- Namur, O., B. Charlier, F. Holtz, C. Cartier, and C. McCammon, Sulfur solubility in reduced mafic silicate melts: Implications for the speciation and distribution of sulfur on mercury, *Earth and Planetary Science Letters*, 448, 102–114, 2016.
- Nanne, J. A., F. Nimmo, J. N. Cuzzi, and T. Kleine, Origin of the non-carbonaceouscarbonaceous meteorite dichotomy, *Earth and Planetary Science Letters*, 511, 44–54, 2019.
- Nie, N. X., and N. Dauphas, Vapor drainage in the protolunar disk as the cause for the depletion in volatile elements of the moon, *The Astrophysical Journal Letters*, 884(2), L48, 2019.
- Nie, N. X., X.-Y. Chen, Z. J. Zhang, J. Y. Hu, W. Liu, F. L. Tissot, F.-Z. Teng, A. Shahar, and N. Dauphas, Rubidium and potassium isotopic variations in chondrites and mars: Accretion signatures and planetary overprints, *Geochimica et Cosmochimica Acta*, 344, 207–229, 2023.
- Nimmo, F., T. Kleine, A. Morbidelli, and D. Nesvorný, Mechanisms and timing of carbonaceous chondrite delivery to the earth, *Earth and Planetary Science Letters*, 648, 119,112, 2024.
- Nittler, L. R., N. L. Chabot, T. L. Grove, and P. N. Peplowski, *The Chemical Composition of Mercury*, p. 3051, Cambridge Planetary Science, Cambridge University Press, 2018.

- Nittler, L. R., et al., The major-element composition of mercurys surface from messenger x-ray spectrometry, *Science*, 333(6051), 1847–1850, 2011.
- Norris, C. A., and B. J. Wood, Earths volatile contents established by melting and vaporization, *Nature*, 549(7673), 507–510, 2017.
- O’Neill, H. S., and H. Palme, Composition of the silicate earth: implications for accretion and core formation, *The Earth’s mantle: Composition, structure, and evolution*, pp. 3–126, 1998.
- O’Neill, H. S. C., The origin of the moon and the early history of the eartha chemical model. part 1: The moon, *Geochimica et Cosmochimica Acta*, 55(4), 1135–1157, 1991.
- O’Neill, H. S. C., and S. M. Eggins, The effect of melt composition on trace element partitioning: an experimental investigation of the activity coefficients of feo, nio, coo, moo2 and moo3 in silicate melts, *Chemical Geology*, 186(1-2), 151–181, 2002.
- O’Neill, H. S. C., and H. Palme, Collisional erosion and the non-chondritic composition of the terrestrial planets, *Philosophical Transactions of the Royal Society A: Mathematical, Physical and Engineering Sciences*, 366(1883), 4205–4238, 2008.
- O’Neill, H. S. C., and M. I. Pownceby, Thermodynamic data from redox reactions at high temperatures. i. an experimental and theoretical assessment of the electrochemical method using stabilized zirconia electrolytes, with revised values for the fe-feo, co-coo, ni-nio and cu-cu2o oxygen buffers, and new data for the w-wo2 buffer, *Contributions to Mineralogy and Petrology*, 114(3), 296–314, 1993.
- O’Neill, H. S. C., D. Canil, and D. C. Rubie, Oxide-metal equilibria to 2500ř c and 25 gpa: Implications for core formation and the light component in the earth’s core, *Journal of Geophysical Research: Solid Earth*, 103(B6), 12,239–12,260, 1998.
- Onyett, I. J., M. Schiller, G. V. Makhatadze, Z. Deng, A. Johansen, and M. Bizzarro, Silicon isotope constraints on terrestrial planet accretion, *Nature*, 619(7970), 539–544, 2023.
- Palme, H., Are there chemical gradients in the inner solar system?, *Space Science Reviews*, 92(1), 237–262, 2000.
- Palme, H., and K. Mezger, Nucleosynthetic isotope variations in chondritic meteorites and their relationship to bulk chemistry, *Meteoritics & Planetary Science*, 59(2), 382–394, 2024.
- Palme, H., and H. S. C. O’Neill, *Treatise on geochemistry*, pp. 1–39, Elsevier Amsterdam, 2014.
- Paniello, R. C., J. M. Day, and F. Moynier, Zinc isotopic evidence for the origin of the moon, *Nature*, 490(7420), 376–379, 2012.
- Paquet, M., P. A. Sossi, and F. Moynier, Origin and abundances of volatiles on mars from the zinc isotopic composition of martian meteorites, *Earth and Planetary Science Letters*, 611, 118,126, 2023.
- Patrick, M. R., T. Orr, A. Sutton, E. Lev, W. Thelen, and D. Fee, Shallowly driven fluctuations in lava lake outgassing (gas pistonning), kilauea volcano, *Earth and Planetary Science Letters*, 433, 326–338, 2016.
- Peplowski, P. N., et al., Variations in the abundances of potassium and thorium on the surface of mercury: Results from the messenger gamma-ray spectrometer, *Journal of Geophysical Research: Planets*, 117(E12), 2012.

- Peplowski, P. N., et al., Remote sensing evidence for an ancient carbon-bearing crust on mercury, *Nature Geoscience*, 9(4), 273–276, 2016.
- Pignatale, F. C., J.-F. Gonzalez, N. Cuello, B. Bourdon, and C. Fitoussi, Size and density sorting of dust grains in SPH simulations of protoplanetary discs, *Monthly Notices of the Royal Astronomical Society*, 469(1), 237–254, 2017.
- Poitrasson, F., A. N. Halliday, D.-C. Lee, S. Levasseur, and N. Teutsch, Iron isotope differences between earth, moon, mars and vesta as possible records of contrasted accretion mechanisms, *Earth and Planetary Science Letters*, 223(3-4), 253–266, 2004.
- Poitrasson, F., T. Zambardi, T. Magna, and C. R. Neal, A reassessment of the iron isotope composition of the moon and its implications for the accretion and differentiation of terrestrial planets, *Geochimica et Cosmochimica Acta*, 267, 257–274, 2019.
- Poole, G. M., M. Rehkämper, B. J. Coles, T. Goldberg, and C. L. Smith, Nucleosynthetic molybdenum isotope anomalies in iron meteorites—new evidence for thermal processing of solar nebula material, *Earth and Planetary Science Letters*, 473, 215–226, 2017.
- Prettyman, T. H., J. Hagerty, R. Elphic, W. Feldman, D. Lawrence, G. McKinney, and D. Vaniman, Elemental composition of the lunar surface: Analysis of gamma ray spectroscopy data from lunar prospector, *Journal of Geophysical Research: Planets*, 111(E12), 2006.
- Pringle, E. A., and F. Moynier, Rubidium isotopic composition of the earth, meteorites, and the moon: Evidence for the origin of volatile loss during planetary accretion, *Earth and Planetary Science Letters*, 473, 62–70, 2017.
- Pringle, E. A., F. Moynier, P. S. Savage, J. Badro, and J.-A. Barrat, Silicon isotopes in angrites and volatile loss in planetesimals, *Proceedings of the National Academy of Sciences*, 111(48), 17,029–17,032, 2014.
- Qin, L., R. W. Carlson, and C. M. Alexander, Correlated nucleosynthetic isotopic variability in cr, sr, ba, sm, nd and hf in murchison and que 97008, *Geochimica et Cosmochimica Acta*, 75(24), 7806–7828, 2011.
- Rafikov, R. R., Protoplanetary disk heating and evolution driven by spiral density waves, *The Astrophysical Journal*, 831(2), 122, 2016.
- Render, J., G. A. Brennecka, C. Burkhardt, and T. Kleine, Solar system evolution and terrestrial planet accretion determined by zr isotopic signatures of meteorites, *Earth and Planetary Science Letters*, 595, 117,748, 2022.
- Ricolleau, A., Y. Fei, A. Corgne, J. Siebert, and J. Badro, Oxygen and silicon contents of earth’s core from high pressure metal–silicate partitioning experiments, *Earth and Planetary Science Letters*, 310(3-4), 409–421, 2011.
- Righter, K., M. J. Drake, and E. Scott, Compositional relationships between meteorites and terrestrial planets, *Meteorites and the early solar system II*, p. 803, 2006.
- Ringwood, A., and S. Kesson, Basaltic magmatism and the bulk composition of the moon: Ii. siderophile and volatile elements in moon, earth and chondrites: Implications for lunar origin, *The Moon*, 16(4), 425–464, 1977.
- Ringwood, A., T. Kato, W. Hibberson, and N. Ware, Partitioning of cr, v, and mn between mantles and cores of differentiated planetesimals: implications for giant impact hypothesis of lunar origin, *Icarus*, 89(1), 122–128, 1991.
- Ringwood, A. E., Chemical evolution of the terrestrial planets, *Geochimica et Cosmochimica Acta*, 30(1), 41–104, 1966.

- Rodríguez-Mozos, J.-M., and A. Moya, Internal structures and magnetic moments of rocky planets-application to the first exoplanets discovered by tess, *Astronomy & Astrophysics*, *661*, A101, 2022.
- Rubie, D., K. Dale, G. Nathan, M. Nakajima, E. Jennings, G. Golabek, S. Jacobson, and A. Morbidelli, Tungsten isotope evolution during earth’s formation and new constraints on the viability of accretion simulations, *Earth and Planetary Science Letters*, *651*, 119,139, 2025.
- Rubie, D. C., C. K. Gessmann, and D. J. Frost, Partitioning of oxygen during core formation on the earth and mars, *Nature*, *429*(6987), 58–61, 2004.
- Rubie, D. C., D. J. Frost, U. Mann, Y. Asahara, F. Nimmo, K. Tsuno, P. Kegler, A. Holzheid, and H. Palme, Heterogeneous accretion, composition and core–mantle differentiation of the earth, *Earth and Planetary Science Letters*, *301*(1-2), 31–42, 2011.
- Rubie, D. C., S. A. Jacobson, A. Morbidelli, D. P. OBrien, E. D. Young, J. de Vries, F. Nimmo, H. Palme, and D. J. Frost, Accretion and differentiation of the terrestrial planets with implications for the compositions of early-formed solar system bodies and accretion of water, *Icarus*, *248*, 89–108, 2015.
- Safronov, V., Evolution of protoplanetary cloud and formation of the earth and planets, nauka, moscow, *NASA Tech. Trans.*, pp. F–677, 1969.
- Salvador, A., and H. Samuel, Convective outgassing efficiency in planetary magma oceans: insights from computational fluid dynamics, *Icarus*, *390*, 115,265, 2023.
- Savage, P. S., F. Moynier, H. Chen, G. Shofner, J. Siebert, J. Badro, and I. Puchtel, Copper isotope evidence for large-scale sulphide fractionation during earths differentiation, *Geochemical Perspectives Letters*, 2015.
- Savage, P. S., F. Moynier, and M. Boyet, Zinc isotope anomalies in primitive meteorites identify the outer solar system as an important source of earth’s volatile inventory, *Icarus*, *386*, 115,172, 2022.
- Schiller, M., M. Bizzarro, and V. A. Fernandes, Isotopic evolution of the protoplanetary disk and the building blocks of earth and the moon, *Nature*, *555*(7697), 507–510, 2018.
- Schiller, M., M. Bizzarro, and J. Siebert, Iron isotope evidence for very rapid accretion and differentiation of the proto-earth, *Science advances*, *6*(7), eaay7604, 2020.
- Schneider, J. M., C. Burkhardt, and T. Kleine, Distribution of s-, r-, and p-process nuclides in the early solar system inferred from sr isotope anomalies in meteorites, *The Astrophysical Journal Letters*, *952*(1), L25, 2023.
- Schoenberg, R., S. Zink, M. Staubwasser, and F. von Blanckenburg, The stable cr isotope inventory of solid earth reservoirs determined by double spike mc-icp-ms, *Chemical Geology*, *249*(3-4), 294–306, 2008.
- Schoenberg, R., A. Merdian, C. Holmden, I. C. Kleinhanns, K. Haßler, M. Wille, and E. Reitter, The stable cr isotopic compositions of chondrites and silicate planetary reservoirs, *Geochimica et cosmochimica acta*, *183*, 14–30, 2016.
- Schramm, D., and E. Norman, Heavy element nucleosynthesis, *3rd International Conference on Nuclei Far from Stability*, 1976.
- Scott, E. R., and J. T. Wasson, Classification and properties of iron meteorites, *Reviews of Geophysics*, *13*(4), 527–546, 1975.

- Shah, O., R. Helled, Y. Alibert, and K. Mezger, Possible chemical composition and interior structure models of venus inferred from numerical modelling, *The Astrophysical Journal*, 926(2), 217, 2022.
- Shahar, A., and E. D. Young, An assessment of iron isotope fractionation during core formation, *Chemical Geology*, 554, 119,800, 2020.
- Shahar, A., K. Ziegler, E. D. Young, A. Ricolleau, E. A. Schauble, and Y. Fei, Experimentally determined si isotope fractionation between silicate and fe metal and implications for earth’s core formation, *Earth and Planetary Science Letters*, 288(1-2), 228–234, 2009.
- Shakura, N., and R. Sunyaev, A theory of the instability of disk accretion on to black holes and the variability of binary x-ray sources, galactic nuclei and quasars, *Monthly Notices of the Royal Astronomical Society*, 175(3), 613–632, 1976.
- Shakura, N. I., and R. A. Sunyaev, Black holes in binary systems. observational appearance., *Astronomy and Astrophysics*, Vol. 24, p. 337-355, 24, 337–355, 1973.
- Shu, F. H., H. Shang, A. E. Glassgold, and T. Lee, X-rays and fluctuating x-winds from protostars, *Science*, 277(5331), 1475–1479, 1997.
- Siebert, J., J. Badro, D. Antonangeli, and F. J. Ryerson, Terrestrial accretion under oxidizing conditions, *Science*, 339(6124), 1194–1197, 2013.
- Siebert, J., P. A. Sossi, I. Blanchard, B. Mahan, J. Badro, and F. Moynier, Chondritic mn/na ratio and limited post-nebular volatile loss of the earth, *Earth and Planetary Science Letters*, 485, 130–139, 2018.
- Sossi, P. A., and B. Fegley, Thermodynamics of element volatility and its application to planetary processes, *High Temperature Gas-Solid Reactions in Earth and Planetary Processes*, pp. 393–460, 2018.
- Sossi, P. A., and A. Shahar, Ironing out isotopic differences among rocky bodies, *Elements: An International Magazine of Mineralogy, Geochemistry, and Petrology*, 17(6), 407–412, 2021.
- Sossi, P. A., O. Nebel, and J. Foden, Iron isotope systematics in planetary reservoirs, *Earth and Planetary Science Letters*, 452, 295–308, 2016.
- Sossi, P. A., F. Moynier, and K. Van Zuilen, Volatile loss following cooling and accretion of the moon revealed by chromium isotopes, *Proceedings of the National Academy of Sciences*, 115(43), 10,920–10,925, 2018a.
- Sossi, P. A., O. Nebel, H. S. C. O’Neill, and F. Moynier, Zinc isotope composition of the earth and its behaviour during planetary accretion, *Chemical Geology*, 477, 73–84, 2018b.
- Sossi, P. A., S. Klemme, H. S. C. O’Neill, J. Berndt, and F. Moynier, Evaporation of moderately volatile elements from silicate melts: experiments and theory, *Geochimica et Cosmochimica Acta*, 260, 204–231, 2019.
- Sossi, P. A., I. L. Stotz, S. A. Jacobson, A. Morbidelli, and H. S. C. O’Neill, Stochastic accretion of the earth, *Nature astronomy*, 6(8), 951–960, 2022.
- Sossi, P. A., M. Nakajima, and A. Khan, Composition, structure and origin of the moon, *Treatise of Geochemistry*, 3rd edition, 7, 417–479, 2025.
- Spitzer, F., C. Burkhardt, G. Budde, T. S. Kruijer, A. Morbidelli, and T. Kleine, Isotopic evolution of the inner solar system inferred from molybdenum isotopes in meteorites, *The Astrophysical Journal Letters*, 898(1), L2, 2020.

- Spitzer, F., C. Burkhardt, T. S. Kruijer, and T. Kleine, Comparison of the earliest nc and cc planetesimals: Evidence from ungrouped iron meteorites, *arXiv preprint arXiv:2503.15102*, 2025.
- Spitzer, F., et al., The ni isotopic composition of ryugu reveals a common accretion region for carbonaceous chondrites, *Science Advances*, 10(39), eadp2426, 2024.
- Stammler, S. M., T. Lichtenberg, J. Drażkowska, and T. Birnstiel, Leaky dust traps: How fragmentation impacts dust filtering by planets, *Astronomy & Astrophysics*, 670, L5, 2023.
- Steele, R. C., C. D. Coath, M. Regelous, S. Russell, and T. Elliott, Neutron-poor nickel isotope anomalies in meteorites, *The Astrophysical Journal*, 758(1), 59, 2012.
- Steenstra, E., J. Berndt, S. Klemme, A. Rohrbach, E. Bullock, and W. Van Westrenen, An experimental assessment of the potential of sulfide saturation of the source regions of eucrites and angrites: Implications for asteroidal models of core formation, late accretion and volatile element depletions, *Geochimica et Cosmochimica Acta*, 269, 39–62, 2020.
- Steinmeyer, M.-L., P. Woitke, and A. Johansen, Sublimation of refractory minerals in the gas envelopes of accreting rocky planets, *Astronomy & Astrophysics*, 677, A181, 2023.
- Steller, T., C. Burkhardt, C. Yang, and T. Kleine, Nucleosynthetic zinc isotope anomalies reveal a dual origin of terrestrial volatiles, *Icarus*, 386, 115,171, 2022.
- Stephens, I. W., et al., Alma reveals transition of polarization pattern with wavelength in hl taus disk, *The Astrophysical Journal*, 851(1), 55, 2017.
- Stoll, M. H. R., and W. Kley, Vertical shear instability in accretion disc models with radiation transport, *A&A*, 572, A77, 2014.
- Suer, T.-A., J. Siebert, L. Remusat, N. Menguy, and G. Fiquet, A sulfur-poor terrestrial core inferred from metal–silicate partitioning experiments, *Earth and Planetary Science Letters*, 469, 84–97, 2017.
- Suzuki, T. K., and S.-i. Inutsuka, Disk winds driven by magnetorotational instability and dispersal of protoplanetary disks, *The Astrophysical Journal*, 691(1), L49, 2009.
- Tabone, B., G. P. Rosotti, A. J. Cridland, P. J. Armitage, and G. Lodato, Secular evolution of mhd wind-driven discs: analytical solutions in the expanded α -framework, *Monthly Notices of the Royal Astronomical Society*, 512(2), 2290–2309, 2022.
- Tang, H., and N. Dauphas, 60fe–60ni chronology of core formation in mars, *Earth and Planetary Science Letters*, 390, 264–274, 2014.
- Tang, H., and E. Young, Evaporation from the lunar magma ocean was not the mechanism for fractionation of the moons moderately volatile elements, *The Planetary Science Journal*, 1(2), 49, 2020.
- Tartèse, R., P. A. Sossi, and F. Moynier, Conditions and extent of volatile loss from the moon during formation of the procellarum basin, *Proceedings of the National Academy of Sciences*, 118(12), e2023023,118, 2021.
- Thibault, Y., and M. J. Walter, The influence of pressure and temperature on the metal-silicate partition coefficients of nickel and cobalt in a model c1 chondrite and implications for metal segregation in a deep magma ocean, *Geochimica et Cosmochimica Acta*, 59(5), 991–1002, 1995.

- Tian, Z., H. Chen, B. Fegley Jr, K. Lodders, J.-A. Barrat, J. M. Day, and K. Wang, Potassium isotopic compositions of howardite-eucrite-diogenite meteorites, *Geochimica et Cosmochimica Acta*, 266, 611–632, 2019.
- Tian, Z., B. L. Jolliff, R. L. Korotev, B. Fegley Jr, K. Lodders, J. M. Day, H. Chen, and K. Wang, Potassium isotopic composition of the moon, *Geochimica et Cosmochimica Acta*, 280, 263–280, 2020.
- Tian, Z., et al., Potassium isotope composition of mars reveals a mechanism of planetary volatile retention, *Proceedings of the National Academy of Sciences*, 118(39), e2101155,118, 2021.
- Tissot, F. L., M. Collinet, O. Namur, and T. L. Grove, The case for the angrite parent body as the archetypal first-generation planetesimal: Large, reduced and mg-enriched, *Geochimica et Cosmochimica Acta*, 338, 278–301, 2022.
- Tomascak, P. B., T. Magna, R. Dohmen, et al., *Advances in lithium isotope geochemistry*, Springer, 2016.
- Toplis, M., et al., Chondritic models of 4 vesta: Implications for geochemical and geophysical properties, *Meteoritics & Planetary Science*, 48(11), 2300–2315, 2013.
- Trinquier, A., J.-L. Birck, and C. J. Allegre, Widespread 54cr heterogeneity in the inner solar system, *The Astrophysical Journal*, 655(2), 1179, 2007.
- Trinquier, A., T. Elliott, D. Ulfbeck, C. Coath, A. N. Krot, and M. Bizzarro, Origin of nucleosynthetic isotope heterogeneity in the solar protoplanetary disk, *Science*, 324(5925), 374–376, 2009.
- Turner, N. J., T. Sano, and N. Dziourkevitch, Turbulent mixing and the dead zone in protostellar disks, *The Astrophysical Journal*, 659(1), 729, 2007.
- Umebayashi, T., The Densities of Charged Particles in Very Dense Interstellar Clouds, *Progress of Theoretical Physics*, 69(2), 480–502, 1983.
- Urey, H. C., and H. Craig, The composition of the stone meteorites and the origin of the meteorites, *Geochimica et Cosmochimica Acta*, 4(1-2), 36–82, 1953.
- van Kooten, E., X. Zhao, I. Franchi, P.-Y. Tung, S. Fairclough, J. Walmsley, I. Onyett, M. Schiller, and M. Bizzarro, The nucleosynthetic fingerprint of the outermost protoplanetary disk and early solar system dynamics, *Science Advances*, 10(24), eadp1613, 2024.
- Visscher, C., and B. Fegley, Chemistry of impact-generated silicate melt-vapor debris disks, *The Astrophysical Journal Letters*, 767(1), L12, 2013.
- Volkov, A. N., R. E. Johnson, O. J. Tucker, and J. T. Erwin, Thermally driven atmospheric escape: Transition from hydrodynamic to jeans escape, *The Astrophysical Journal Letters*, 729(2), L24, 2011.
- von Strandmann, P. A. P., T. Elliott, H. R. Marschall, C. Coath, Y.-J. Lai, A. B. Jeffcoate, and D. A. Ionov, Variations of li and mg isotope ratios in bulk chondrites and mantle xenoliths, *Geochimica et Cosmochimica Acta*, 75(18), 5247–5268, 2011.
- Wade, J., and B. Wood, Core formation and the oxidation state of the earth, *Earth and Planetary Science Letters*, 236(1-2), 78–95, 2005.
- Wadhwa, M., Redox conditions on small bodies, the moon and mars, *Reviews in Mineralogy and Geochemistry*, 68(1), 493–510, 2008.

- Wang, B., F. Moynier, M. G. Jackson, F. Huang, X. Hu, S. A. Halldórsson, W. Dai, and G. Devos, Rubidium isotopic fractionation during magmatic processes and the composition of the bulk silicate earth, *Geochimica et Cosmochimica Acta*, 354, 38–50, 2023.
- Wang, B., F. Moynier, and Y. Hu, Rubidium isotopic compositions of angrites controlled by extensive evaporation and partial recondensation, *Proceedings of the National Academy of Sciences*, 121(1), e2311402, 2024.
- Wang, H., B. P. Weiss, X.-N. Bai, B. G. Downey, J. Wang, J. Wang, C. Suavet, R. R. Fu, and M. E. Zucolotto, Lifetime of the solar nebula constrained by meteorite paleomagnetism, *Science*, 355(6325), 623–627, 2017.
- Wang, X., C. Fitoussi, B. Bourdon, B. Fegley Jr, and S. Charnoz, Tin isotopes indicative of liquid–vapour equilibration and separation in the moon-forming disk, *Nature Geoscience*, 12(9), 707–711, 2019.
- Wang, Z., V. Laurenz, S. Petitgirard, and H. Becker, Earth’s moderately volatile element composition may not be chondritic: Evidence from in, cd and zn, *Earth and Planetary Science Letters*, 435, 136–146, 2016.
- Warren, P. H., Stable-isotopic anomalies and the accretionary assemblage of the earth and mars: A subordinate role for carbonaceous chondrites, *Earth and Planetary Science Letters*, 311(1-2), 93–100, 2011.
- Wasson, J. T., and G. W. Kallemeyn, Compositions of chondrites, *Philosophical Transactions of the Royal Society of London. Series A, Mathematical and Physical Sciences*, 325(1587), 535–544, 1988.
- Weidenschilling, S., Aerodynamics of solid bodies in the solar nebula, *Monthly Notices of the Royal Astronomical Society*, 180(2), 57–70, 1977.
- Weidenschilling, S., and J. N. Cuzzi, Formation of planetesimals in the solar nebula, in *Protostars and planets III*, pp. 1031–1060, 1993.
- Weider, S. Z., et al., Evidence from messenger for sulfur-and carbon-driven explosive volcanism on mercury, *Geophysical Research Letters*, 43(8), 3653–3661, 2016.
- Whipple, F. L., On certain aerodynamic processes for asteroids and comets, in *From plasma to planet*, p. 211, 1972.
- Williams, C. D., M. E. Sanborn, C. Defouilloy, Q.-Z. Yin, N. T. Kita, D. S. Ebel, A. Yamakawa, and K. Yamashita, Chondrules reveal large-scale outward transport of inner solar system materials in the protoplanetary disk, *Proceedings of the National Academy of Sciences*, 117(38), 23,426–23,435, 2020.
- Williams, J. G., Contributions to the earth’s obliquity rate, precession, and nutation, *The Astronomical Journal*, vol. 108, no. 2, p. 711–724, 108, 711–724, 1994.
- Wimpenny, J., L. Borg, and C. K. I. Sio, The gallium isotopic composition of the moon, *Earth and Planetary Science Letters*, 578, 117,318, 2022.
- Witt-Eickschen, G., H. Palme, H. S. C. Oneill, and C. M. Allen, The geochemistry of the volatile trace elements as, cd, ga, in and sn in the earths mantle: New evidence from in situ analyses of mantle xenoliths, *Geochimica et Cosmochimica Acta*, 73(6), 1755–1778, 2009.
- Wolf, A. S., N. Jäggi, P. A. Sossi, and D. J. Bower, Vaporock: thermodynamics of vaporized silicate melts for modeling volcanic outgassing and magma ocean atmospheres, *The Astrophysical Journal*, 947(2), 64, 2023.
- Woo, J. M. Y., R. Brasser, S. L. Grimm, M. L. Timpe, and J. Stadel, The terrestrial planet formation paradox inferred from high-resolution n-body simulations, *Icarus*, 371, 114,692, 2022.

- Wood, B. J., and J. Wade, Activities and volatilities of trace components in silicate melts: a novel use of metal–silicate partitioning data, *Contributions to Mineralogy and Petrology*, 166, 911–921, 2013.
- Wood, B. J., E. S. Kiseeva, and F. J. Mirolo, Accretion and core formation: The effects of sulfur on metal–silicate partition coefficients, *Geochimica et Cosmochimica Acta*, 145, 248–267, 2014.
- Wood, B. J., D. J. Smythe, and T. Harrison, The condensation temperatures of the elements: A reappraisal, *American Mineralogist*, 104(6), 844–856, 2019.
- Wood, J. A., and A. Hashimoto, Mineral equilibrium in fractionated nebular systems, *Geochimica et Cosmochimica Acta*, 57(10), 2377–2388, 1993.
- Worsham, E. A., K. R. Bermingham, and R. J. Walker, Characterizing cosmochemical materials with genetic affinities to the earth: genetic and chronological diversity within the iab iron meteorite complex, *Earth and Planetary Science Letters*, 467, 157–166, 2017.
- Wulf, A., H. Palme, and K. Jochum, Fractionation of volatile elements in the early solar system: evidence from heating experiments on primitive meteorites, *Planetary and Space Science*, 43(3-4), 451–468, 1995.
- Yang, X., Z. Du, and Y. Li, Experimental constraints on metal-silicate partitioning of chlorine and implications for planetary core formation, *Geochimica et Cosmochimica Acta*, 355, 62–74, 2023.
- Yap, T. E., and F. L. Tissot, The nc-cc dichotomy explained by significant addition of cai-like dust to the bulk molecular cloud (bmc) composition, *Icarus*, 405, 115,680, 2023.
- York, D., N. M. Evensen, M. L. Martinez, and J. De Basabe Delgado, Unified equations for the slope, intercept, and standard errors of the best straight line, *American journal of physics*, 72(3), 367–375, 2004.
- Yoshizaki, T., and W. F. McDonough, The composition of mars, *Geochimica et Cosmochimica Acta*, 273, 137–162, 2020.
- Young, E., A. Shahar, F. Nimmo, H. Schlichting, E. Schauble, H. Tang, and J. Labidi, Near-equilibrium isotope fractionation during planetesimal evaporation, *Icarus*, 323, 1–15, 2019.
- Young, E. D., R. D. Ash, P. England, and D. Rumble III, Fluid flow in chondritic parent bodies: Deciphering the compositions of planetesimals, *Science*, 286(5443), 1331–1335, 1999.
- Zahnle, K. J., and J. F. Kasting, Mass fractionation during transonic escape and implications for loss of water from mars and venus, *Icarus*, 68(3), 462–480, 1986.
- Zhu, K., P. A. Sossi, J. Siebert, and F. Moynier, Tracking the volatile and magmatic history of vesta from chromium stable isotope variations in eucrite and diogenite meteorites, *Geochimica et Cosmochimica Acta*, 266, 598–610, 2019.
- Zhu, K., J.-A. Barrat, A. Yamaguchi, O. Rouxel, Y. Germain, J. Langlade, and F. Moynier, Nickel and chromium stable isotopic composition of ureilites: Implications for the earth’s core formation and differentiation of the ureilite parent body, *Geophysical Research Letters*, 49(7), e2021GL095,557, 2022.
- Zhu, K., et al., Chromium stable isotope panorama of chondrites and implications for earth early accretion, *The Astrophysical Journal*, 923(1), 94, 2021.
- Zuber, M. T., H. Y. McSween, R. P. Binzel, L. T. Elkins-Tanton, A. S. Konopliv, C. M. Pieters, and D. E. Smith, Origin, internal structure and evolution of 4 vesta, *Space science reviews*, 163, 77–93, 2011.